Zeolite and Metal-Organic Framework Membranes for Pervaporation and Gas Separation

Von der Naturwissenschaftlichen Fakultät der

Gottfried Wilhelm Leibniz Universität Hannover

zur Erlangung des Grades

Doktorin der Naturwissenschaften

Dr. rer. nat.

genehmigte Dissertation

von

M. Sc. Nanyi Wang

geboren am 26.11.1986 in Jiangsu, China

2015

Preface

The presented original results of this thesis were obtained from January 2012 until January 2015 during my Ph. D. study at the Institute of Physical Chemistry and Electrochemistry at the Gottfried Wilhelm Leibniz University Hannover under the supervision of Prof. Dr. Jürgen Caro. In this period, I worked as a member of scientific research staff for the European project CARENA (CAtalytic REactors based on New mAterials).

Five research articles, in which I have participated as the first author or the co-author, are presented in this thesis. The following statement will point out my contribution to the articles collected in this thesis. For all these articles, I would like to appreciate valuable comments and helpful discussion from the co-authors, referees, and cooperation partners in CARENA project, particularly from Prof. Dr. Jürgen Caro, Prof. Dr. Aisheng Huang (Institute of New Energy Technology, Ningbo Institute of Material Technology and Engineering) and Dr. Yi Liu (Humboldt Research Fellow).

The two articles about zeolites, *Supported SOD membrane with steam selectivity by a two-step repeated hydrothermal synthesis* and *Hydrophilic SOD and LTA membranes for membrane-supported methanol, dimethylether and dimethylcarbonate synthesis*, which are collected in Chapter 2, were written by me with the help of Prof. Dr. Jürgen Caro. I prepared the samples of zeolite SOD and LTA membranes and powders, did the ion-exchange experiments, performed the corresponding characterizations like scanning electron microscopy (SEM), the energy-dispersive X-Ray spectroscopy (EDXS) and the X-Ray diffraction (XRD) analysis and carried out the measurement of gas separation performances. However, I kindly thank Frank Steinbach for his helpful suggestions and technical support for EDXS. I appreciate Dr. Yi Liu for his discussion and support during the experiments and writing. Prof. Dr. Aisheng Huang helped me to revise and improve the manuscript.

The first article about MOF membrane in Chapter 3.2, *Amine-modified Mg-MOF-74/CPO-27-Mg membrane with enhanced H_2/CO_2 separation*, was written by me. I prepared the Mg-MOF-74 membranes and powders, performed the corresponding characterizations of SEM and XRD analysis and did the measurement of gas separation performances. Alexander Mundstock shared his experiences with me during the

experiments and characterization. The idea of this paper was born during the discussion with Prof. Dr. Aisheng Huang. Prof. Dr. Jürgen Caro and Dr. Yi Liu have made a significant contribution to improve the manuscript.

Another article about MOF membrane in Chapter 3.3, *Polydopamine-based synthesis of zeolite imidazolate framework ZIF-100 membrane with high H_2/CO_2 selectivity*, was written by me. I also prepared the ZIF-100 membranes and powders, performed the corresponding characterizations and did the gas separation measurements. I would like to thank Zhiwei Qiao and Jian Zhou (Guangdong Provincial Key Lab for Green Chemical Product Technology, South China University of Technology) for the simulation study of gas adsorption isotherm of ZIF-100. Lisa Diestel helped me to build the structure model of ZIF-100. Prof. Dr. Jürgen Caro, Prof. Dr. A. Huang and Dr. Yi Liu have helped me to improve the manuscript.

The last article in Chapter 3.4, *Organosilica-functionalized zeolitic imidazolate framework ZIF-90 membrane with high gas-separation performance*, was written by Prof. Dr. Aisheng Huang. My contribution was to modify the proposed way of membrane preparation, to provide experimental assistance characterizations and to carry out the gas separation performances.

Acknowledgement

To those who have helped me during my Ph.D. thesis research at the Institute of Physical Chemistry and Electrochemistry at the Gottfried Wilhelm Leibniz University Hannover, I would like to give my appreciation.

First and foremost, I would like to express the deepest gratitude to my supervisor Prof. Dr. Jürgen Caro for giving me this opportunity to carry out my scientific work in his group. He never hesitates to give me support and patient guidance during my research. I am also deeply impressed by his hard-working attitude, high efficiency and honest passion for science. Prof. Caro's international group gives me a comfort atmosphere, where people always show their enthusiasm, kindness and friendship.

Furthermore, I would like to appreciate Prof. Dr. Aisheng Huang (Institute of New Energy Technology at Ningbo Institute of Material Technology and Engineering) for his contribution. I cannot have so many research articles without his help and cooperation.

The financial support of the European project CARENA is acknowledged. I am grateful to my project collaboration partners, particularly Thijs de Groot and Gerrald Bargeman from AkzoNobel, Marcel den Exter from ECN and William McDonnell from Johnson Matthey for the suggestions and cooperation in research of zeolite membranes.

I would like to thank Dr. Yi Liu for his valuable discussions and experimental help during my work. I would also like to give many thanks to current and former members in Prof. Caro's group, namely M. Sc. Lisa Diestel, Dipl. NanoSc. Alexander Mundstock, M. Sc. Alexander Schulz and M. Sc. Sebastian Friebe in porous membrane group for their experimental help and suggestions in my research work, as well as Prof. Dr. Armin Feldhoff, Dr. Yanying Wei, Dr. Fangyi Liang, Dr. Zhengwen Cao, Dipl.-Chem. Olga Ravkina, M. Sc. Kaveh Partovi, M. Sc. Jian Xue, M. Sc. Wei Fang and M. Sc. Benjamin Geppert, for their discussions and exchanges of knowledge throughout my work. Yvonne Gabbey-Uebe, Kerstin Janze, and Frank Steinbach are appreciated for their kind supports in the administrative or technical aspects.

At last but not least, I would like to thank my parents Daoping Wang and Xiao Hong for their understandings and unlimited support, and my husband Luyu Hao for his encouragement and unconditional love.

Abstract

The present thesis is dedicated to investigation of microporous zeolite and metal-organic framework (MOF) membranes for pervaporation and gas separation on a laboratory scale. Different experimental synthesis methods and modification methods were used to improve the membrane quality, reproducibility, and separation performance.

Two strong hydrophilic zeolite membranes, SOD and LTA membranes, were synthesized on alumina supports for vapor permeation or water pervaporation. A repeated synthesis method was used to prepare zeolite SOD membranes. As the first candidate to separate water vapor at high temperatures, zeolite SOD membrane shows high thermal and chemical stability and has a small pore size. The removal of steam from other components allows the possibility to support the chemical reaction like methanol, dimethylether (DME) and dimethylcarbonate (DMC) formation. Another candidate to separate water is zeolite LTA membrane, which we used at room temperature for water/methanol and water/DMC pervaporation. Na-LTA membrane was ion-exchanged with K^+ to further improve the pervaporation selectivity.

Supported Mg-MOF-74, ZIF-90 and ZIF-100 membranes were prepared for gas separation. For synthesis of these MOF membranes, different pre- or post-modification methods were used. Mg-MOF-74 membrane was prepared on MgO-seeded alumina support, and the H_2/CO_2 selectivity could be improved by the post-modification of the open Mg sites with ethylenediamine. The dense ZIF-100 membrane was prepared on a polydopamine (PDA)-modified support. After the pre-modification, the ZIF-100 crystals could grow better on the support surface through the formation of covalent chemical bonds. Attributing to its high CO_2 uptake behavior, ZIF-100 membrane has a high H_2/CO_2 selectivity. A post-functionalization method was developed for ZIF-90 membrane by using 3-aminopropyltriethoxysilane (APTES). Via the covalent linkages between the free aldehyde groups of the ZIF-90 and the amino group of APTES, the pore was narrowed and the defects were sealed, thus the gas separation selectivity of ZIF-90 was enhanced.

Keywords: Zeolite membrane, MOF membrane, gas separation, pervaporation, ion-exchange, pre- and post-modification method.

Zusammenfassung

Die Arbeit behandelt Synthese, Charakterisierung und Ausprüfung mikroporöser Zeolith- und Metal-Organic Framework (MOF)-Membranen durch Pervaporation und Gasseparation. Verschiedenste Synthesestrategien und Modifikationen wurden entwickelt, um Qualität, Reproduzierbarkeit und Trennleistung der Membranen zu verbessern.

Zur permeativen Dampftrennung und Pervaporation wässriger Gemische wurden zwei hydrophile Zeolithmembranen, SOD und LTA, auf Al_2O_3-Trägern synthetisiert. Die SOD-Membran kann für Wasser-Trennungen bis zu Temperaturen von mind. 200 °C verwendet werden. Grund hierfür ist die hohe thermische und chemische Stabilität der SOD-Gerüststruktur und der kleine Porendurchmesser von SOD, der molekulares Sieben ermöglicht. Die Entfernung von Wasser unter gleichgewichtskontrollierten Reaktionsbedingungen könnte z.B. zu einer höheren Ausbeute bei der Synthese von Dimethylcarbonat (DMC) oder Dimethylether (DME) in Membranreaktoren führen. Ein weiterer Kandidat für die Wasserabtrennung ist die LTA-Membran. Diese wurde für die Pervaporation von Wasser/Methanol- und Wasser/DMC-Gemischen bei Raumtemperatur verwendet. Die Natriumionen der Na-LTA-Membran wurden durch Kaliumionen ausgetauscht, um die Selektivität der Pervaporation weiter zu verbessern.

Trägergestützte Mg-MOF-74-, ZIF-90- und ZIF-100-Membranen wurden für die Gastrennung hergestellt. Zur Synthese dieser MOF-Membranen wurden verschiedene Pre- oder Post-Modifikationsverfahren entwickelt. Die Mg-MOF-74-Membran wurde auf einem mit MgO-Keimkristallen beschichtetem Al_2O_3-Träger hergestellt. Nach der Post-Modifikation der Mg-Positionen durch Ethylendiamin konnte die H_2/CO_2-Selektivität verbessert werden. Eine ZIF-100-Membran wurde auf einem Polydopamin (PDA)-modifizierten Träger hergestellt. Nach der PDA-Modifikation konnten die ZIF-100-Kristalle besser auf der Oberfläche des Trägers wachsen. Wegen der guten adsorptiven CO_2-Bindung besaß die ZIF-100-Membran eine hohe H_2/CO_2-Selektivität. Die ZIF-90-Membran wurde mit 3-Aminopropyltriethoxysilan (APTES) post-funktionalisiert. Über die kovalenten Bindungen zwischen den Aldehydgruppen des ZIF-90 und den Aminogruppen von APTES wurden Poren der ZIF-90-Membran verengt und Defekte versiegelt, und so die Selektivität der ZIF-90-Membran verbessert.

Schlagwörter: Zeolith-Membranen, MOF-Membranen, Gastrennung, Pervaporation, Ionenaustausch, Pre- und Post-Funktionalisierung.

Content

1 Introduction

1.1 Motivation

In the past five decades, membrane separation technology has attracted intense attention and membrane separation processes have already had a direct impact on large scale industrial applications due to the lower energy consumption and investment cost in comparison with conventional distillation and adsorption.[1-2] A membrane can be simply defined as a semipermeable two-dimensional material which allows preferential passage of selected components of a mixture or solution. Depending on different driving forces and sizes of the selected components, membrane processes can be applied in microfiltration (potable water treatment), ultrafiltration (waste water treatment), nanofiltration (water softening), reverse osmosis (seawater desalination), dialysis (medical applications) and electrodialysis (aqueous solution deionization).[3]

Gas separation and pervaporation are relative new membrane separation processes in industry during the past decades. Among the gas separations, hydrogen purification is one of the most important tasks due to the growing demand for energy and environmental issues. Currently, hydrogen is mainly produced by steam-methane reforming (SMR) followed by the water-gas shift (WGS). Before H_2 can be used in fuel cell, it has to be purified from the SMR/WGS products which mainly contain CO_2, but also CH_4 and CO.[4] Membrane gas separation can be more economical compared with traditional separation methods like pressure swing adsorption (PSA) and cryogenic distillation.[5] In pervaporation, liquid mixture can be separated. Pervaporation process can be applied for dehydration of organic solvents, removal of organic compounds from aqueous solution and separation of anhydrous organic mixtures.[6] Moreover, pervaporation can realize some separations which are difficult by distillation, extraction and sorption.[7] Therefore, as potential membrane separation progresses, gas separation and pervaporation have been attracted significant attention recently.

Membranes can be roughly classified into organic and inorganic membranes. Unfortunately, a lot of organic membranes like polymers suffer from instability problems at high temperatures, swelling in contact with solvents or decomposition in sterilization progress. In contrast, inorganic membranes display a much higher thermal and solvent stability. Therefore, inorganic membranes have been studied increasingly in

new applications fields like fuel cells and catalytic membrane reactors.[8]

Inorganic membranes can be classified into dense membranes like Pd-based membranes[9-10] and perovskite membranes[11], as well as porous membranes, such as amorphous microporous silica[12] and carbon membranes[13]. The distinction of dense or porous membranes is not much a matter to the absolute pore size, but rather relative to the different transport mechanisms. The dense membranes permeate atomic or ionic forms of hydrogen or oxygen by a solution-diffusion mechanism, while the porous membranes separate the components through other mechanisms, such as adsorption-diffusion effect, molecular sieving effect, Knudsen diffusion, viscous flow, surface diffusion and capillary condensation.[14] Compared to the dense inorganic membranes, porous membranes have received increasing attention in the recent years, since they can be applied to separate a broad range of chemical components.

Among the porous inorganic membranes, molecular sieve zeolite membranes have attached great interest in the past two decades. Attributed to their uniform pore structure and high thermal stability, zeolite membranes have wide potential applications such as catalysts in reactors, sensors and as devices for gas and/or liquid separations.[15-16] Zeolite LTA membranes were already commercialized for dehydration in steam permeation. Due to their molecular sieving effect, high thermal stability and low-cost for synthesis, zeolites are good candidates for pervaporation and gas separation.

Synthesis of most zeolites requires the use of organic structure directing agent (SDA), in order to control the process of the crystallization of zeolites. After the synthesis, the organic SDA can be removed by calcination, which always requires high temperatures of 450 to 500 ℃. Attributing to its high thermal stability, zeolite itself is still stable at high temperature, and zeolite crystals will not be destroyed. However, the membrane layers will form cracks easily due to the lack of mechanical stability and the expansion/shrimking effect during the calcination.[17] In this thesis, therefore, we focus on the zeolite SOD and LTA membranes, which can be synthesized free of SDA.

In the past two decades, a new class of porous materials, metal-organic frameworks (MOFs) has been developed. As a recently-identified class of porous materials, MOFs have porous structure based on metal ions and organic ligands. Due to the wide choice of metals and ligands, different kinds of MOFs can be designed with rich possibilities

for structures and properties, such as adsorption, magnetic, electrical, optical and catalytic properties.[18] Based on the adjustable pore structure and controllable properties, MOFs are another promising candidates for gas storage and gas separation besides zeolites.

Compared to zeolites, MOFs have not only higher porosity and specific surface area[19], but also rich possibilities to be pre- and post-modified with functional groups[20]. The pre-modification can promote the nucleation of MOF membranes on the support surface, while the post-modification allows the possibilities to modulate the physical can chemical properties of MOFs, change the pore size of the framework structure, or make the MOFs interacting with guest species as well.

The aims of this thesis are to optimize the synthesis method of supported zeolite and MOF membranes, develop dense zeolite and MOF membranes for pervaporation and gas separation, and use different methods like ion-exchange and post-modification to improve the selectivity.

1.2 Zeolite

1.2.1 Structure and properties of zeolites

The name of "zeolite" is derived from two Greek words "zeo" and "lithos" which mean "to boil" and "a stone".[21] Zeolites are three-dimensional crystalline microporous or mesoporous aluminosilicates with well-defined structures, which mainly contain silicon, aluminum and oxygen atoms in their framework structures. The silicon and aluminum atoms are tetrahedrally connected to each other by using the oxygen atoms as bridge. The building unit of every zeolite framework is mostly tetrahedral TO_4 blocks
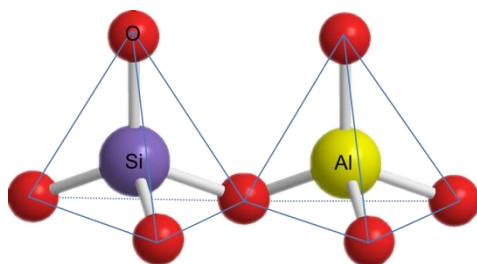

Figure 1: TO_4 blocks: units of zeolite framework.

(some new architectures involve other polyhedral like octahedral TO_6, pentacoordinated TO_5 or pyramidal TO_4 or TO_3 blocks)[22], where T is the tetrahedrally coordinated atom like Al or Si, as shown in Figure 1. Since each oxygen atom is shared by two units, the net formal charge of the tetrahedral SiO_4 unit is 0, but not like the isolated unit with a charge of -4. In contrast, AlO_4 unit carries a formal charge of -1. Consisting of SiO_4 and AlO_4 units, therefore, the entire zeolite framework is negatively charged. The negative charges can be compensated either by cations or proton in the acidic form in pores and channels or by pentavalent T-atoms instead of Si like P^{5+} (such as ALPO's).[23] Therefore, the aluminosilicate zeolite has a general formula of $A_{x/n}[Si_{1-x}Al_xO_2]$ mH_2O, where A is the cation with a valence n.[22] The typical cations in natural zeolites are alkali metal, like Na^+, K^+ and alkaline earth metals such as Ca^{2+} und Mg^{2+}.[24] The Si/Al ratio can range from 1 as a minimum to infinity. By varying the Si/Al ratio in zeolites, the ionicity and hydrophilicity of the material is also changed, which can impact the crystal size, morphology, surface area, thermal and chemical stability and acidity of the zeolites.[25]

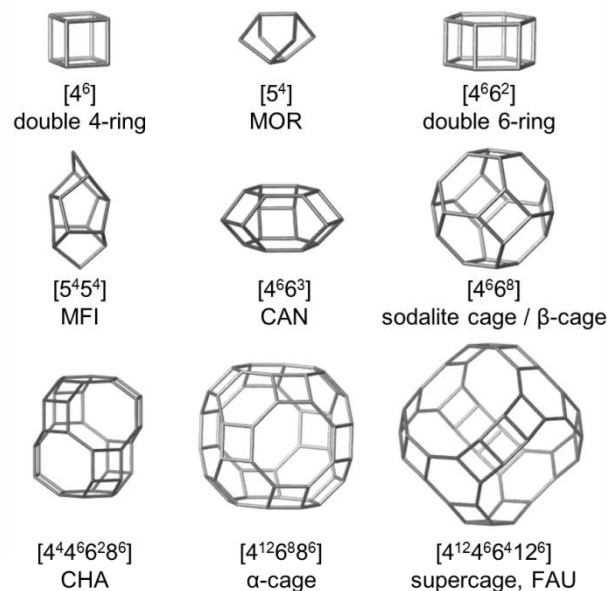**Figure 2**: Examples of CBUs in zeolites with their pore symbols.[21]

Depending on their framework symmetry, zeolites can be classified with an identification code consisting of three capital letters by the International Zeolite Association (IZA).[23] The structure types of zeolite can be described by the composite building units (CBUs), which are built by several TO_4 tetrahedral blocks.[21] Some

commonly found CBUs are shown in Figure 2 as examples with their corresponding pore symbols (e.g. 4^66^2 means six 4-membered rings with two 6-membered rings) and common names. According to the different window apertures of pore structures, zeolites can be classified into small (with 6-, 8- and 9-membered rings), medium (with 10-membered rings), large (with 12-membered rings) and ultralarge (with 14-, 18- or 20-membered rings) pore materials.[23] The molecular sieving effect of a zeolite is determined by the largest channel in the framework structure.

Due to their unique properties, like uniform pore structure, ion-exchange property, high thermal stability and high internal surface area, zeolites have found a lot of applications such as adsorbents, catalysts, sensors, ion-exchangers, and electrical insulators. Potential applications are growing up such as membranes.

1.2.2 Introduction to zeolite membranes

Recently, much effort has been devoted to fabrication of zeolite membranes. Zeolite membranes can be classified into self-supported (symmetric) or supported (asymmetric) membranes, and both of them have been reported. However, self-supported zeolite membranes always suffer from mechanical stability problems due to their heterogeneous thickness. Therefore, zeolite membranes were usually synthesized on substrates, and the substrate can either combine with the zeolite to form a composite membrane, or be removed after the synthesis.[23]

In 1987, Suzuki prepared the first zeolite membrane on a porous support of metal.[26] After that, Haag and Tsikoyiannis investigated the standalone, mechanically unstable ZSM-5 membrane in 1991.[27-28] Then Geus et al. reported the first supported silicalite-1 membrane in 1992.[29] Since then, significant progress has been made to develop different kinds of zeolite membranes, and there are several reviews on zeolite membranes.[15, 23, 30] Today, various zeolite membranes, typically SOD[31-32], SAPO-34 (CHA-type)[33-34], DDR[35], LTA[36-39], FER[40], ZSM-5 or silicalite 1 (MFI-type)[41-42], MOR[43], $AlPO_4$-5 (AFI-type)[44] and FAU[45-47] are developed on porous or non-porous supports.

So far, various supported zeolite membranes have been successfully synthesized for the separation of gas and/or liquid mixtures. As summerized in Table 1, zeolite

membranes on different supports have been used for separations like n-/iso-butane separation, hydrogen purification, water pervaporation and organic mixture separation.[48] In our work, we usually use asymmetric α-Al$_2$O$_3$ discs to support our membranes.

Table 1: Summary of supported zeolite membranes developed for gas/vapor/liquid permeation and separation

n-Butane and iso-butane separation		
	Silicalite	γ-alumia tube, stainless steel disk
	ZSM-5	α-alumia disk or tube, stainless steel tube
	MFI	α-alumia disk
Hydrogen purification		
	LTA	α-alumia disk or tube
	FAU	α-alumia disk or tube
	Silicalite	γ-alumia tube, stainless steel disk,
	ZSM-5	α-alumia disk or tube, γ-alumia tube
Carbon dioxide and methane separation		
	FAU	α-alumia tube
	SAPO-34	α-alumia tube
	ZSM-5	γ-alumia tube
Carbon dioxide and nitrogen separation		
	ZSM-5	α-alumia disk
	NaY	α-alumia tube
	SAPO-34	α-alumia tube
Water pervaporation		
	NaA	α-alumia tube, Ceramesh sheet, carbon tube
	FAU	α-alumia disk or tube
Organic solvents pervaporation		
	Silicate	stainless steel disk or tube
	ZSM-5	α-alumia disk
Organic mixture separation		
	NaA	α-alumia disk or tube
	FAU	α-alumia disk or tube
	Silicate	stainless steel disk or tube
	FER	α-alumia disk or tube

1.2.3 Structure, properties and applications of zeolite SOD and zeolite LTA

Zeolite A (Linde Type A, LTA), with a chemical composition of [Na$_{12}$(H$_2$O)$_{27}$]$_8$ [Al$_{12}$Si$_{12}$O$_{48}$]$_8$, has a cubic symmetry. The LTA framework type consists of β-cages linked by double 4-rings (both of the CBUs are shown in Figure 2), which results in a

α-cage with a pore diameter of about 4.1 Å.[49] The framework structure is shown in Figure 3 (left).

Among numerous zeolites, the zeolite LTA membranes have been extensively studied due to the strong hydrophilicity and suitable pore size. [38-39, 50-51] Moreover, zeolite LTA membranes were the first commercialized zeolite membrane, which are applied for dehydration of water/alcohol mixtures by membrane-based steam permeation.[52-56]
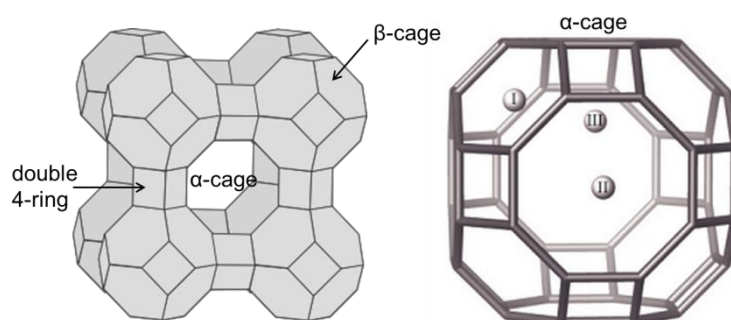

Figure 3: Framework structures of zeolite LTA (left) and α-cage in LTA (right)[21].

As hydrated low-silica zeolite (1< Si/Al <2), zeolite LTA is also used widely for ion-exchange applications, since the high cation content results in a high exchange ability.[22] As shown in Figure 3 (right), site I (centered on the 6-ring), II (near the center of 8-ring) and III (centered on the 4-ring) in every α-cage of LTA can accommodate 8, 3 and 12 cations, respectively. The cations tend to prefer sites following the order I > II > III, and the cations which occupy site II are rather mobile and can diffuse since site II is near to the center of the 8-membered ring. With a Si/Al ratio of 1, each α-cage in LTA consists of 12 cations, which occupy fully sites I and II. Normally, the cations in synthesized LTA are Na^+. By ion-exchange, the Na^+ which occupy site II can diffuse into the cavity and be exchanged by other cations. By replacing the Na^+ with Ca^{2+}, the number of cations will be reduced thus the Ca-LTA has a pore size of 5 Å. When the sodium cations were replaced by larger K^+ ions, the pore size of K-LTA will be narrowed to 3 Å.[21] This ion-exchange behavior allows the applications such as water-softening, gas adsorption and gas separation.

Zeolite sodalite (SOD) is an aluminosilicate with 3-dimentional channel network.[57] It was first discovered by Thomson in 1811[58] and its structure was

described by Pauling in 1930[59].The chemical composition of mineral sodalite is [Na$_8$Cl$_2$][Al$_6$Si$_6$O$_{24}$].[60] As shown in Figure 4, SOD consists of only sodalite cages (also called β-cages shown in Figure 2) and has, therefore, only 4- and 6-membered rings. Hydroxy sodalite (H-SOD) has the same structure as sodalite. In the framework of H-SOD, the 4-membered rings are too small to allow the passage of any molecules, but the window aperture of the 6-membered ring of Si-O-Si bonds with a diameter of 2.7 Å can allow the passage of small molecules like helium, ammonia and water, with kinetic diameters of 2.60, 2.55 and 2.65 Å, respectively.[61] Compared with LTA, zeolite SOD has the same Si/Al ratio of 1, but shows a higher framework density (number of T-atoms per Å^3: for SOD 16.7 T/1000 Å^3). Therefore, zeolite SOD has a higher structural stability.
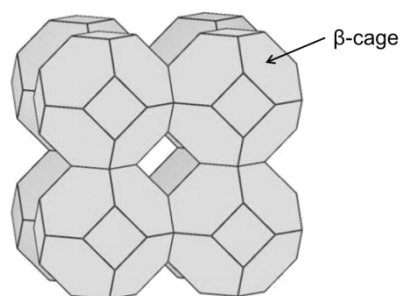
Figure 4: Framework structure of zeolite SOD.

Due to its small pore size and strong hydrophilicity, hydroxy sodalite membrane has an important potential for esterification[62], sea water desalination[63], separation of small molecules from gas mixtures and the removal of water from industrial streams, such as in the synthesis of dimethyl ether (DME) and dimethyl carbonate (DMC) (see Eq. 1 and 2).

$$2\ CO_2 + 6\ H_2 \leftrightharpoons DME + 3\ H_2O \qquad\qquad\qquad\text{(Eq. 1)}$$

$$CO_2 + 2\ MeOH \leftrightharpoons DMC + H_2O \qquad\qquad\qquad\text{(Eq. 2)}$$

1.2.4   Synthesis of zeolite membranes

As explained in section 1.2.2, most of the zeolite membranes are prepared on supports, therefore, only synthesis of supported zeolite membranes are discussed in this

part. The commonly used synthesis methods to prepare a supported zeolite membrane consist of *in-situ* hydrothermal synthesis, secondary growth method and microwave synthesis.

In-situ hydrothermal synthesis is the mostly used preparation method for zeolite membranes. In this simple synthesis method, the support is contacted directly with a synthesis solution or an aqueous gel, and the membrane will grow on the support surface under hydrothermal conditions, which should be carefully controlled so that the zeolite crystals can nucleate and intergrow into a membrane. This method requires heterogeneous nucleation on the support surface and crystal growth to form a continuous layer which can cover the support. [48] The flow diagram for the *in-situ* hydrothermal synthesis is shown in Figure 5.
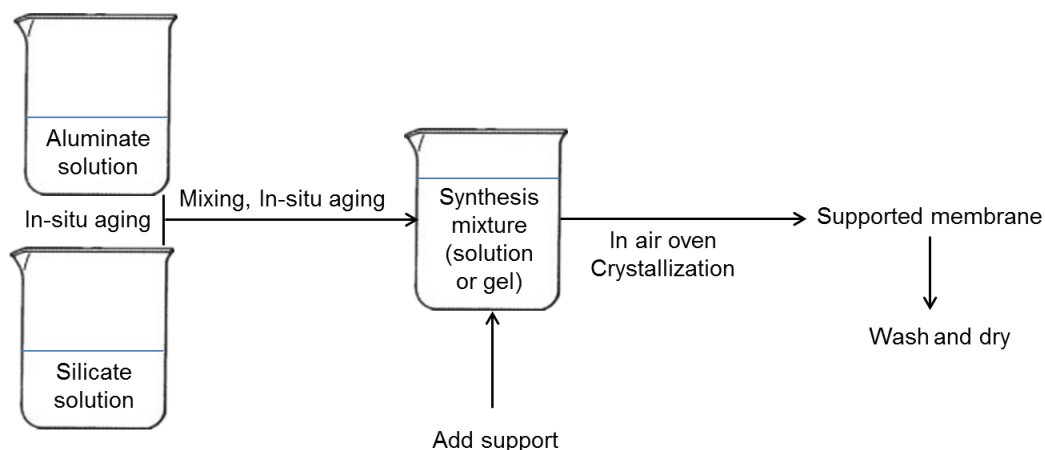
Figure 5: Schematic diagram of *in-situ* hydrothermal synthesis.

This method is commonly used and easy to operate. However, it usually takes long crystallization time, which can result in the formation of impurity. In addition, the size of the zeolite crystals, which are formed on the surface of the support, are not uniform due to the low heating rate and inhomogeneous heating in hydrothermal synthesis.[64] Therefore, it is usually difficult to prepare a dense membrane on the support by using this method.

In the **secondary growth method**, supports are firstly coated with a layer of zeolite seeds, after that, the membrane is formed through the further growth of the seeds during the following hydrothermal synthesis.[64] The seeding can be attached on the surface of the membrane by mechanical scrubbing the support surface with zeolite

crystals or by dip-coating in seed-solution.[48] In this method, the microstructure of the membrane such as thickness and orientation can be controlled, thus the quality and reproducibility of the membrane can be improved.[64] Since the problem of heterogeneous nucleation in normal *in-situ* hydrothermal synthesis is solved, the membranes prepared by secondary growth method are dense and have uniform crystal size. However, as a multi-step synthesis, this method is relatively complicated. It is also necessary to simplify the seeding process, in order to attach the seeds effectively.[65]

Recently, **microwave synthesis method** was started to be used for the synthesis of zeolite membrane. In microwave synthesis, the heating process was carried out in a microwave instead of an air oven. The electromagnetic filed supplies the energy directly to the materials, which leads to an effective heating process. Compared to the conventional hydrothermal synthesis, therefore, microwave synthesis method has lot of advantages like reduced synthesis time, small crystal size, high purity as well as narrow particle size distribution. [64] However, microwave synthesis was still not widely used, since the synthesis conditions for only a few kinds of zeolites were optimized and the mechanism of crystal nucleation and growth by microwave heating is not clear yet.

1.3 Metal-organic framework

1.3.1 Naming and history of MOFs

In the past two decades, metal-organic frameworks (MOFs), a new class of synthetic porous materials, have been developed into one of the most fruitful research areas.[66-67] Due to the lack of a general definition during the explosion of the development of MOFs, various appellations have been appeared, such as porous coordination polymer (PCP) [68] and porous coordination network (PCN)[69] or other names. Following the tradition of naming for zeolites, acronym of the laboratory was also used to name the MOFs, like the series of MILs (matériauxs de l'Institut Lavoisier)[70] and HKUST (Hong-Kong University of Science and Technology)[71].

The interest in porous coordination polymer started around 1990 by Hoskins and Robson[72-73]. Then the development of MOFs was promoted by Yaghi et al.[74-75] and Kitagawa et al.[76] in 1995 and 1997. In 1999, the structures of MOF-5[77] and

HKUST-1[71] were published, which are still among the most studied MOFs up to now. In 2002, the series of MILs were reported by Férey et al.[78-79] and in the same year, imidazolate-based MOF with zeolite-related topology was published[80], which are later organized in sub-group of MOFs: zeolitic imidazole frameworks (ZIFs). Up to now, a large number of different MOFs has been investigated and successively developed for gas separation and other potential applications.

1.3.2   Structure and properties of MOFs

MOFs are inorganic-organic hybrid materials, which are built of inorganic single metal ions or metal-containing clusters and organic ligands called linkers. The inorganic part and organic part link with each other through coordination bonds and build a well-defined framework structure.[81] As shown in Figure 6, the framework structure of MOF-5[82-83] was taken as an example to describe the basic construction of MOFs, which consists of inorganic metal clusters $(Zn_4O)^{6+}$ and organic linkers 1,4-benzenedicarboxylate (BDC).
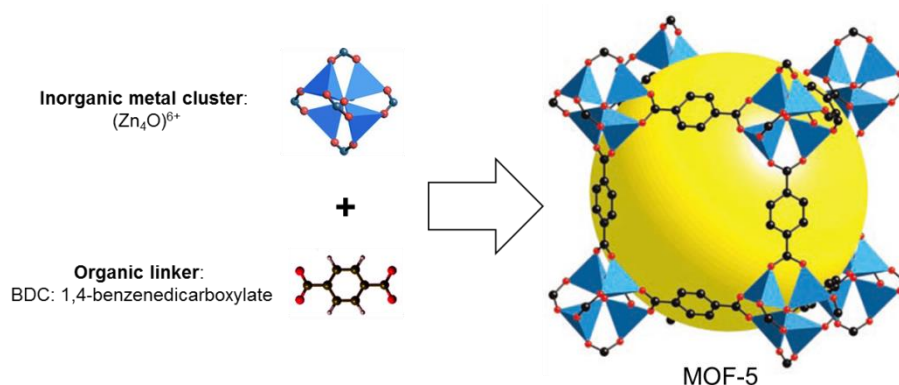
Figure 6: Framework structure of MOF-5 ($Zn_4(O)O_{12}C_6$), which is built of inorganic metal cluster (Zn_4O^{6+}) and organic linker 1,4-benzenedicarboxylate (BDC). The metal clusters are shown on the left as a ball and stick model and on the right with the ZnO_4 tetrahedra. The yellow sphere shows the cavity of MOF-5.[82-83]

Although the structure description and classification of MOF is still debatable, two approaches are proposed to explain the structure principles of MOFs. The first approach by Yaghi et al.[84] used nets and vertex symbols, namely (N, M)-connected nets, to describe the topologies of MOFs. N and M are the numbers of connections from two

nodes, and the edges are links between vertices. An (N, M)-connected net was defined to have some vertices connected to N neighbors and some to M neighbors. Here nodes can be metal ions, clusters or polyhedrons, while edges can be linker molecules or multiple bonds.[84-85] To describe the structure of MOF-5, for instance, the nodes (Zn_4O^{6+} clusters) are linked by 6 edges (BDC) to form an octahedral geometry. The second concept was proposed by Férey et al.[86], which describe the MOF framework by building units (BUs). The BU is defined as a building block of the framework, which acts as a "brick" to form coherent structures.[86] Following this concept, the cubic MOF-5 framework can by described as eight BUs, and each BU consists of a Zn_4O^{6+} cluster coordinated by 6 BDCs.

As a light material with highest porosities, MOFs have high inner surface areas.[87] A typical example is MOF-177[88], which was reported with an inner surface of 4500 $m^2 \ g^{-1}$. With this property, therefore, MOFs can be used for gas adsorption and separation. Based on the construction principle of MOFs, the structure and properties of MOFs can be designed by judicious combination of metal clusters and organic linkers.[81] Besides adsorption-based properties, MOFs can also display other unique properties like optic, magnetic and electronic properties, when special metals or organic linkers were chosen.[89] Based on the various properties, MOFs have a lot of potential applications like gas storage, gas separation, catalysis, sensing, ion-exchange and drug delivery.[81] However, so far MOFs have not found industrial application.

1.3.3   Structure and properties of Mg-MOF-74, ZIF-90 and ZIF-100

Magnesium dioxybenzenedicarboxylate (**Mg-MOF-74**)[90], which is also termed Mg/dobdc or CPO-27-Mg[91-92], is one of the iso-structural compounds of $M_2(dhtp)(H_2O)_2 \ 8H_2O$ (M-MOF-74, M can be Ni, Co, Zn, Mg, Mn, dhtp is dihydroxyterephthalic acid).[93-94] Due to its significantly high adsorption capacities, Mg-MOF-74 is under intense investigation.[95-96] As shown in Figure 7, Mg-MOF-74 is constructed by the linkage of the Mg^{2+} ions (yellow) with 2,5-dioxido-1,4-benzenedicarboxylate (DOBDC). The metal cations Mg^{2+} build a distorted octahedron and the carboxylate groups act as ligands of Mg^{2+}, then a well-defined hexagonal, one-dimensional (1D) pore structure (Figure 7 left) is formed with a pore diameter of

about 11 Å.[97-98]

In the framework structure of Mg-MOF-74, the metal cations Mg^{2+} are bonded with five oxygen atoms to form square-pyramid coordination, and the open and accessible unsaturated metal sites, which locate in the center of the square plane, are free to interact with CO_2 molecules. Attributing to this unique feature of the structure, Mg-MOF-74 has a high CO_2 adsorption capacity (380 mg CO_2/g at room temperature under dry conditions[99]).
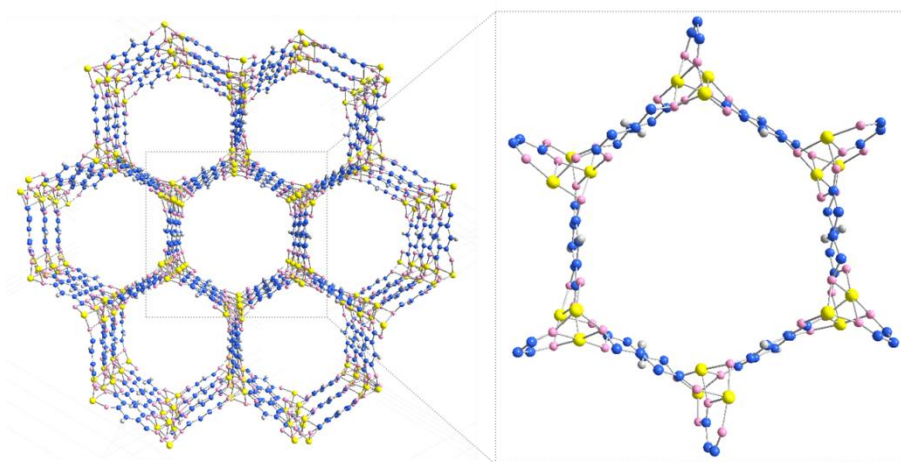
Figure 7: Framework structure of Mg-MOF-74 as viewed along the [100] direction. Yellow, red, blue and gray spheres represent Mg, O, C and H atoms, respectively.
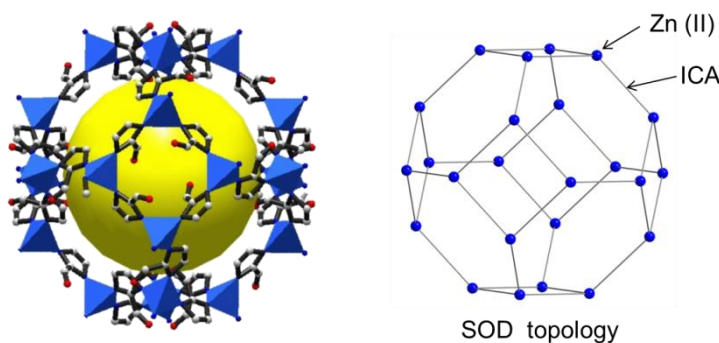
Figure 8: Left: Framework structure of ZIF-90 as viewed along the [100] direction. Violet tetrahedron represents ZnN_4; gray and red spheres represent C and O atoms, respectively; Right: SOD topology of ZIF-90.

Zeolite imidazolate frameworks (ZIFs) are a sub-group of MOFs, which are constructed from metal ions bridged by imidazolate linkers with zeolite-type tetrahedral topologies.[100] In 2008, Yaghi et al.[101] have reported a new crystalline ZIF structure

which termed **ZIF-90**. It is synthesized through a solvothermal reaction of $Zn(NO_3)_2$ $4H_2O$ with imidazolate-2-carboxyaldehyde (ICA). The structure of ZIF-90 is shown in Figure 8 left, which is related to the SOD topology (Figure 8 right) by replacing the Si/Al and O with Zn(II) and ICA linkers. ZIF-90 has an inner sphere with a diameter of 11.2 Å (yellow sphere in Figure 8) and a narrow aperture of the six-membered ring pores of about 3.5 Å.[101-102] ZIF-90 has not only high chemical and thermal stability[101], but also various possibility to be functionalized due to the aldehyde group in the framework structure[103].
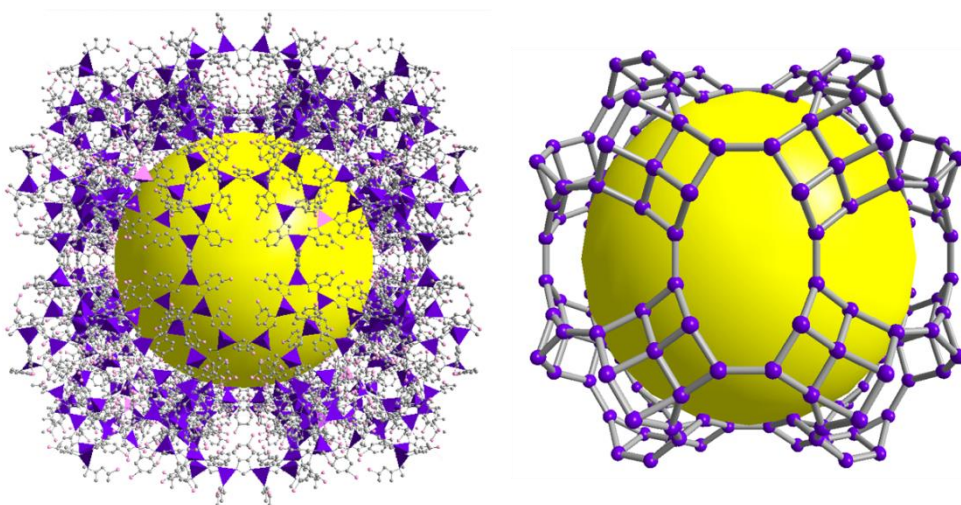
Figure 9: Framework structure of the MOZ cage in ZIF-100 as viewed along the [100] direction. Left: Violet tetrahedron represents ZnN_4; gray and pink spheres represent C and Cl atoms, respectively; O and H are not shown here. Right: ball and stick diagram of MOZ cage in ZIF-100. The yellow sphere shows the cavity of ZIF-100.

The structure of zeolite imidazolate framework **ZIF-100** was first published by Yaghi et al.[104] in 2008. ZIF-100 has a composition of $Zn_{20}(cbIM)_{39}(OH)$, which is obtained through the reaction of $Zn(O_3SCF_3)_2$ with 5-chlorobenzimidazole (cbIM). As shown in Figure 9, ZIF-100 has a rather complex structure, whose unit cell has a MOZ topology, which is constructed from 7524 atoms (Figure 9 left). This MOZ cage has a large inner sphere with a diameter of 35.6 Å (the yellow sphere in Figure 9 right) and a constricted window aperture of only 3.35 Å.

As reported by Yaghi et al.[104], mainly CO_2 can be retained in the pore structure of ZIF-100, since ZIF-100 shows a strong adsorption of CO_2 due to the strong quadrupolar interactions of carbon with nitrogen atoms in the linkers of ZIF-100 framework, which

results in an outstanding CO_2 adsorption affinity. The CO_2 uptake of ZIF-100 for CO_2 outperforms ZIF-95 and BPL carbon[105], which is already widely used in industry for gas separation. Besides the CO_2 adsorption capacity, ZIF-100 has also a high thermal stability up to 500 °C.[104]

### 1.3.4   Synthesis of MOF membranes: Pre- and post-modification method

The first MOF membranes were IRMOF-1 membrane which reported by Lai and Jeong et al.[106-107] in 2009. After that, different MOF membranes were prepared like HKUST-1[108-109], MMOF[95], ZIF-7[110], ZIF-8[111], ZIF-22[112], ZIF-69[113], ZIF-90[114] and MIL-53[115]. Resembling the synthesis methods of zeolite membranes, MOF membranes were usually fabricated by hydrothermal synthesis method (*in-situ* growth)[109,112-114] or secondary growth method[95,108,115], and based on these two synthesis methods, microwave synthesis[110-111] was also developed to control the crystal size of the membrane. Since MOF is a novel material, despite a lot of progress in MOF membranes synthesis, the robust synthetic strategies are still not developed to obtain dense membranes with high gas selectivities.

Despite much progress in MOF membranes synthesis, there is still a long road ahead before robust synthetic strategies can be developed that allow the facile synthesis of highly selective MOF membranes, as highlighted recently.[116] One major reason that the MOF films cannot grow on supports, is the bad interaction between the organic linkers in MOF materials and support surface. Due to the poor heterogeneous nucleation of MOF crystals on support surfaces, it is rather difficult to grow continuous and dense MOF membranes by direct hydrothermal synthesis. [117-118] Therefore, pre-modifications of the supports[112,118] and secondary growth method by seeding are usually used to promote the growth of continuous MOF layers. The pre-modification methods can provide additional linkage groups which can form bonds with groups on the support surface (e.g. OH group on alumina support), while the secondary growth method can avoid heterogeneous nucleation and promote the nucleation of MOF crystals on the support.

Compared to the secondary growth method, **pre-modification** of the support is a relatively simple and effective strategy to improve the membrane growth, when a

suitable modification agent was chosen. For instance, the free aldehyde groups in the framework of ZIF-90 allow the possibility of imine condensation reaction with amine groups.[101] Based on this coupling, we report a covalent functionalization strategy to modify the support surface with amine groups by using 3-aminopropyltriethoxysilane (APTES).[114,119] The APTES functions as covalent linkers between the ZIF-90 layer and Al_2O_3 support, so that the MOF layer can grow better on the APTES-modified support due to the imine condensation reaction, as shown in Eq. 3. Another pre-modification method we reported is using polydopamine (PDA). By adding dopamine in the modification solution, dopamine can easily polymerize to PDA (Eq. 4) and stick on the support surface during the pre-modification process, since PDA has various functional groups which can have interactions with different kinds of organic and inorganic surfaces.[120] The PDA-pre-modified support can be used as a platform for further reactions.[121-123] This pre-modification method was already used for synthesis of ZIF-8 and zeolite LTA membranes to improve their gas separation performance and reproducibility.[124-126]

$$MOF\text{-}CHO + H_2N\text{-}Support \rightarrow MOF\text{-}CH=N\text{-}Support + H_2O \qquad (Eq.\ 3)$$

(Eq. 4)
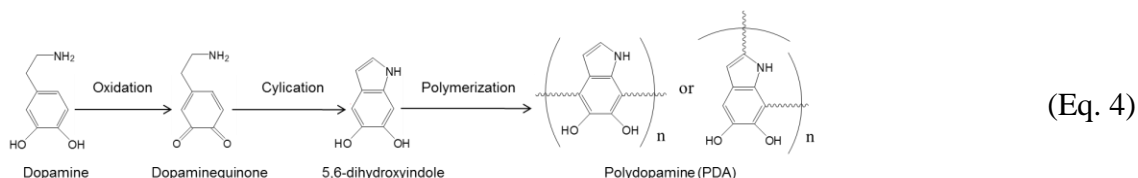
After the MOF membranes are prepared, it is found that the synthesized MOF layers have a polycrystalline structure which usually contains intercrystalline defects. Therefore, **post-modification** method for the as-prepared MOF membranes were investigated to minimize the intercrystalline gaps and improve the membrane selectivity.[127-128] There are already at least three strategies for the post-modification[129]: covalent modification by using functionalized ligands to modify 1) the organic building blocks[119,130-131] or 2) metal ions[132-133], as well as 3) non-covalent modification to demonstrate the framework with cartridge molecules.[134]

The covalent modification of organic linkers can be explained by ZIF-90 as an example. The free aldehyde groups in ZIF-90 framework allow the possibility to be modified.[101] The covalent post-functionalization of ZIF-90 with amine groups through an imine condensation reaction was reported,[135-138] and we used this post-modification

method to improve the hydrogen selectivity of as-prepared ZIF-90 membrane by ethanolamine[128] and APTES[119]. The post-synthesis modification of Mg-MOF-74 membrane is a representative for the modification of metal sites. In the unique framework structure of Mg-MOF-74, the metal cations Mg^{2+} have unsaturated metal sites, which can be modified with amine groups.[139] H_2/CO_2 selectivity can be improved by post-modification of Mg-MOF-74 membranes with ethylenediamine, whose one side can bind to the open coordination sites of the Mg by direct ligation, the other side remains free in space for CO_2 adsorption.[132]

1.4 Mass transport in microporous membranes

1.4.1 Important parameters

To evaluate the quality of a membrane, two aspects should be considered: how permeable and how selective the membrane is.

In gas separation measurement, the most commonly used parameters to describe the permeability of a membrane are flux F, permeance P and permeability PE, while the ideal or mixture separation factor α was used to describe the selectivity. The flux (Eq. 5) is the amount of gas n which has passed through the membrane pre time t and membrane area A. The permeance P is obtained by division of the flux by the transmembrane pressure difference Δp, as shown in Eq. 6, and the permeability (Eq. 7) is the permeance multiplied by the membrane thickness d. The separation factor $\alpha_{i,j}$ of a binary mixture permeation is defined as the quotient of the molar ratios of the components (i, j) in the permeate, divided by the quotient of those in the retentate, as shown in Eq. 8. Since in our case less than 1 % of the feed gas pass the membrane, the retentate composition is de facto identical with the feed composition.

$$J = \frac{n}{A \cdot t} \tag{Eq. 5}$$

$$P = \frac{n}{A \cdot t \cdot \Delta p} \tag{Eq. 6}$$

$$PE = \frac{n \cdot d}{A \cdot t \cdot \Delta p} \tag{Eq. 7}$$

$$\alpha_{i/j} = \frac{y_{i,p}/y_{j,p}}{y_{i,r}/y_{j,r}} \tag{Eq. 8}$$

In pervaporation, the total flux J and the separation factor α are always used, which are defined following Eqs. 9 and 10, where W is total weight of the permeate (kg), Δt is collecting time (h), A is separation area of the membrane (m^2), $x_{i,p}$ and $x_{i,f}$ are the weight fractions of species i in the permeate and in the feed, respectively.

$$J = \frac{W}{\Delta t \cdot A} \tag{Eq. 9}$$

$$\alpha_{i/j} = \frac{x_{i,p}}{x_{i,f}} \cdot \frac{x_{j,f}}{x_{j,p}} \tag{Eq. 10}$$

With the equations given above, the quality of a membrane can be characterized easily by the experimental measurement. However, to investigate the permeation behaviour of our membranes, the mechanism of mass transport should be focused on. Mass transfer through a membrane can only take place, when a driving force exists. The driving force in our measurements is always the pressure difference between the feed and permeate sides of a membrane, which can be also described as a concentration gradient ∇c across the membrane layer. In the following discussion, the permeation behaviour of a microporous membrane will be explained in details.

1.4.2   General aspects

Our crystalline microporous membranes were always prepared on asymmetric alumina substrates, as descried in section 1.2.2. From comparing the permeation behaviour of the neat alumina supports and the supported zeolite/MOF membranes, it can be concluded that the support does not remarkably ($< 5\%$) impact the flux and selectivity. Therefore, the influence from the macroporous substrate can be usually neglected (Figure 10).

As shown in Figure 10, the process of gas or liquid molecule transport through a microporous membrane can be descried as follows: 1) adsorption of a molecule from the bulk phase to membrane surface; 2) diffusion from the surface to the inside of the

pore, through the pore and from the pore to external surface; 3) desorption from the surface to the permeate side.[2] Therefore, there are two major factors which affect the mass transport: adsorption and diffusion. The interplay of adsorption and diffusion determines the permeation behavior of a microporous membrane, and the selectivity of the membrane can be expressed by the adsorption selectivity S_{ads} multiplied by diffusion selectivity S_{diff}.[140-141] However, the effect of adsorption and diffusion is only considered, when more than one component in a mixture can go through the membrane layer.[141] If real molecular sieving occurs, namely only one component of a binary mixture can go through the pores, the interplay of adsorption and diffusion is not important any more.
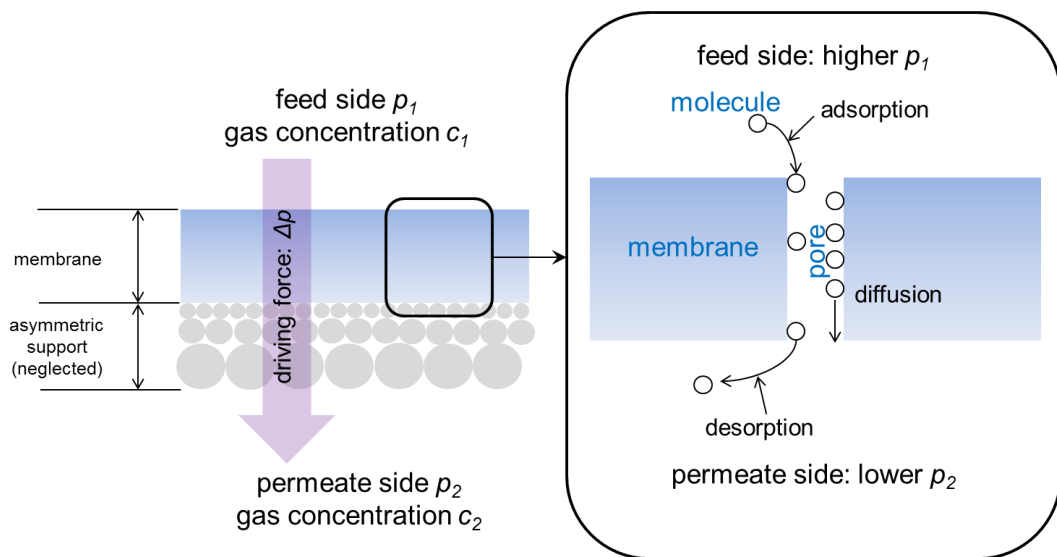
Figure 10: Scheme of mass transfer though a membrane. The gases on the feed and permeate side have pressures p_1 and p_2, concentrations c_1 and c_2, respectively. By a driving force of Δp, the molecule on the feed side was adsorbed on the membrane surface, diffused through the membrane, and desorbed from the membrane to the permeate side.

Adsorption takes place physically (physisorption) or chemically (chemisorption) at the interface of gas and membrane surface, while diffusion deals with the rate of the gas passage through the bulk membrane depending on the interaction between the diffusing gas molecules and pore channels (van der Waals force or chemical bond) under a driving force of a partial pressure difference.

1.4.3   Adsorption in microporous membranes

As shown in Eq. 11, adsorption is an equilibrium process between the gas or liquid adsorbate molecules and adsorbent (membrane) either by physical and chemical adsorption.

$$Adsorbate + Adsorbent \xrightleftharpoons[Desorption]{Adsorption} Adsorbate - Adsorbent \qquad\qquad \text{(Eq. 11)}$$
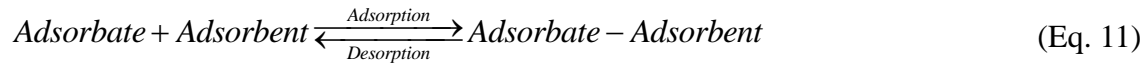
For a certain membrane and gas system, the adsorption amount is related to the experimental conditions like temperature and pressure. Then the adsorption phenomenon can be described through adsorption isotherms (temperature is constant) or adsorption isobar (pressure is constant). Here we only discuss the physisorption through isotherms, which express the amount of adsorbate on the adsorbent as a function of pressure (for gas) or concentration (for liquid). The physisorption isotherms can be classified into six types depending on the pore size of the adsorbent and the different interaction of adsorbate with the adsorbent.[142] Among these six types, type I isotherm can be usually applied for microporous materials, where the adsorption takes place in micropore volume rather than at internal surface area.[142]

The earliest known adsorption isotherm equation was developed by Freundlich[143] in 1906, which can be applied to multilayer adsorption as well as nonideal adsorption on heterogeneous surfaces, but this empirical model does not reduce to Henry's law at low concentrations.

In 1916, Langmuir[144] presented theoretical equilibrium isotherm, which describes an ideal monolayer adsorption on a homogeneous surface with distinct adsorption sites. The Langmuir adsorption model is the most commonly used model for physisorption and a single-site Langmuir adsorption can be expressed by Eq.12: [145]

$$\theta_i = \frac{K_i p_i}{1 + K_i p_i} \qquad \text{with} \qquad K_i = \frac{k_{ads}}{k_{des}} \qquad\qquad \text{(Eq. 12)}$$

where θ_i is the fraction of the surface sites covered with i, k_{adv} and k_{des} are the rate of adsorption and desorption, respectively, and p_i is the partial pressure of i over the surface. The equilibrium constant K_i depends on temperature following the van't Hoff equation. The Langmuir model is not limited by single-site adsorption for single

component. It can also be applied in the case that molecules show preferences for adsorption sites by a dual-site model (especially by larger molecules or molecules at high coverages), or for multicomponent adsorptions.[7, 146] For instance, when the Langmuir model is used for the adsorption in a binary mixture of species a and b, the adsorption fraction of species b should be described as follows:[147]

$$\theta_b = \frac{K_b p_b}{1 + K_a p_a + K_b p_b} \qquad \text{(Eq. 13)}$$

It can be seen, that the Langmuir model shows a linear relationship between θ_i and p_i at low adsorbate concentrations, which follows Henry's law, and a constant sorption capacity at high adsorbate concentrations.[148] Although there are several equilibrium isotherm equations which can describe the experimental adsorption data, here we only use the Langmuir model to explain the mass transport behavior and the gas adsorption on our membranes.

1.4.4 Diffusion in microporous membranes

Diffusion is a mass transfer process, wherein the density of a component increases in a region while it decreases at its starting point due to random thermal motion.[149] Here the region is only considered as a gas or a liquid. In order to describe the diffusion through the membrane and calculate the permeation flux, we usually use Fick's law and Maxwell-Stefan formulation.

Following the Fick's law, the diffusion of the components through the membrane was based on the effect of the concentration gradient on the diffusion rate.[149] The Fick's law can be applied not only for single-component but also for multicomponent diffusion in microporous membranes. Generally the Fick's first law is given by:[150]

$$J_i = -D_i \nabla c_i \qquad \text{with} \qquad \nabla c_i = \frac{\partial c_i}{\partial z} \qquad \text{(Eq. 14)}$$

where J_i, D_i, ∇c_i and c_i are the material flux, the Fickian diffusion coefficient, the concentration gradient and the concentration of component i, respectively, and z is the thickness of the membranes. As given by Eq. 14, the flux is proportional to concentration gradients when the gradient is small.[150]

The Maxwell-Stefan formulation is especially useful for the mass transport in multicomponent or multi-phase systems.[150] The driving force used in Maxwell-Stefan formulation is the chemical potential gradient $\nabla \mu$. By consideration both of the driving force of one component as well as the frictional force exerted by other components (related to the corresponding diffusive velocity), the Maxwell-Stefan approach is proposed. When the simplest case, a two-component system, was taken as an example, the Maxwell-Stefan diffusion coefficient $Đ$ has a following relationship with chemical potential gradient and frictional force:[150-151]

$$-\nabla \mu_i = RTx_j \left(\frac{v_i - v_j}{Đ_{ij}} \right) \quad \text{with} \quad \nabla \mu_i = \frac{\partial \mu_i}{\partial z} \tag{Eq. 15}$$

where R is the ideal gas constant, T is the temperature, x_j is the mole fraction of component j; v_i, v_j are the diffusive velocities of component 1 and 2, respectively. For a single-component Maxwell-Stefan diffusion by expressing the chemical potential gradient by concentration gradient and partial pressure, the diffusive flux of component i can be given as:[150-151]

$$J_i = v_i \cdot c_i = -Đ_{i,s} \frac{\partial \ln p_i}{\partial \ln c_i} \nabla c_i \tag{Eq. 16}$$

where $D_{i,s}$ is the single-component Maxwell-Stefan diffusivity of component i. In gas phase, the partial pressure p is usually replaced by partial fugacity f, which is equal to the partial pressure by ideal gas at low pressures. When we compare Eq. 14 with Eq. 16, the single-component Fickian diffusivity has the following relationship with the single-component Maxwell-Stefan diffusivity:[150-151]

$$D_i = Đ_{i,s}\Gamma \quad \text{with} \quad \Gamma = \left(\frac{\partial \ln p_i}{\partial \ln c_i} \right)_T \tag{Eq. 17}$$

where Γ is defined as the "thermodynamic correction factor". For an ideal gas or liquid phase, D_i is identical to $Đ_{i,s}$.

Krishna and van Baten[152] have investigated the different diffusion behaviors of various kinds of porous materials, and they have found two categories. The first one is for cage-structure porous materials with narrow window, like ZIF-8, DDR, ITQ-29 membranes. They primarily follow the rule, that $S_{ads} > 1$ and $S_{diff} > 1$. In this case, the

diffusivities are mainly influenced by molecular size and framework structure. Other materials are classified into the second case, where the binding energies determinate the diffusivities, like 1D channel materials (MOF-74, MIL53), intersecting channels materials (MIF) or materials with open structures with large cavities (NaY, CuBTC). In this category, the diffusion selectivity favors the poorly adsorbed molecules, and it is found that $S_{ads} > 1$ with $S_{diff} \ll 1$.[152]

1.5 Bibliography

[1]   R. D. Noble, S. A. Stern, Membrane science and technology series 2: Membrane separations technology principles and applications, *Elsevier 1st Edition* 1995.

[2]   N. W. Ockwig, T. M. Nenoff, Membranes for hydrogen separation, *Chem. Rev.* 2007, 107, 4078-4110.

[3]   H. P. Hsieh, Membrane science and technology series 3: Inorganic membranes for separation and reactions, *Elsevier 1st Edition* 1996.

[4]   J. R. Rostrup-Nielsen, T. Rostrup-Nielsen, Large-scale hydrogen production, *CATTECH* 2002, 6, 150-159.

[5]   A. J. Brown, N. A. Brunelli, K. Eum, F. Rashidi, J. R. Johnson, W. J. Koros, C. W. Jones, S. Nair, Interfacial microfluidic processing of metal-organic framework hollow fiber membranes, *Science*, 2014, 345, 72-75.

[6]   X. Feng and R.Y. M. Huang, Liquid separation by membrane pervaporation: a Review, *Ind. Eng. Chem. Res.* 1997, 36, 1048-1066.

[7]   T. C. Bowen, R. D. Noble, J. L. Falconer, Fundamentals and applications of pervaporation through zeolite membranes, *J. Membr. Sci.* 2004, 245, 1-33.

[8]   R. Soria; Overview on industrial membranes, *Catal. Today*, 1995, 25, 285-290.

[9]   F. Gallucci, E. Fernandez, P. Corengia and M. S. Annaland, Recent advances on membranes and membrane reactors for hydrogen production, *Chem. Eng. Sci.*, 2013, 92, 40-66.

[10]   S. Uemiya, T. Matsuda, E. Kikuchi, Hydrogen permeable palladium-silver alloy membrane supported on porous ceramics, *J. Membr. Sci.* 1991, 56, 315-325.

[11]   Z. Shao, W. Yang, Y. Cong, H. Dong, J. Tong, G. Xiong, Investigation of the permeation behavior and stability of a $Ba_{0.5}Sr_{0.5}Co_{0.8}Fe_{0.2}O_3$-delta oxygen membrane, *J. Membr. Sci.* 2000, 172, 177-188.

[12]   R. M. de Vos, H. Verweij, High-selectivity, high-flux silica membranes for gas separation, *Science* 1998, 279, 1710-1711.

[13]   M. B. Shiflett, H. C. Foley, Ultrasonic deposition of high-selectivity nanoporous carbon membranes, *Science* 1999, 285, 1902-1905.

[14]   S. T. Oyama, S. M. Stagg-Williams, Membrane science and technology series 14: Inoganic, polymeric and composite membranes, *Elsevier 1st Edition* 2011.

[15]   J. Caro, M. Noack, Zeolite membranes - recent developments and progress, *Micropor. Mesopor. Mater.* 2008, 115 , 215-233.

[16] D. W. Bruce, D. O'Hare, R. I. Walton, Inorganic Materials Series*: Porous Materials*, *Wiley 1st Edition* 2011.

[17] M. Noacka, M. Schneider, A. Dittmar, G. Georgi, J. Caro, The change of the unit cell dimension of different zeolite types by heating and its influence on supported membrane layers, *Micropor. Mesopor. Mater.* 2009, 117, 10-21.

[18] S. L. James, Metal-organic framewoks, *Chem. Soc. Rev.* 2003, 32, 276-288.

[19] J. Li, J. Sculley, H. Zhou, Metal-organic frameworks for separations, Chemical Reviews, 2012, 112, 869-932.

[20] R. Banerjee, H. Furukawa, D. Britt, C. Knobler, M. O'Keeffe, O. M. Yaghi, Control of pore size and functionality in isoreticular zeolitic imidazolate frameworks and their carbon dioxide selective capture properties, *J. Am. Chem. Soc.* 2009, 131, 3875-3877.

[21] S. Kulprathipanja, Zeolites in industrial separation and catalysis, *Wiley-VCH 1st Edition* 2010.

[22] A. K. Cheetham, G. Férey, T. Loiseau, Open-Framework Inorganic Materials, *Angew. Chem. Int.* Ed. 1999, 38, 3268-3292.

[23] A. Tavolaro, E. Drioli, Zeolite membranes, *Adv. Mater.* 1999, 11, 975-996.

[24] M. E. Davis, R. F. Lobo, Zeolite and molecular sieve synthesis, *Chem. Mater.* 1992, 4, 756-768.

[25] L. Shirazi, E. Jamshidi and M. R. Ghasemi, The effect of Si/Al ratio of ZSM-5 zeolite on its morphology, acidity and crystal size, *Cryst. Res. Technol.* 2008, 43, 1300-1306.

[26] H. Suzuki, *US Patent* 1987, *4,699,892*.

[27] J. G. Tsikoyiannis, W.O. Haag, Synthesis and characterization of a pure zeolitic membrane, *Zeolites* 1992, 12, 126-130.

[28] W. O. Haag; J.G. Tsikoyiannis; *US Patent* 1992, *5,019,263*.

[29] E. R. Geus, M. J. den Exter, H. Bekkum, Synthesis and characteriazation of zeolite (MFI) membranes on porous ceramic supports, *J. Chem. Soc. Faraday Trans.* 1992, 88, 3101-3110.

[30] J. Caro, M. Noack, P. Kölsch, R. Schäfer, Zeolite membranes - state of their development and perspective, *Micropor. Mesopor. Mater.* 2000, 38, 3-24.

[31] S. Khajavi, F. Kapteijn, J. C. Jansen, Synthesis of thin defect-free hydroxy sodalite membranes: New candidate for activated water permeation, *J. Membr. Sci.* 2007, 299, 63-72.

[32] N. Wang, Y. Liu, A. Huang, J. Caro, Supported SOD membrane with steam selectivity by a two-step repeated hydrothermal synthesis, *Micropor. Mesopor. Mater.* 2014, 192, 8-13.

[33] M.A. Carreon, S. Li, J. L. Falconer, R.D. Noble, Alumina-supported SAPO-34 membranes for CO_2/CH_4 separation, *J. Am. Chem. Soc.* 2008, 130, 5412-5413.

[34] S. Lin, J. Li, R. P. Sharma, J. Yu, R. Xu, Fabrication of SAPO-34 Crystals with Different Morphologies by Microwave Heating, *Top. Catal.* 2010, 53, 1304-1310.

[35] Z. Zheng, A. S. Hall, V. V. Guliants, Synthesis, characterization and modification of DDR membranes grown on alpha-alumina supports, *J. Mater. Sci.* 2008, 43, 2499-2502.

[36] T. Masuda, H. Hara, M. Kouno, K. Hashimoto, Preparation of A-type zeolite film on the surface of an alumina ceramic filter, *Micro. Mater.* 1995, 3, 565-571.

[37] A. Huang, F. Liang, F. Steinbach, T.M. Gesing, J. Caro, Neutral and cation-free LTA-type aluminophosphate (AlPO4) molecular sieve membrane with high hydrogen permselectivity, *J. Am. Chem. Soc.* 2010, 132, 2140-2141.

[38] A. Huang, J. Caro, Cationic polymer used to capture zeolite precursor particles for the facile synthesis of oriented zeolite LTA molecular sieve membrane, *Chem. Mater.* 2010, 22, 4353-4355.

[39] K. Aoki, K. Kusakabe, S. Morooka, Gas permeation properties of A-type zeolite membrane formed on porous substrate by hydrothermal synthesis, *J. Membr. Sci.* 1998, 141, 197-205.

[40] R. Rakoczy, Doctor thesis: Hydrothermalsynthese ausgewählter Zeolithe und ihre Charakterisierung durch Adsorption, Stuttgart 2003.

[41] K. Keizer, A. J. Burggraaf, Z. A. E. P. Vroon, H. Verweij, Two component permeation through thin zeolite MFI membranes, *J. Membr. Sci.* 1998, 147, 159-172.

[42] R. Lai, Y. Yan, G. R. Gavalas, Growth of ZSM-5 films on alumina and other surfaces, *Micropor. Mesopor. Mater.* 2000, 37, 9-19.

[43] G. Li, E. Kikuchi, M. Matsukata, Separation of water-acetic acid mixtures by pervaporation using a thin mordenite membrane, *Sep. Purif. Technol.* 2003, 32, 199-206.

[44] K. J. Balkus, L. J. Ball, B.E. Gnade, J. M. Anthony, A capacitance type chemical sensor based on AlPO4-5 molecular sieves, *Chem. Mater.* 1997, 9, 380-386.

[45] H. Kita, T. Inoue, H. Asamura, K. Tanaka, K. I. Okamoto, NaY zeolite membrane for the pervaporation separation of methanol-methyl tert-butyl ether mixtures, *Chem. Commun.* 1997, 1, 45-46.

[46] K. Kusakabe, T. Kuroda, A. Murata, S. Morooka, Formation of a Y-type zeolite membrane on a porous alpha-alumina tube for gas separation, *Ind. Eng. Chem. Res.* 1997, 36, 649-655.

[47] A. Huang, N. Wang, J. Caro, Seeding-free synthesis of dense zeolite FAU membranes on 3-aminopropyltriethoxysilane-functionalized alumina supports, *J. Membr. Sci.* 2012, 389, 272-279.

[48] Y. S. Lin, I. Kumakiri, B. N. Nair, H. Alsyouri, Microporous inorganic membranes, *Sep. Purif. Methods* 2002, 31, 229-379.

[49] D. W. Breck, Zeolite molecular sieves, *Wiley, New York* 1974.

[50] Y. Li, W. Yang, Microwave synthesis of zeolite membranes: A review, *J. Membr. Sci.* 2008, 316, 3-17.

[51] A. Huang, J. Caro, Steam-stable hydrophobic ITQ-29 molecular sieve membrane with H_2 selectivity prepared by secondary growth using Kryptofix 222 as SDA, *Chem. Commun.* 2010, 46, 7748-7750.

[52] J. J. Jafar, P. M. Budd, Separation of alcohol/water mixtures by pervaporation through zeolite A membranes, *Micropor. Mater.* 1997, 12, 305-311.

[53] M. Kondo, M. Komori, H. Kita, K. I. Okamota, Tubular-type pervaporation module with zeolite NaA membrane, *J. Membr. Sci.* 1997, 133, 133-141.

[54] D. Shah, K. Kissick, A. Ghorpade, R. Hannah, D. Bhattacharyya, Pervaporation of alcohol-water and dimethylformamide-water mixtures using hydrophilic zeolite NaA membranes: mechanisms and experimental results, *J. Membr. Sci.* 2000, 179, 185-205.

[55] K. Sato, K. Aoki, K. Sugimoto, K. Izumi, S. Inoue, J. Saito, S. Ikeda, T. Nakane, Dehydrating performance of commercial LTA zeolite membranes and application to fuel grade bio-ethanol production by hybrid distillation/vapor permeation process, *Micropor. Mesopor. Mater.* 2008, 115, 184-188.

[56] Y. Li, H. Chen, J. Liu, H. Li, W. Yang, Pervaporation and vapor permeation dehydration of Fischer-Tropsch mixed-alcohols by LTA zeolite membranes, *Separ. Purif. Technol.* 2007, 57, 140-146.

[57] A. van Niekerk, J. Zah, J. C. Breytenbach, H. M. Krieg, Direct crystallisation of a hydroxy sodalite membrane without seeding using a conventional oven, *J. Membr. Sci.* 2007, 300, 156-164.

[58]   W. Thomson, *Trans. R. Soc. Edinb.* 1881, 1, 390.

[59]   L. Pauling, The structure of sodalite and helvite, *Z. Kristallogr.* 1930, 74, 213-225.

[60]   S. Khajavi, F. Kapteijn, J. C. Jansen, Synthesis of thin defect-free hydroxy sodalite membranes: New candidate for activated water permeation, *J. Membr. Sci.* 2007, 299, 63-72.

[61]   S. Khajavi, J. C. Jansen, F. Kapteijn, Application of hydroxy sodalite films as novel water selective membranes, *J. Membr. Sci.* 2009, 326, 153-160.

[62]   S. Khajavi, J. C. Jansen, F. Kapteijn, Application of a sodalite membrane reactor in esterification-Coupling reaction and separation, *Catal. Today* 2010, 156, 132-139.

[63]   S. Khajavi, J. C. Jansen, F. Kapteijn, Production of ultra pure water by desalination of seawater using a hydroxy sodalite membrane, *J. Membr. Sci.* 2010, 326, 52-57.

[64]   S. Wee, C. Tye, S. Bhatia, Membrane separation process - Pervaporation through zeolite membrane, *Separ. Purif. Technol.* 2008, 63, 500-516.

[65]   H. Jiang, B. Zhang, Y. S. Lin, Y. Li, Synthesis of zeolite membranes, *Chin. Sci. Bull.* 2004, 49, 2547-2554.

[66]   J. L.C. Rowsell, O. M. Yaghi, Metal-organic frameworks: a new class of porous materials, *Micropor. Mesopor. Mater.* 2004, 73, 3-14.

[67]   J. R. Long, O. M. Yaghi, The pervasive chemistry of metal-organic frameworks, *Chem. Soc. Rev.* 2009, 38, 1213-1214.

[68]   S. Kitagawa, R. Kitaura, S. Noro, Functional porous coordination polymers, *Angew. Chem. Int. Ed.* 2004, 43, 2334-2375.

[69]   S. Ma, H. Zhou, A metal-organic framework with entatic metal centers exhibiting high gas adsorption affinity, *J. Am. Chem. Soc.* 2006, 128, 11734-11735.

[70]   G. Ferey, C. Mellot-Draznieks, C. Serre, F. Millange, J. Dutour, S. Surble, I. Margiolaki, A chromium terephthalate-based solid with unusually large pore volumes and surface area, *Science* 2005, 309, 2040-2042.

[71]   S. S. Y. Chui, S. M. F. Lo, J. P. H. Charmant, A. G. Orpen, I. D. Williams, A chemically functionalizable nanoporous material $[Cu_3(TMA)_2(H_2O)_3]_n$, *Science* 1999, 283, 1148-1150.

[72]   B. F. Hoskins, R. Robson, Infinite polymeric frameworks consisting of 3

dimensionally linked rod-like segments, *J. Am. Chem. Soc.* 1989, 111, 5962-5964.

[73] B. F. Hoskins, R. Robson, Design and construction of a new class of scaffolding-like materials comprising infinite polymeric frameworks of 3D-linked molecular rods. A reappraisal of the $Zn(CN)_2$ and $Cd(CN)_2$ structures and the synthesis and structure of the diamond-related frameworks $[N(CH_3)_4][Cu^IZn^{II}(CN)_4]$ and $Cu^I[$ 4,4''4'',4'''-tetracyanotetraphenylmethane] BF4 $xC_6H_5NO_2$, *J. Am. Chem. Soc.* 1990, 112, 1546-1554.

[74] O. M. Yaghi, G. Li, H. Li, Selective binding and removal of guests in a microporous metal-organic framework, *Nature* 1995, 378, 703-706.

[75] O. M. Yaghi, H. Li, Hydrothermal synthesis of a metal-organic framework containing large rectangular channels, *J. Am. Chem. Soc.* 1995, 117, 10401-10402.

[76] M. Kondo, T. Yoshitomi, K. Seki, H. Matsuzaka, S. Kitagawa, Three-dimensional framework with channeling cavities for small molecules: $\{[M_2(4,4'-bpy)_3(NO_3)_4] xH_2O\}_n$ (M = Co, Ni, Zn)**, *Angew. Chem. Int. Ed.* 1997, 36, 1725-1727.

[77] H. Li, M. Eddaoudi, M. O'Keeffe, O. M. Yaghi, Design and synthesis of an exceptionally stable and highly porous metal-organic framework, *Nature* 1999, 402, 276-279.

[78] K. Barthelet, J. Marrot, D. Riou, G. Ferey, A breathing hybrid organic-inorganic solid with very large pores and high magnetic characteristics, *Angew. Chem. Int. Ed.* 2002, 41, 281-284.

[79] C. Serre, F. Millange, C. Thouvenot, M. Nogues, G. Marsolier, D. Louër, G. Ferey, Very large breathing effect in the first nanoporous chromium(III)-based solids: MIL-53 or $Cr^{III}(OH) \{O_2C-C_6H_4-CO_2\} \{HO_2C-C_6H_4-CO_2H\}_x H_2O_y$, *J. Am. Chem. Soc.* 2002, 124, 13519-13526.

[80] Y. Q. Tian, C. X. Cai, Y. Ji, X. Z. You, S. M. Peng, G. H. Lee, $[Co_5(im)_{10} 2MB]_\infty$: A metal-organic open-framework with zeolite-like topology, *Angew. Chem. Int. Ed.* 2002, 41, 1384-1386.

[81] J. Li, R. J. Kuppler, H. Zhou, Selective gas adsorption and separation in metal-organic frameworks, *Chem. Soc. Rev.* 2009, 38, 1477-1504.

[82] H. Li, M. Eddaoudi, M. O'Keeffe, O. M. Yaghi, Design and synthesis of an exceptionally stable and highly porous metal-organic framework, *Nature* 1999, 402, 276-279.

[83] N. L. Rosi, J. Eckert, M. Eddaoudi, D., T. Vodak, J. Kim, M. O'Keeffe, O. M.

Yaghi, Hydrogen storage in microporous metal-organic frameworks, *Science* 2003, 300, 1127-1129.

[84] M. O'Keeffe, M. Eddaoudi, H. Li, T. Reineke, O. M. Yaghi, Frameworks for extended solids: geometrical design principles, *J. Solid State Chem.* 2000, 152, 3-20.

[85] N. W. Ockwig, O. Delgado-Friedrichs, M. O'Keeffe, O. M.Yaghi, Reticular chemistry: occurrence and taxonomy of nets and grammar for the design of frameworks, *Acc. Chem. Res.* 2005, 38,176-182.

[86] G. Férey, Building units design and scale chemistry, J. Solid State Chem. 2000, 152, 37-48.

[87] U. Mueller, M. Schubert, F. Teich, H. Puetter, K. Schierle-Arndt, J. Pastré, Metal-organic frameworks-prospective industrial applications, *J. Mater. Chem.* 2006, 16, 626-636.

[88] H. K. Chae, D. Y. Siberio-Peŕez, J. Kim, Y. B. Go, M. Eddaoudi, A. J. Matzger, M. O'Keeffe, O. M. Yaghi, A route to high surface area, porosity and inclusion of large molecules in crystals, Nature 2004, 427, 523-527.

[89] J. Li, J. Sculley, H. Zhou, Metal-organic frameworks for separations, *Chem. Rev.* 2012, 112, 869-932.

[90] N. L. Rosi, J. Kim, M. Eddaoudi, B. L. Chen, M. O'Keeffe, O. M. Yaghi, Rod packings and metal-organic frameworks constructed from rod-shaped secondary building units, *J. Am. Chem.Soc.* 2005,127, 1504-1518.

[91] P. D. C. Dietzel, Y. Morita, R. Blom, H. Fjellvag, An in situ high-temperature single-crystal investigation of a dehydrated metal-organic framework compound and field-induced magnetization of one-dimensional metaloxygen chains, *Angew. Chem. Int. Ed.* 2005, 44, 6354-6358.

[92] P. D. C. Dietzel, B. Panella, M. Hirscher, R. Blom, H. Fjellvag, Hydrogen adsorption in a nickel based coordination polymer with open metal sites in the cylindrical cavities of the desolvated framework, *Chem. Comm.* 2006, 9, 959-961.

[93] P. D. C. Dietzel, R. E. Johnsen, R. Blom, H. Fjellvag, Structural changes and coordinatively unsaturated metal atoms on dehydration of honeycomb analogous microporous metal-organic frameworks, *Chem. Eur. J.* 2008, 14, 2389-2397.

[94] D. Britt, H. Furukawa, B. Wang, T. G. Glover, O. M. Yaghi, Highly efficient separation of carbon dioxide by a metal-organic framework replete with open metal sites, *Proc. Natl. Acad. Sci.* 2009, 106, 20637-20640.

[95] R. Ranjan, M. Tsapatsis, Microporous metal organic framework membrane on porous support using the seeded growth method, *Chem. Mater.* 2009, 21, 4920-4924.

[96] P. D. C. Dietzel, V. Besikiotis, R. Blom, Application of metal-organic frameworks with coordinatively unsaturated metal sites in storage and separation of methane and carbon dioxide, *J. Mater. Chem.* 2009, 19, 7362-7370.

[97] S. R. Caskey, A. G. Wong-Foy, A. J. Matzger, Dramatic tuning of carbon dioxide uptake via metal substitution in a coordination polymer with cylindrical pores, *J. Am. Chem. Soc.* 2008, 130, 10870-10871

[98] A. Bétard, D. Zander, R. A. Fischer, Dense and homogeneous coatings of CPO-27-M type metal-organic frameworks on alumina substrates, *CrystEngComm* 2010, 12, 3768-3772.

[99] A. Ö. Yazaydin, R. Q. Snurr, T. Park, K. Koh, J. Liu, M. D. LeVan, A. I. Benin, P. Jakubczak, M. Lanuza, D. B. Galloway, J. J. Low, R. R.Willis, Screening of metal-organic frameworks for carbon dioxide capture from flue gas using a combined experimental and modeling approach, *J. Am. Chem. Soc.* 2009, 131, 18198-18199.

[100] A. Phan, C. J. Doonan, F. J. Uribe-Romo, C. B. Knobler, M. O'Keeffe, O. M. Yaghi, Synthesis, structure, and carbon dioxide capture properties of zeolitic imidazolate frameworks, *Acc. Chem. Res.* 2010, 43, 58-67.

[101] W. Morris, C. J. Doonan, H. Furukawa, R. Banerjee, O. M. Yaghi, Crystals as molecules: Postsynthesis covalent functionalization of zeolitic imidazolate frameworks, *J. Am. Chem. Soc.* 2008, 130, 12626-12627.

[102] S. R. Venna, M. A. Carreon, Highly permeable zeolite imidazolate framework-8 membranes for CO_2/CH_4 separation, *J. Am. Chem. Soc.* 2010, 132, 76-78.

[103] T. Haneda, M. Kawano, T. Kawamichi, M. Fujita, Direct observation of the labile imine formation through single-crystal-to-single-crystal reactions in the pores of a porous coordination network, *J. Am. Chem. Soc.* 2008, 130, 1578-1579.

[104] B. Wang, A. P. Côté, H. Furukawa, M. O'Keeffe, O. M. Yaghi, Colossal cages in zeolitic imidazolate frameworks as selective carbon dioxide reservoirs, *Nature* 2008, 453, 207-212.

[105] S. Sircar, T. C. Golden, M. B. Rao, Activated carbon for gas separation and storage, Carbon 1996, 34, 1-12.

[106] Y. Yoo, Z. Lai, H. K. Jeong, Fabrication of MOF-5 membranes using

microwave-induced rapid seeding and solvothermal secondary growth, *Micropor. Mesopor. Mater.* 2009, 123, 100-106.

[107] Y. Liu, Z. Ng, E. A. Khan, H. K. Jeong, C. Ching, Z. Lai, Synthesis of continuous MOF-5 membranes on porous alpha-alumina substrates, *Micropor. Mesopor. Mater.* 2009, 118, 296-301.

[108] J. Gascon, S. Aguado, F. Kapteijn, Manufacture of dense coatings of Cu-3(BTC)(2) (HKUST-1) on alpha-alumina, *Micropor. Mesopor. Mater.* 2008, 113, 1-3.

[109] H. Guo, G. Zhu, I. J. Hewitt, S. Qiu, "Twin copper source" growth of metal-organic framework membrane: $Cu_3(BTC)_2$ with high permeability and selectivity for recycling H_2, *J. Am. Chem. Soc.* 2009, 131, 1646-1647.

[110] Y. Li, F. Liang, H. Bux, A. Feldhoff, W. Yang, J. Caro, Molecular sieve membrane: supported metal-organic framework with high hydrogen selectivity, *Angew. Chem. Int. Ed.* 2010, 49, 548-551.

[111] H. Bux, F. Liang, Y. Li, J. Cravillon, M. Wiebcke, J. Caro, Zeolitic imidazolate framework membrane with molecular sieving properties by microwave-assisted solvothermal synthesis, *J. Am. Chem. Soc.* 2009, 131, 16000-16001.

[112] A. Huang, H. Bux, F. Steinbach, J. Caro, Molecular-sieve membrane with hydrogen permselectivity: ZIF-22 in LTA topology prepared with 3-aminopropyltriethoxysilane as Covalent Linker, *Angew. Chem. Int. Ed.* 2010, 49, 4958-4961.

[113] Y. Liu, E. Hu, E. A. Khan, Z. Lai, Synthesis and characterization of ZIF-69 membranes and separation for CO_2/CO mixture, *J. Membr. Sci.* 353, 36-40.

[114] A. Huang, W. Dou, J. Caro, Steam-Stable zeolitic imidazolate framework ZIF-90 membrane with hydrogen selectivity through covalent functionalization, *J. Am. Chem. Soc.* 2010, 132, 15562-15564.

[115] F. Zhang, X. Zou, X. Gao, S. Fan, F. Sun, H. Ren, G. Zhu, Hydrogen selective NH_2-MIL-53(Al) MOF membranes with high permeability, *Adv. Funct. Mater.* 2012, 22, 3583-3590.

[116] J. Gascon, F. Kapteijn, Metal-organic framework membranes-high potential, bright future?, *Angew. Chem. Int. Ed.* 2010, 49, 1530-1532.

[117] E. Biemmi, C. Scherb, T. Bein, Oriented growth of the metal organic framework $Cu_3(BTC)_2(H_2O)_3$ xH_2O tunable with functionalized self-assembled monolayers, *J. Am. Chem. Soc.* 2007, 129, 8054-8055.

[118] S. Hermes, F. Schroder, R. Chelmowski, C. Woll, R. A. Fischer, Selective

nucleation and growth of metal-organic open framework thin films on patterned COOH/CF$_3$-terminated self-assembled monolayers on Au(111), *J. Am. Chem. Soc.* 2005, 127, 13744-13745.

[119] A. Huang, N. Wang, C. Kong, J. Caro, Organosilica-functionalized zeolitic imidazolate framework ZIF-90 membrane with high gas-separation performance, *Angew. Chem. Int. Ed.* 2012, 51, 10551-10555.

[120] H. Lee, S. M. Dellatore, W. M. Miller, P. B. Messersmith, Mussel-inspired surface chemistry for multifunctional coatings, *Science* 2007, 318, 426-430.

[121] H. Lee, J. Rho, P. B. Messersmith, Facile conjugation of biomolecules onto surfaces via mussel adhesive protein inspired coatings, *Adv. Mater.* 2009, 21, 431-434.

[122] J. Ryu, S. H. Ku, H. Lee, C. B. Park, Mussel-inspired polydopamine coating as a universal route to hydroxyapatite crystallization, *Adv. Funct. Mater.* 2010, 20, 2132-2139.

[123] D. Ling, W. Park, Y. I. Park, N. Lee, F. Li, C. Song, S. Yang, S. H. Choi, K. Na, T. Hyeon, Multiple-interaction ligands inspired by mussel adhesive protein: synthesis of highly stable and biocompatible nanoparticles, *Angew. Chem. Int. Ed.* 2011, 50, 11360-11365.

[124] Q. Liu, N. Wang, J. Caro, A. Huang, Bio-inspired polydopamine: a versatile and powerful platform for covalent synthesis of molecular sieve membranes, *J. Am. Chem. Soc.* 2013, 135, 17679.

[125] A. Huang, Q. Liu, N. Wang, J. Caro, Highly hydrogen permselective ZIF-8 membranes supported on polydopamine functionalized macroporous stainless-steel-nets, *J. Mater. Chem. A* 2014, 2, 8246-8251.

[126] C. Yuan, Q. Liu, H. Chen, A. Huang, Mussel-inspired polydopamine modification of supports for the facile synthesis of zeolite LTA molecular sieve membranes, *RSC Adv.* 2014, 4, 41982-41988.

[127] Y. Yoo, V. Varela-Guerrero, H.-K. Jeong, Isoreticular metal-organic frameworks and their membranes with enhanced crack resistance and moisture stability by surfactant-assisted drying, *Langmuir* 2011, 27, 2652-2657.

[128] A. Huang, J. Caro, Covalent post-functionalization of zeolitic imidazolate framework ZIF-90 membrane for enhanced hydrogen selectivity, *Angew. Chem. Int. Ed.* 2011, 50, 4979-4982.

[129] Z. Wang, M. Cohen, Postsynthetic modification of metal-organic frameworks, *Chem. Soc. Rev.* 2009, 38, 1315-1329.

[130] D. Maspoch, D. Ruiz-Molina, K. Wurst, N. Domingo, M. Cavallini, F. Biscarini, J. Tejada, C. Rovira, J. Veciana, *Nat. Mater.* 2003, 2, 190-195.

[131] R. Custelcean, M. G. Gorbunova, A metal-organic framework functionalized with free carboxylic acid sites and its selective binding of a $Cl(H_2O)_4^-$ cluster, *J. Am. Chem. Soc.* 2005, 127, 16362-16363.

[132] N. Wang, A. Mundstock, Y. Liu, A. Huang, J. Caro, Amine-modified Mg-MOF-74/CPO-27-Mg membrane with enhanced H_2/CO_2 separation, *Chem. Eng. Sci.* 2015, 124, 27-36.

[133] R. Kitaura, G. Onoyama, H. Sakamoto, R. Matsuda, S. Noro, S. Kitagawa, Immobilization of a metallo Schiff base into a microporous coordination polymer, *Angew. Chem. Int. Ed.* 2004, 43, 2684-2687.

[134] M. Kawano,. T. Kawamichi,.T. Haneda, T. Kojima, M. Fujita, The modular synthesis of functional porous coordination networks, *J. Am. Chem. Soc.* 2007, 129, 15418-15419

[135] Z. Wang, S. M. Cohen, Tandem modification of metal-organic frameworks by a postsynthetic approach, *Angew. Chem. Int. Ed.* 2008, 47, 4699-4702.

[136] S. M. Cohen, Postsynthetic methods for the functionalization of metal-organic frameworks, *Chem. Rev.* 2012, 112, 970-1000.

[137] T. Haneda, M. Kawano, T. Kawamichi, M. Fujita, Direct observation of the labile imine formation through single-crystal-to-single-crystal reactions in the pores of a porous coordination network, *J. Am. Chem. Soc.* 2008, 130, 1578-1579.

[138] A. D. Burrows, C. G. Frost, M. F. Mahon, C. Richardson, Post-synthetic modification of tagged metal-organic frameworks, *Angew. Chem. Int. Ed.* 2008, 47, 8482-8486.

[139] S. Choi, T. Watanabe, T. Bae, D. S. Sholl, C. W. Jones, Modification of the Mg/DOBDC MOF with amines to enhance CO_2 adsorption from ultradilute gases, *J. Phys. Chem. Lett.* 2012, 3, 1136-1141.

[140] J. Caro, M. Noack, P. Kölsch, R. Schäfer, Zeolite membranes - state of their development and perspective, *Micropor. Mesop. Mater.* 2000, 38, 3-24.

[141] J. Caro, M. Noack, P. Kölsch, Zeolite membranes: from the laboratory scale to technical applications, *Adsorption* 2005, 11, 215-227.

[142] K. S. W. Sing, D. H. Everett, R. A. W. Haul, L. Moscou, R. A. Pierotti, J. Rouquérol, T. Siemieniewska, Reporting physisorption data for gas/solid systems with special reference to the determination of surface area and porosity,

Pure Appl. Chem. 1985, 57, 603-619.

[143] H. M. F. Freundlich, Over the adsorption in solution, *J. Phys. Chem.* 1906, 57, 385-470.

[144] I. Langmuir, The adsorption of gases on plane surface of glass, mica and platinum, *J. Am. Chem. Soc.* 1916, 40, 1361-1368.

[145] P. W. Atkins, Physikalische Chemie, *Wiley-VCH, Weinheim* 2001.

[146] R. Krishna, Diffusion of binary mixtures across zeolite membranes, entropy effects on permeation selectivity, *Int. Comm. Heat Mass Transfer* 2001, 28, 227-346.

[147] R. Krishna, L. J. P. van den Broeke, The Maxwell-Stefan description of mass transport across zeolite membranes, *Chem. Eng. J.* 1995, 57, 155-162.

[148] Y. S. Ho, J. F. Porter, G. Mckay, Equilibrium isotherm studies for the sorption of divalent metal ions onto peat: copper, nickel and lead single component systems, *Water, Air, Soil Pollut.* 2001, 141, 1-33.

[149] A. Cooksy, Physical chemistry: thermodynamic, statistical mechanics & kinetics, *International ed. Boston, Pearson* 2014.

[150] J. Kärger, S. Vasenkov, S. M. Auerbach, Diffusion in zeolites, in handbook of zeolite science and technology, *Marcel-Dekker Inc., New York* 2003.

[151] J. Kärger, D. M. Ruthven, D. N. Theodorou, Diffusion in nanoporous materials, *Wiley-VCH* 2012.

[152] R. Krishna, J. M. van Baten, Investigating the relative influences of molecular dimensions and binding energies on diffusivities of guest species inside nanoporous crystalline materials, *J. Phys. Chem. C* 2012, 116, 23556-23568.

2 Zeolite membranes for water pervaporation and separation

2.1 Summary

As described in Section 1.2.2, zeolite membranes have attracted great attention due to their potential applications in the gas/liquid mixture separations. Zeolite LTA membranes with strong hydrophilicity and suitable pore size of about 4.0 Å shows the feasibility to separate water from large molecules, and LTA membranes were already first commercialized to separate water from alcohol by steam permeation. Compared to zeolite LTA, zeolite SOD has a higher framework density, thus showing higher chemical and thermal stability. With a relatively small pore size of 2.8 Å, zeolite SOD membranes can be applied for separation of water from other molecules. In this chapter, dense zeolite SOD and LTA membranes were developed for water vapor (steam) separation at high temperatures and for water pervaporation at room temperature.

The publication in Section 2.2 describes a two-step repeated synthesis method for supported zeolite SOD membrane and reports its gas separation behavior for water vapor against other gas molecules and methanol in the temperature window between 125 and 200 °C. By repeated synthesis, dense SOD membranes with water selectivity could be obtained on the alumina support. The synthesized SOD membranes show not only good selectivity, but also high reproducibility. The gas separation factors were found to decrease slightly as the temperature increases, since less water could be adsorbed in the SOD framework at higher temperatures.

In the publication in Section 2.3, zeolite SOD and LTA membranes were proposed to support the production of DME and DMC, and they were used to separate water in different temperature range. SOD membranes can separate water from molecules like DME and DMC from 125 to 200 °C. Due to its small pore size, SOD membranes displayed good selectivities for H_2O/DME and H_2O/DMC. On the other side, LTA membranes were used for water pervaporation at room temperature. Since the kinetic diameter of MeOH (about 3.8 Å) is smaller than the pore size of LTA, selectivity of water against methanol through LTA membrane is not good. In Section 2.3, LTA membranes were ion-exchanged with K^+ ions. After the ion-exchange, the H_2O/MeOH

selectivity was improved since the pore size of LTA could be narrowed to about 3 Å by replacing the smaller Na^+ by larger K^+.

2.2 Supported SOD membrane with steam selectivity by a two-step repeated hydrothermal synthesis
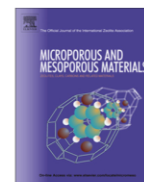
Nanyi Wang, Yi Liu, Aisheng Huang and Jürgen Caro

Supported SOD membrane with steam selectivity by a two-step repeated hydrothermal synthesis

N. Wang [a,*], Y. Liu [a], A. Huang [b], J. Caro [a]

[a] Institute of Physical Chemistry and Electrochemistry, Leibniz University Hannover, Callinstr. 3 – 3A, D-30167 Hannover, Germany
[b] Institute of New Energy Technology, Ningbo Institute of Material Technology and Engineering, CAS, 519 Zhuangshi Road, 315201 Ningbo, PR China

ARTICLE INFO

ABSTRACT

By a two-step repeated hydrothermal synthesis, supported SOD membranes have been prepared. Compared with LTA membranes, SOD membranes are more stable and can be used in the removal of steam in catalytic membrane reactors in the presence of other species like H_2, CH_4 and CO_2 in the feed or retentate. Under practice-relevant conditions, the mixture separation factors for equimolar mixtures of steam with possible reactants and products have been evaluated between 125 and 200 °C. The mixed gas separations factors for H_2O/H_2, H_2O/CH_4, and H_2O/CO_2 were found to decrease slightly with increasing temperatures from 125 to 200 °C and decrease from 8.1 to 4.6, from 17.9 to 14.5, and from 33.4 to 22.6, respectively. For the water separation from methanol a mixture separation factor of 200 was found.

© 2014 Published by Elsevier Inc.

1. Introduction

The hydrophilic LTA membrane is the first commercialized zeolite membranes and it is used increasingly for the de-watering of (bio) ethanol and i-propanol by membrane-based steam permeation. Impressive capacities have been installed in the last few years [1]. However, the handling of LTA zeolite membrane requires careful membrane treatment in the permeation operation to avoid structural damage. Compared with LTA, the zeolite structure SOD shows a higher framework density and has, therefore, with the same Si/Al ratio of 1, a higher structural stability. The supported SOD layers show even a higher thermal stability than non-supported SOD material [2]. Consequently, for water separation under harsh conditions such as from (catalytic) membrane reactors, powerful SOD type membranes have been successfully developed [3–5]. However, since the SOD structure itself is stabilized through hydrogen bonding between adsorbed water and the framework oxygen atoms, complete dehydration of SOD weakens these hydrogen bonds and may cause a partial damage of the SOD structure [6]. By intercalation of sulphur into the framework, the hydrothermal (or steam, depending on the reference) stability of SOD could be improved [7].

On the other hand, in the presence of steam, SOD membranes show remarkable stability under acidic and basic conditions [8], and SOD membranes have been successfully evaluated in membrane reactors for esterification [9] and seawater desalination [10]. SOD membranes can also be used in gas separation. As an

example, by microwave-assisted hydrothermal synthesis, Xu et al. could prepare hydrogen-selective SOD zeolite membranes with a H_2/n-butane selectivity >1000 [11]. Also mixed matrix membranes based on SOD with polyimide [12] or clay [13] are reported.

Because of its Si/Al = 1, SOD is hydrophilic with a pore diameter of around 2.7 Å [14], which allows the passage of small molecules like e.g. H_2O (2.6 Å). Therefore, a SOD membrane is an excellent candidate to remove steam formed in chemical reactions at elevated temperatures such as in the synthesis of dimethylether (DME) and dimethylcarbonate (DMC) starting with carbon dioxide, hydrogen or methanol (MeOH) as reactants according to $2\ CO_2 + 6H_2 \rightarrow DME + 3H_2O$ and $CO_2 + 2MeOH \leftrightharpoons DMC + H_2O$, respectively. Also the removal of water in MeOH synthesis starting from carbon dioxide according to $CO_2 + 3H_2 \rightarrow MeOH + H_2O$ seems possible. Another challenging goal for the development of SOD membranes is the water extraction in the Fischer Tropsch synthesis [15]. The difficulty in the steam/water separations is the simultaneous presence of other small molecules like hydrogen (2.9 Å), carbon dioxide (3.3 Å) and methane (3.8 Å) in the gaseous reaction mixture, which are expected to remain in the feed. With other words, high H_2O/H_2, H_2O/CH_4, and H_2O/CO_2 selectivities are needed. Further, a high $H_2O/MeOH$ selectivity would allow the in situ removal of water in the membrane supported methanol synthesis starting with carbon dioxide as feed.

It is worth to note that the papers published so far on water permeation on SOD membranes report only pervaporation studies of liquid mixtures under 100 °C or - when using pressurized feeds - up to 165 °C [8,10,3]. It is the aim of this paper to study the separation behaviour of SOD membranes for the steam/gas mixtures

---

2 Zeolite membranes for water pervaporation and separation

H_2O/H_2, H_2O/CH_4 and H_2O/CO_2 under practice-relevant conditions at higher temperatures between 125 and 200 °C.

2. Experimental

2.1. Materials

Chemicals were used as received: LUDOX AS-40 colloidal silica (40% SiO_2 in water, Aldrich) as Si source; aluminum foil (Fisher Scientific); sodium hydroxide (>99%, Merck); doubly distilled water. Porous α-Al_2O_3 disks (Fraunhofer Institute IKTS, former HITK/Inocermic, Hermsdorf, Germany: 18 mm in diameter, 1.0 mm in thickness, 70 nm particles in the top layer) were used as supports.

2.2. Preparation of zeolite SOD membranes by repeated synthesis

A clear precursor solution with the molar ratio $50Na_2O$: $1Al_2O_3$:$5SiO_2$:$1005H_2O$, was prepared according to the procedure reported elsewhere [3]. Typically, 11.11 g sodium hydroxides were dissolved in 25 g deionized water at room temperature, then 0.15 g aluminum foil was added to obtain the aluminate solution. The silicate solution was prepared by mixing 2.08 g LUDOX AS-40 colloidal silica and 23.75 g deionized water at 60 °C under vigorous stirring. The prepared aluminum solution was added into the silicate solution and stirred overnight at room temperature to produce a clear solution. α-Al_2O_3 support was then horizontally placed face down in a Teflon-lined stainless steel autoclave which was filled with synthesis solution. After hydrothermal synthesis over 24 h at 120 °C, the solution was decanted off and the membrane was washed with deionized water and dried in air at 110 °C overnight. To prepare a more compact SOD membrane, the dried membrane was subject to repeated hydrothermal synthesis under identical conditions. Finally, the dried membrane was further characterized and evaluated in gas permeation measurement. Following this recipe, 8 SOD membranes have prepared and all preparations were successful and showed similar separation behaviors (Table 2).

2.3. Characterization of zeolite SOD membranes

The morphology and thickness of the zeolite SOD membranes were characterized by scanning electron microscopy (SEM), which was carried out on a JEOL JSM-6700F with a cold field emission gun operating at 2 kV and 10 μA. The chemical composition of the SOD-layer was characterized by energy-dispersive X-ray spectroscopy (EDXS) using the same SEM microscope at 20 kV and 20 μA. The phase purity and crystallinity of the zeolite SOD membrane layers were confirmed by X-ray diffraction (XRD). XRD patterns were recorded at room temperature under ambient conditions with Bruker D8 ADVANCE X-ray diffractometer using Cu Kα radiation at 40 kV and 40 mA.
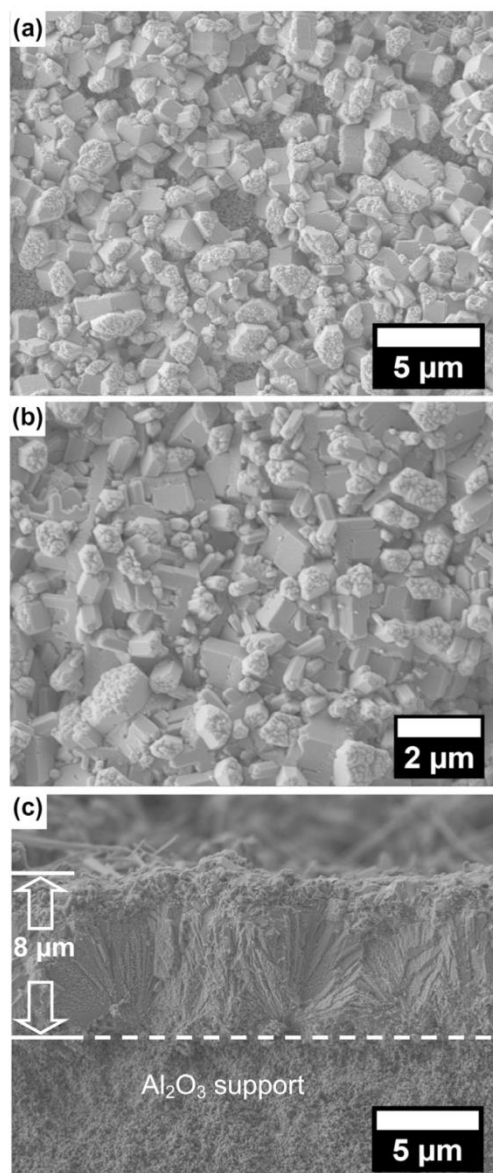
Fig. 2. SEM top view of zeolite SOD membrane by one-step hydrothermal synthesis (a), SEM top view (b) and cross-section (c) of zeolite SOD membrane by two-step repeated hydrothermal synthesis.

Fig. 1. SEM top views (a) (b) and EDXS mapping of top view (c) (orange: SOD islands, green: Al_2O_3 support) of the α-alumina support after hydrothermal SOD synthesis prepared by secondary growth method with SOD seeds deposited by dip-coating, no dense SOD layer has been formed, the uncovered alumina support can be seen.

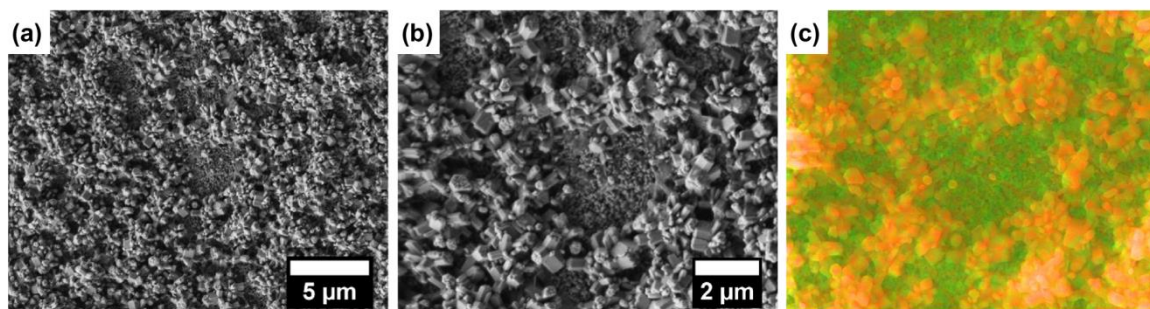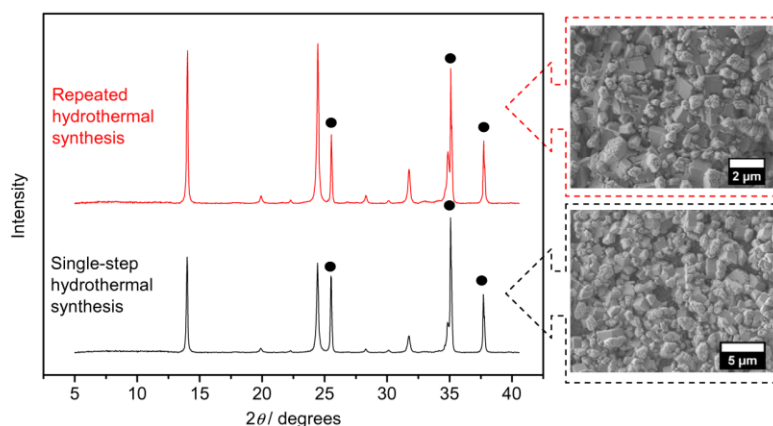**Fig. 3.** XRD patterns of the zeolite SOD membrane by one-step hydrothermal synthesis (black) and by two-step repeated hydrothermal synthesis (red). (●): Al$_2$O$_3$ support, (not marked): zeolite SOD. (For interpretation of the references to colour in this figure legend, the reader is referred to the web version of this article.)

Fig. 4. Mixture separation factors for H$_2$O over other gases from equimolar mixtures (left) and the 48 h stability measurement for the single gas permeances on the SOD membrane (right) at 125 °C and 1 bar.
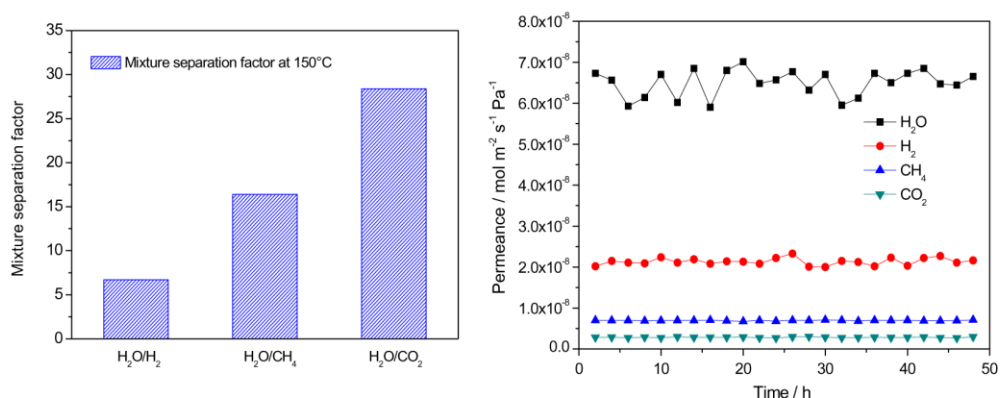
Fig. 5. Mixture separation factors for H$_2$O over other gases from equimolar mixtures (left) and the 48 h stability measurement for the single gas permeances on the SOD membrane (right) at 150 °C and 1 bar.

2.4. Evaluation of single gas permeation and mixed gas separation

Zeolite SOD membranes supported on α-Al$_2$O$_3$ disks were evaluated by single gas permeation and mixed gas separation. For permeation experiments, the supported zeolite SOD membranes were sealed in a permeation module with silicone O-rings. In the feed side, deionized water was heated to 200 °C and vaporized before the measurements. Then the water vapor was led to the permeation cell in a heated pipe, and the permeate gases was kept heated until they were injected into gas chromatograph. The

2 Zeolite membranes for water pervaporation and separation

Fig. 6. Mixture separation factors for H_2O over other gases from equimolar mixtures (left) and the 48 h stability measurement for the single gas permeances on the SOD membrane (right) at 175 °C and 1 bar.
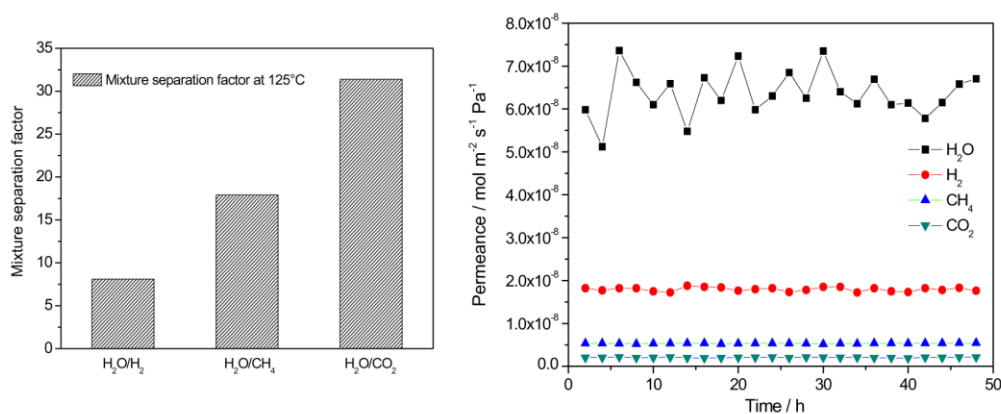

Fig. 7. Mixture separation factors for H_2O over other gases from equimolar mixtures (left) and the 48 h stability measurement for the single gas permeances on the SOD membrane (right) at 200 °C and 1 bar.
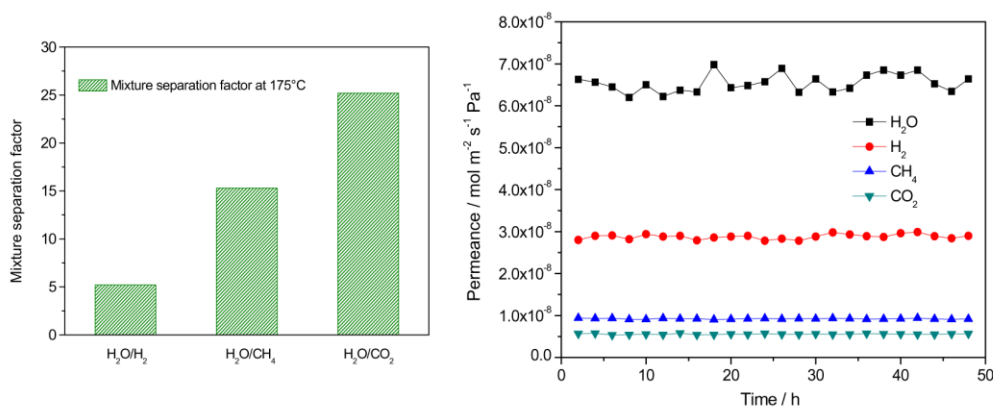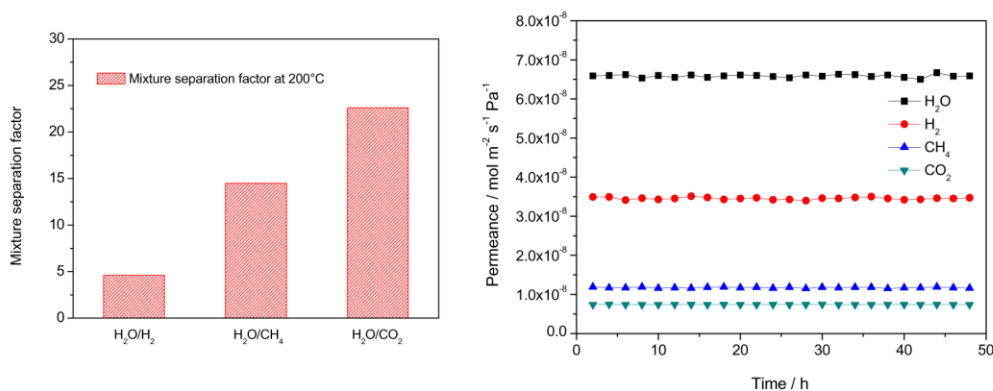
Table 1
Comparison of the mixed gas selectivities α^{real} determined for equimolar mixtures acc. to Eq. (1) and the ideal gas selectivities α^{ideal} determined as the ratio of the single component permeances.

	125 °C		150 °C		175 °C		200 °C	
	α^{real}	α^{ideal}	α^{real}	α^{ideal}	α^{real}	α^{ideal}	α^{real}	α^{ideal}
H_2O/H_2	8.1	4.8	6.7	3.2	5.2	2.7	4.6	1.9
H_2O/CH_4	17.9	12.1	16.4	9.7	15.3	7.8	14.5	6.6
H_2O/CO_2	31.4	26.1	28.4	24	25.2	21.8	22.6	18.9

Fig. 8. Mixture separation factors for H_2O over other gases through a zeolite SOD membrane prepared by two-step repeated hydrothermal synthesis as a function of temperature.

volumetric flow rates of the single gases H_2O, H_2, CO_2, and CH_4 as well as of the equimolar binary mixtures of H_2O with H_2, CO_2 and CH_4 were measured using the Wicke–Kallenbach technique, as shown in detail elsewhere [16]. The sweep gas N_2 was fed on the permeate side to guarantee enough driving force for permeation. To avoid the condensation of water, the measurements were carried out at 125 °C, 150 °C, 175 °C and 200 °C, respectively. Atmospheric pressure was kept on both sides of the membranes. Fluxes of both feed and sweep gases were controlled by mass flow controllers (MFCs) for gases, while the flux of feed water was controlled by a MFC for water. A calibrated gas chromatograph (HP6890) was used to determine the gas concentrations. The separation factor $\alpha_{i,j}$ of a binary mixture permeation is defined as the quotient 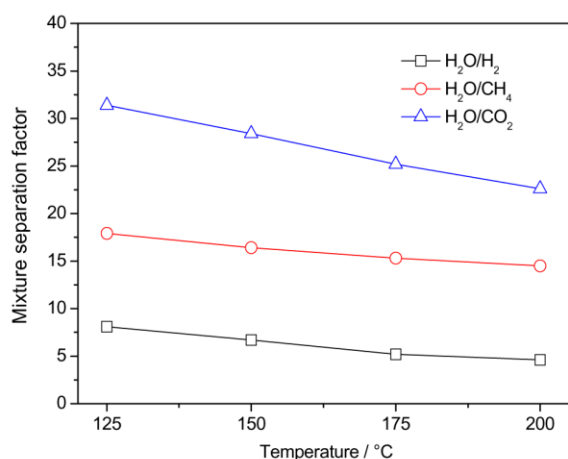of the molar ratios of the components (*i,j*) in the permeate, divided by the quotient of the molar ratio of the components (*i,j*) in the retentate, as shown in Eq. (1).

$$\alpha_{i/j} = \frac{y_{i,Perm}/y_{j,Perm}}{y_{i,Ret}/y_{j,Ret}} \tag{1}$$

3. Results

In situ growth and secondary growth methods are the most common techniques for the preparation of zeolite membranes. Due to the separation of nucleation (at high supersaturation) and crystal growth (at low supersaturation), the seeded growth method suppresses non-desired secondary nucleation and growth, and allows therefore more control of the microstructure of zeolite membranes. In view of this, we first tried to prepare SOD membranes by secondary growth. Initially, SOD seeds have been prepared and successfully deposited on the α-alumina supports by dip-coating. Then the SOD membrane was prepared in the same synthesis solution as described in 2.2 over 24 h at 120 °C. However, the SEM shows that after secondary growth, the SOD seed crystallites are not intergrown to a dense SOD layer (Fig. 1). Accordingly, the permeation of steam/gas mixtures shows that the SOD membrane has no H_2O/H_2 H_2O/CH_4 or H_2/CO_2 selectivity at all.

Therefore, we decided to develop an "*in situ*" seeding method for the direct growth of the SOD layer on the substrate [17]. In this method, the bare α-alumina support is immersed in a SOD precursor solution and then subjected to hydrothermal growth at 120 °C. After the first hydrothermal SOD synthesis, SEM indicates that no compact SOD seed layer had formed and on some spots the support surface can be seen (Fig. 2a). Although SOD crystallites could not fully cover the entire substrate surface after the first hydrothermal synthesis, after repeated synthesis the surface of the alumina support has been completely covered by a tightly packed SOD layer (Fig. 2b), and no visible intercrystalline defects can be detected.

The cross-section image (Fig. 2c) shows a well-intergrown SOD membrane layer with a thickness of about 8 μm. One could assume from the top views, that the SOD layers prepared by single-step (Fig. 2a) and repeated hydrothermal synthesis (Fig. 2b) are rather heterogeneous due to the different size and shape of the crystallites, and contain different crystalline phases. However, the XRD results confirmed that in both the SOD layers prepared by single-step and repeated hydrothermal synthesis, no foreign crystalline phase is present (Fig. 3). After the repeated hydrothermal synthesis, the membrane shows stronger SOD peaks relative to the alumina support because of the increased SOD layer thickness (XRD were done in the grazing incidence technique).

Figs. 4–7 shows the mixture separation factors for the three equimolar mixtures H_2O/H_2, H_2O/CH_4, and H_2O/CO_2 as well as the single gas permeances for a 48 h permeation time at 125 °C, 150 °C, 175 °C and 200 °C, respectively. It can be seen that the permeances of H_2, CH_4 and CO_2 kept unchanged for 48 h, indicating the stability of the SOD membrane at high temperatures (above 125 °C) even for steam as undiluted feed. In complete accordance with this stable permeation behavior, no structural degradation of the SOD structure could be observed by XRD and electron microscopy (not shown here). The scattering of the steam permeances (Figs. 4–7) is a measuring effect due to the repeated condensation/evaporation of water vapor in the equipment at low temperatures which settles with increasing permeation temperature. Table 1 shows that, surprisingly, all mixture separation factors α^{real} are higher than the ideal selectivities α^{ideal} calculated from the single gas permeances. This experimental finding can be explained by the extreme hydrophilicity of the SOD structure. In the case of the mixed gas permeation, the water becomes strongly adsorbed in the SOD framework in the whole temperature window between 125 and 200 °C. This strongly adsorbed water effectively suppresses the adsorption and diffusion of the second component.

Fig. 8 and Table 1 show the mixture separation factors for H_2O over other gases through a zeolite SOD membrane as a function of temperature. It was found that the mixed gas separations factors
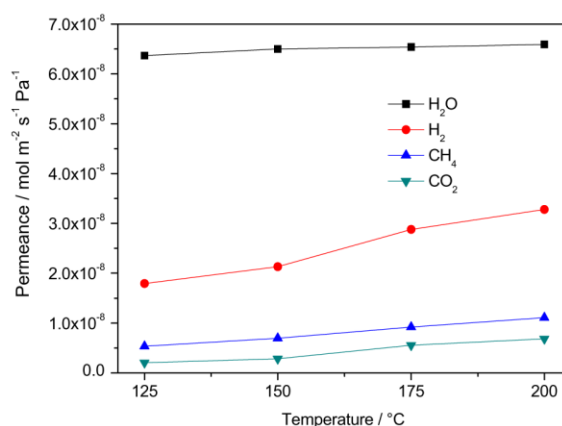

Fig. 9. Single gas permeances of H_2O, H_2, CH_4 and CO_2 through a zeolite SOD membrane prepared by two-step repeated hydrothermal synthesis as a function of temperature.

Table 2
Single gas permeances of H_2O and mixture separation factors for H_2O over other gases from equimolar mixtures at 150 °C and 1 bar of 8 different zeolite SOD membranes.

SOD-membrane number	H_2O permeance $(mol\ m^{-2}\ s^{-1}\ Pa^{-1})$	Mixture separation factors		
		H_2O/H_2	H_2O/CH_4	H_2O/CO_2
1	6.50×10^{-8}	6.7	16.4	28.4
2	6.48×10^{-8}	7.1	16.9	28.6
3	6.73×10^{-8}	6.3	16.1	27.8
4	6.31×10^{-8}	6.7	16.5	28.5
5	6.08×10^{-8}	7.2	17.2	29.3
6	6.70×10^{-8}	6.6	15.9	28.1
7	6.32×10^{-8}	6.9	16.0	27.9
8	6.88×10^{-8}	6.1	16.2	28.6

for the three systems under study H_2O/H_2, H_2O/CH_4, and H_2O/CO_2 decreased slightly with increasing temperature (from 8.1 to 4.6, from 17.9 to 14.5, and from 33.4 to 22.6), respectively. Permeation of a species through the membrane is a result of the interplay of adsorption and diffusion. The "membrane selectivity" can be estimated as product of "diffusion selectivity" multiplied by "adsorption selectivity". In the whole temperature window between 125 and 200 °C, the hydrophilic SOD preferentially adsorbs water thus restraining the diffusion of the rarely adsorbed H_2, CH_4, and CO_2. As temperature increases, slightly less H_2O becomes adsorbed and, thus, the other components H_2, CH_4, and CO_2 can diffuse in the resulting free volume, leading to a reduction of the selectivity of H_2O/H_2, H_2O/CH_4, and H_2O/CO_2. The SOD membrane switches with increasing temperature from "adsorption control" in the direction of "diffusion control". This temperature-dependent interplay of adsorption and diffusion has been developed for describing permeation through organic polymer membranes [18], but it has been successfully applied to permeation through MFI pore membrane with hydrogen as the weakly and i-butane as the strongly adsorbed component [19]. In the adsorption-controlled state at low temperature, the MFI membrane is butane-selective, with increasing temperature the MFI membrane becomes hydrogen-selective. Fig. 9 presents the increase of the single component permeances with increasing temperature. Obviously, the decreased adsorption with increasing temperature has been over compensated by the increased diffusivity of the guest species. However, from the only slight increase of the water single component permeance with increasing temperature (Fig. 9) it can

Table 3
Mixture gases separation performances of H_2O over MeOH for equimolar mixtures through a zeolite SOD membrane prepared by two-step repeated hydrothermal synthesis at different temperatures.

Temperature (°C)	H_2O permeance (mol m^{-2} s^{-1} Pa^{-1})	CH_3OH permeance (mol m^{-2} s^{-1} Pa^{-1})	Mixture separation factor
125	8.98×10^{-8}	4.97×10^{-10}	180
150	9.48×10^{-8}	4.15×10^{-10}	228
175	1.05×10^{-7}	4.84×10^{-10}	235
200	1.08×10^{-7}	4.96×10^{-10}	233

be concluded that reduced water adsorption and increased diffusion in SOD almost compensate. This increase of the permeance with increasing temperature has been also observed in pervaporation studies up to 165 °C with pressurized liquid water as feed [3,10].

As a proof of the good reproducibility of the two-step repeated hydrothermal synthesis method, Table 2 shows the gas permeation performances of 8 different zeolite SOD membranes prepared following identical synthesis protocols. The mixed gas selectivities and water permeances at 150 °C do not scatter more than ±10%, which proofs both the good reproducibility of the SOD membrane preparation as well as of the SOD membrane testing.

Table 3 shows the mixture separation performance for H_2O over MeOH through a zeolite SOD membrane at different temperatures (from 125 °C to 200 °C), which indicates that the removal of water from methanol is also successful in the whole temperature window due to molecular sieving (pore size SOD ≈ 2.7 Å, water 2.6 Å, MeOH 3.8 Å). This finding recommends SOD membrane for *in situ* water removal in methanol synthesis acc. to $CO_2 + 3H_2 \rightarrow$ MeOH + H_2O.

4. Conclusions

After a two-step repeated hydrothermal crystallization, a well intergrown SOD membrane layer with a thickness of about 8 μm could be obtained on the α-alumina support. The SOD membrane displayed water selectivity in steam permeation of equimolar mixtures of H_2O/H_2, H_2O/CH_4, and H_2O/CO_2 under practice-relevant conditions. The mixed gas separation factors of H_2O/H_2, H_2O/CH_4, and H_2O/CO_2 were found to decrease slightly with increasing temperature. These selectivity data of steam removal in the presence of hydrogen, methane, and carbon dioxide are promising for the use of SOD membranes in (catalytic) membrane reactors. However, the selectivity has to be improved further. It was found that the mixed gas separations factors for the three systems under study H_2O/H_2, H_2O/CH_4, and H_2O/CO_2 decreased slightly from 125 to 200 °C (from 8.1 to 4.6, from 17.9 to 14.5, and from 33.4 to 22.6), respectively. Water is also separated from methanol with mixture separation factors near 200. However, the water permeance of

0.43 kg/m^{2}h bar at 200 °C is relative low due to the 8 μm thickness of the SOD membrane.

References

[1] Industrial applications of LTA membranes between 2009 and 2012: (a) Mitsui–Sulzer Chemtech at 130 °C: Singapore, 27 t IPA/day, 100 m^2 membrane area; Finland, 216 t EtOH/day, 800 m^2; Ucraina, 150 t EtOH/day, 400 m^2; (b) Fraunhofer IKTS-GFT Membrane Systems at140 °C: Lithuania, 80 t EtOH/day, 400 m^2; (c) Dalian Univ. of Techn.-Yancheng Inst. of Techn. at 140 °C: 150 t IPA/day, 200 m^2; (d) Nanjing Jiangsu Nine-Heaven Hi-Tec Co.: 7.5 t IPA/day, 35 m^2, 6 t IPA/day, 52 m^2, 9 t MeOH/day, 84 m^2, 9 t IPA/day, 56 m^2; (e) Dalian DIPC of CAS-Xinhua Chemical Co. Ltd. At 140 °C: 140 t IPA/day, 350 m^2; Dalian DIPC of CAS-Sopo China at 120 °C: 80 t EtOH/day, 350 m^2.
[2] S. Khajavi, S. Sartipi, J. Gascon, J.C. Jansen, F. Kapteijn, Microporous Mesoporous Mater. 132 (2010) 510–517.22.
[3] S. Khajavi, F. Kapteijn, J.C. Jansen, J. Membr. Sci. 299 (2007) 63–72.
[4] S.-R. Lee, Y.-H. Son, A. Julbe, J.-H. Choy, Thin Solid Films 495 (2006) 92–96.
[5] A. Julbe, J. Motuzas, F. Cazeville, G. Volle, C. Guizard, Sep. Purif. Technol. 32 (2003) 139–149.
[6] R. Szostak, Handbook of Molecular Sieves, Van Nostrand Reinhold, New York, 1992.
[7] C. Günther, H. Richter, I. Voigt, Chem. Eng. Trans. 31 (2013) 000.
[8] S. Khajavi, J.C. Jansen, F. Kapteijn, J. Membr. Sci. 356 (2010) 1–6.
[9] S. Khajavi, J.C. Jansen, F. Kapteijn, Catal. Today 156 (2010) 132–139.
[10] S. Khajavi, J.C. Jansen, F. Kapteijn, J. Membr. Sci. 326 (2010) 52–57.
[11] X. Xu, Y. Bao, C. Song, W. Yang, J. Liu, L. Lin, Microporous Mesoporous Mater. 75 (2004) 173–181.
[12] D. Li, H.Y. Zhu, K.R. Ratinac, S.P. Ringer, H. Wang, Microporous Mesoporous Mater. 126 (2009) 14–19.
[13] S. Workneh, A. Shukla, J. Membr. Sci. 309 (2008) 189–195.
[14] D.W. Breck, Zeolite Molecular Sieves, John Wiley, New York, 1974.
[15] M.P. Rhode, G. Schaub, S. Khajavi, J.C. Jansen, F. Kapteijn, Microporous Mesoporous Mater. 115 (2008) 123–136.
[16] A. Huang, F. Liang, F. Steinbach, J. Caro, J. Membr. Sci. 350 (2010) 5–9.
[17] Y. Li, H. Chen, J. Liu, W. Yang, J. Membr. Sci. 277 (2006) 230–239.
[18] C.E. Rogers, V. Stannet, M. Szwark, J. Polym. Sci. XLV (1960) 61–82.
[19] U. Illgen, R. Schäfer, M. Noack, P. Kölsch, A. Kühnle, J. Caro, Catal. Commun. 2 (2001) 339–345.

2.3 Hydrophilic SOD and LTA membranes for membrane-supported methanol, dimethylether and dimethylcarbonate synthesis

Nanyi Wang**,** Yi Liu, Aisheng Huang and Jürgen Caro

Hydrophilic SOD and LTA membranes for membrane-supported methanol, dimethylether and dimethylcarbonate synthesis

N. Wang [a, *], Y. Liu [a], A. Huang [b], J. Caro [a]

[a] Institute of Physical Chemistry and Electrochemistry, Leibniz University Hannover, Callinstr. 22, D-30167 Hannover, Germany
[b] Institute of New Energy Technology, Ningbo Institute of Material Technology and Engineering, CAS, 519 Zhuangshi Road, 315201 Ningbo, PR China

A B S T R A C T

Hydrophilic LTA and SOD membranes have been tested in the selective water removal from methanol (MeOH), dimethylcarbonate (DMC) and dimethylether (DME) thus simulating their synthesis in membrane reactors with CO_2 as feed. To further improve the pervaporation selectivity of LTA membranes for an aqueous MeOH solution, Na^+ ions located in the 8-membered oxygen ring of LTA were ion-exchanged with larger K^+ ions in a KNO_3 solution, leading to an improvement of the pervaporation separation factor of the H_2O/MeOH mixture from 2.8 to 7.4 at room temperature. Furthermore, the selective removal of steam from the organic compounds MeOH, DME and DMC on supported SOD membranes was investigated at high temperatures by steam permeation. The separation performances of SOD membranes for equimolar mixtures of steam with H_2, CO_2, MeOH, DME or DMC, were evaluated in the temperature range from 125 to 200 °C. The mixture separation factors for steam from DME and DMC through the SOD membrane were found to be higher than 200 and 1000, respectively.

1. Introduction

Zeolite membranes have attracted widespread attention due to their great potential in the separation of gas or liquid mixtures. Among them, the fabrication of LTA-type zeolite membranes has been extensively studied, and supported LTA membranes have also been successfully prepared [1–6]. Because of the strong hydrophilicity and suitable pore size, zeolite LTA membranes were first commercialized in the dehydration of alcohol/water mixtures by steam permeation [7–12].

While past decades had witnessed great progress made in LTA membranes, some problems still existed, which had hindered the improvement of the dehydration performance. One critical problem encountered is the pore size control. Usually LTA membranes are synthesized in the Na^+ form. However, their pore size of about 4 Å is not small enough for the molecular sieving of H_2O/MeOH (kinetic diameters about 2.6 Å and 3.8 Å, respectively) mixtures. One possible solution of pore size-engineering is ion-exchange of the Na^+ with bigger K^+ ions. The formula of one cubo-octaheder $Na_{12}[Si_{12}Al_{12}O_{48}]$ represents one large cavity. 8 of the 12 Na^+ are located inside the large cavity near to the eight six-rings. 3 of remaining 4 Na^+ ions are located in the 8-membered oxygen rings between the large cavities thus hindering the molecular passage. The fourth of these remaining Na^+ is not located. Zeolite Na^+-LTA has a pore size of about 4.1 Å, when the sodium ions are exchanged with K^+, the pore size will be narrowed to about 3 Å. Theoretically, when Na^+ are ion-exchanged with even larger cations like Rb^+ for Cs^+, the pore size of LTA is expected to be further reduced [13]. On the contrary, when the Na^+ are replaced with smaller cations like Li^+, the pore size of the framework will be increased [14]. If the Na^+ are replaced by two-valent ions like Ca^{++} or Mg^{++}, these ions go into the large cavity and the cation positions in the 8-membered oxygen rings become unoccupied which "opens" the window to about 5 Å [15,16]. Because of the potential industrial applications like water-softening, gas adsorption and gas separation, the ion-exchange behavior of zeolite LTA has been studied extensively [17–23]. It was found that the Li^+-exchanged LTA can adsorb NO better relative to the Na-LTA [24]. The Rb^+ and Cs^+-exchanged LTA was also investigated [16] and the Rb^+ and Cs^+-exchanged LTA membranes supported on carbon discs were used for hydrogen purification [13]. However, ion-exchanged LTA membranes have been investigated in only a few gas separation studies [4–6,25]. Morooka et al. [5] found that K-LTA membranes show better separation performance for a H_2/N_2 system compared to the Na-LTA
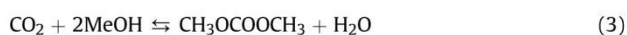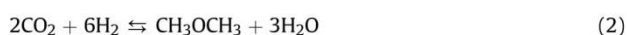
and Ca-LTA membranes. Huang et al. [6] used Ca-LTA membranes to separate n-butane (4.3 Å) from i-butane (5.1 Å).

Zeolite SOD is also hydrophilic, but with a higher framework density of 17.2 T/1000 $Å^3$ which shows a higher chemical and thermal stability compared with zeolite LTA (12.9 T/1000 $Å^3$) [26,27]. The small pore size of about 2.7 Å allows molecular sieving, that is to say the permeation of small molecules like H_2O with 2.6 Å through the membrane should be possible while the large molecules are excluded. Therefore, due to their hydrophilicity and molecular sieving properties, SOD membranes are advantageous in the removal of steam under harsh conditions [28–30] and could be used in the synthesis of methanol (MeOH, Eq. (1)), dimethylether (DME, Eq. (2)) and dimethylcarbonate (DMC, Eq. (3)) in catalytic membrane reactors with carbon dioxide, hydrogen or methanol as reagents:

$$CO_2 + 3H_2 \leftrightarrows CH_3OH + H_2O \tag{1}$$

$$2CO_2 + 6H_2 \leftrightarrows CH_3OCH_3 + 3H_2O \tag{2}$$

$$CO_2 + 2MeOH \leftrightarrows CH_3OCOOCH_3 + H_2O \tag{3}$$

In the present work, the K^+-exchanged LTA membrane was prepared and exhibited improved H_2O/MeOH pervaporation performance at room temperature in comparison with the as-synthesized Na^+-LTA membrane. We further studied the pervaporation behavior of SOD membranes in the separation of H_2O/MeOH, H_2O/DME and H_2O/DMC mixtures in the temperature range between 125 and 200 °C.

2. Experimental

2.1. Materials

The following chemicals were used as received: LUDOX AS-40 colloidal silica (40% SiO_2 in water, Aldrich); aluminum foil (Fisher Scientific); sodium hydroxide (>99%, Merck); potassium nitrate (≥99%, Roth); doubly distilled water; 3-aminopropyltriethoxysilane (98%, Abcr); toluene (99.8%, Acros). Porous α-Al_2O_3 disks (Fraunhofer Institute IKTS, former HITK/Inocermic, Hermsdorf, Germany. diameter: 18 mm; thickness: 1.0 mm; pore size: 70 nm) were used as supports.

2.2. Preparation of zeolite LTA membrane

The zeolite LTA membranes were prepared on APTES-functionalized α-Al_2O_3 supports following the procedure reported elsewhere [31,32]. The porous alumina supports were treated with APTES (0.2 mM) in 10 mL toluene at 110 °C for 30 min under argon. A clear synthesis solution with the molar ratio of 50Na_2O:1Al_2O_3:5SiO_2:1000H_2O was used as precursor solution. The aluminate solution was prepared by adding 0.15 g aluminum foil to 25 g deionized water containing 11.11 g sodium hydroxides at room temperature. The silicate solution was prepared by mixing 2.08 g LUDOX AS-40 colloidal silica and 23.75 g deionized water at 60 °C under stirring. Then the prepared silicate solution was added into the aluminate solution and stirred overnight to produce a clear, homogenous solution. The APTES-functionalized alumina supports were horizontally placed face down in a Teflon-lined stainless steel autoclave and immersed in the precursor solution. After the in-situ growth at 60 °C for 24 h, the solution was decanted off and the membranes were washed with deionized water several times and immersed in deionized water overnight, and then dried in air at 110 °C for characterization and permeation measurement.

To prepare the K^+-ion-exchanged LTA membranes, as-prepared LTA membranes were immersed into a 1 M KNO_3 solution for 12 h at room temperature. Then the membranes were thoroughly washed with deionized water several times and dried in air at 110 °C overnight.

2.3. Preparation of zeolite SOD membrane

The clear precursor solution with the molar ratio 50Na_2O:1Al_2O_3:5SiO_2:1005H_2O was prepared according to the procedure reported elsewhere [28]. To prepare the aluminate solution, 11.11 g sodium hydroxides were dissolved in 25 g deionized water at room temperature, then 0.15 g aluminum foil was added into the solution. The silicate solution was prepared by mixing 2.08 g LUDOX AS-40 colloidal silica and 23.75 g deionized water at 60 °C under stirring. The prepared silicate solution was added into the aluminate solution and stirred overnight at room temperature to produce a clear solution. α-Al_2O_3 support was then horizontally placed face down in a Teflon-lined stainless steel autoclave which was filled with synthesis solution. After hydrothermal synthesis over 24 h at 120 °C, the solution was decanted off. The membrane was washed with deionized water and immersed in deionized water overnight, and then dried in air at 110 °C. To prepare a more compact SOD membrane, the dried membrane was subjected to repeated hydrothermal synthesis under identical conditions. Finally, the dried membrane after the repeated synthesis was further characterized and evaluated in gas permeation measurement.

2.4. Characterization of zeolite LTA and SOD membranes

The morphology and thickness of the zeolite LTA and SOD membranes were characterized by scanning electron microscopy (SEM, JEOL JSM-6700F with a cold field emission gun operating at 2 kV and 10 μA). The chemical composition of the cross-section of ion-exchanged LTA-layer was characterized by energy-dispersive X-ray spectroscopy (EDXS) using the same SEM microscope at 10 kV and 20 μA. The phase purity and crystallinity of the zeolite LTA and SOD membrane layers were measured by X-ray diffraction (XRD). XRD patterns were recorded at room temperature under ambient conditions with Bruker D8 ADVANCE X-ray diffractometer using CuK_α radiation at 40 kV and 40 mA.

2.5. Evaluation of pervaporation

Pervaporation performance of prepared LTA membranes were evaluated as follows: The supported LTA membrane was sealed in a home-built permeation cell with silicone O-rings and tested at room temperature by pervaporation. The concentration on the feed side was 5 wt% water against 95 wt% MeOH or DMC. The H_2O/MeOH or H_2O/DMC mixtures were fed to the feed side of the LTA membrane in the membrane model, and the permeate side of the membrane was evacuated with a vacuum pump. The permeate was collected in liquid nitrogen cooled traps. The flux was calculated by weighing before and after pervaporation, and the composition of the permeate were analyzed by gas chromatograph (HP6890). The total flux J and the separation factor α are defined following Eqs. (4) and (5)

$$J = \frac{W}{\Delta t \cdot A} \tag{4}$$

$$\alpha_{i,j} = \frac{x_{ip}}{x_{if}} \cdot \frac{x_{jf}}{x_{jp}} \tag{5}$$

where W is total weight of the permeate (kg), Δt is collecting time (h), A is separation area of the membrane (m^2), x_{ip} is the weight fraction of species i in the permeate and x_{if} is the weight fraction of species i in the feed.

2.6. Evaluation of single gas permeation and mixed gas separation

Both single and mixed gas permeation behaviors of prepared SOD membranes were evaluated as follows: For permeation experiments, the zeolite SOD membranes were sealed in a permeation module with silicone O-rings. On the feed side, deionized water, methanol, DME or DMC was heated to 200 °C in advance and vaporized before the measurements. Then the gas or liquid vapor was given to the permeation cell via a heated pipe. The permeated gases were kept heated until they were injected into gas chromatograph. The volumetric flow rates of the single gases H$_2$O, methanol, DME and DMC as well as of the equimolar binary mixtures of H$_2$O with methanol, DME and DMC were measured with the Wicke–Kallenbach technique, as shown in detail elsewhere [25]. The sweep gas N$_2$ was fed on the permeate side to guarantee enough driving force for permeation. To avoid the condensation of the liquids, the measurements were carried out in the temperature range from 125 °C to 200 °C. Atmospheric pressure was kept on both sides of the membranes. Fluxes of both feed and sweep gases were controlled by mass flow controllers (MFCs) for gases, while the fluxes of feed water, methanol and DMC were controlled by a MFCs for liquids. A calibrated gas chromatograph (HP6890) was used to determine the gas concentrations. The separation factor $\alpha_{i,j}$ of a binary mixture permeation is defined as the quotient of the molar ratios of the components (i,j) in the permeate, divided by the quotient of the molar ratio of the components (i,j) in the retentate, as shown in Eq. (6).

$$\alpha_{i,j} = \frac{y_{i,Perm} \big/ y_{j,Perm}}{y_{i,Ret} \big/ y_{j,Ret}} \qquad (6)$$

3. Results and discussion

3.1. Preparation of Na-LTA membrane and ion-exchanged K-LTA membrane

Fig. 1 shows top view and cross-section of the supported K$^+$-exchanged LTA membrane. After hydrothermal synthesis for 24 h, a dense and well-intergrown Na-LTA membrane with a thickness of around 3.5 μm was formed on the α-alumina support without any
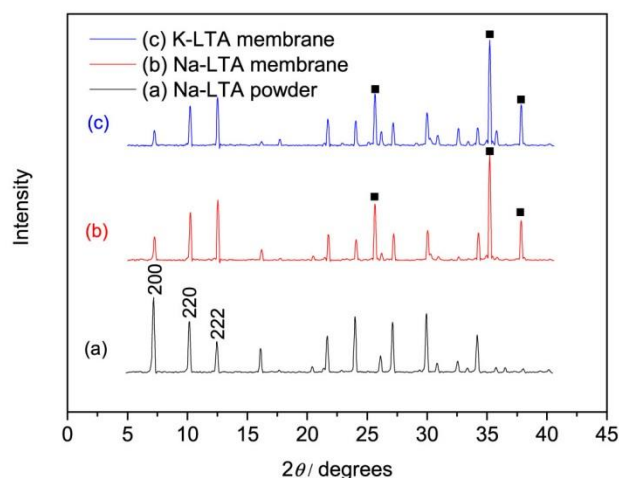

Fig. 2. XRD patterns of the zeolite Na-LTA membrane (b) K-LTA membrane after ion-exchange (c) compared with XRD patterns of the zeolite Na-LTA powder (a). (■): Al$_2$O$_3$ support (not marked): zeolite LTA.

macroscopic cracks or pinholes. After the 12 h ion-exchange with potassium ion, the morphology of the zeolite LTA membrane remained unchanged (Fig. 1a). The formation of a phase-pure zeolite LTA membrane with high crystallinity can also be confirmed by XRD patterns (Fig. 2). Referring to the XRD pattern of zeolite LTA powders (Fig. 2a), no other foreign crystalline phase of both Na-LTA and K-LTA membrane was observed, thus indicating that the ion-exchange process did not influence the LTA framework structure. Compared the XRD patterns of the LTA membrane and of LTA powder, the formation of an oriented LTA membrane can be stated. The LTA membrane shows a much stronger (222) peak, while the intensity of the (200) peaks is obviously decreased, which indicates that the LTA crystals are oriented with their diagonal perpendicular to the support surface. In agreement with the evolutionary selection model by van der Drift growth [33,34], the LTA crystals grow with their diagonal of the cube perpendicular to the support surface with {222} as the fastest growth direction. This finding from XRD correlates with the optical impression of the top view of the membrane (Fig. 1a), showing that the corners of the cube-shaped LTA crystals jut out of the membrane surface.

After the ion-exchange in the KNO$_3$ solution for 12 h, the distribution of the potassium ions in the ion-exchanged K-LTA membrane was investigated by EDXS. Fig. 3a shows the EDXS mapping of
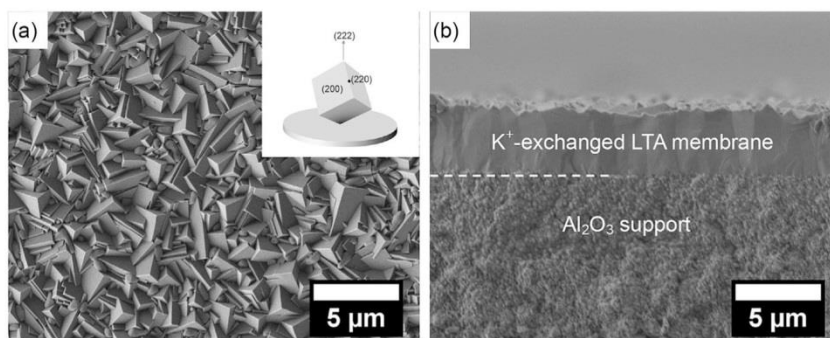

Fig. 1. SEM top views (a) and cross sections (b) of the zeolite LTA membranes on APTES-functionalized alumina supports after the 12 h ion-exchange with potassium ion. The inset of (a) shows the orientation of an individual cubic LTA crystal with (222) perpendicular to the support.

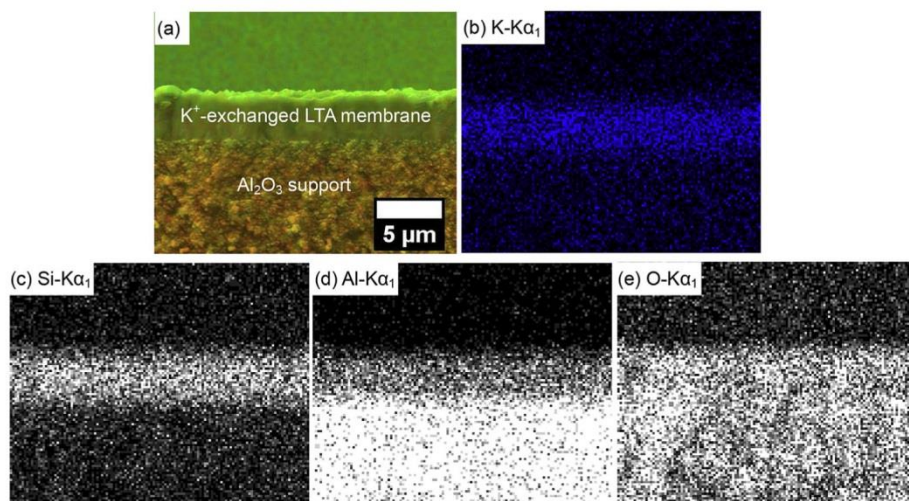# 2 Zeolite membranes for water pervaporation and separation

Fig. 3. (a) EDXS mapping of the cross section of ion-exchanged Na-LTA membrane (green: K in the LTA membrane, orange: Al_2O_3 support) after 12 h ion-exchange in KNO_3 solution. (b–e) Element distribution by EDXS of the area shown in (a). (For interpretation of the references to colour in this figure legend, the reader is referred to the web version of this article.)
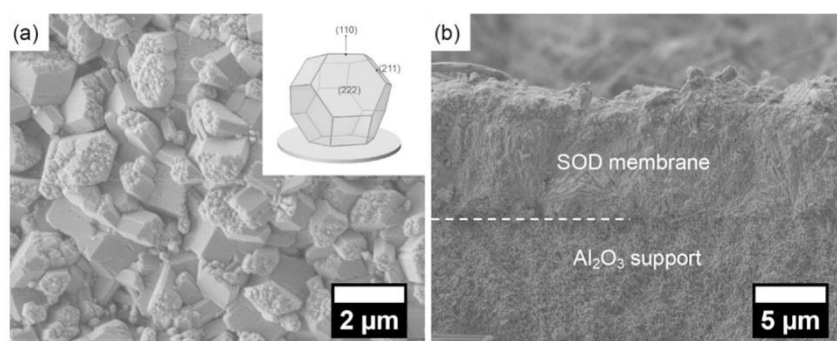
Fig. 4. SEM top view (a) and cross sections (b) of the zeolite SOD membrane by repeated synthesis on alumina support. The inset of (a) shows the orientation of an individual cubo-octahedral SOD crystal with (110) perpendicular to the support.

the cross section of the LTA membrane after K^+-exchange, and the element distribution of K, Si, Al and O of the same area are shown in Fig. 3b–e, respectively. It can be seen that the K^+ ions (blue color in Fig. 3b) were homogeneously distributed in the whole cross section of the K^+-LTA layer. Moreover, the element K was also found underneath the porous alumina substrate (comparing Fig. 3c with Fig. 3d), showing that the LTA precursor solution had partially penetrated into the substrate. This was beneficial since the adhesion stability of the LTA membrane to the porous alumina support could thus be strengthened.

3.2. Preparation of zeolite SOD membrane

According to our previous work [35], zeolite SOD membranes were prepared with a repeated synthesis method. Fig. 4 shows the top view and the cross section of a zeolite SOD membrane prepared by repeated synthesis. After two steps of hydrothermal synthesis, the surface of the α-Al_2O_3 support has been completely covered by a tightly packed SOD layer with a thickness of 8 μm, and no visible intercrystalline defects can be observed. The XRD results confirm that a pure zeolite SOD membrane with high crystallinity has formed on the alumina

Fig. 5. XRD patterns of the zeolite SOD membrane (b) compared with zeolite SOD powder (a). (■): Al_2O_3 support (not marked): zeolite SOD.

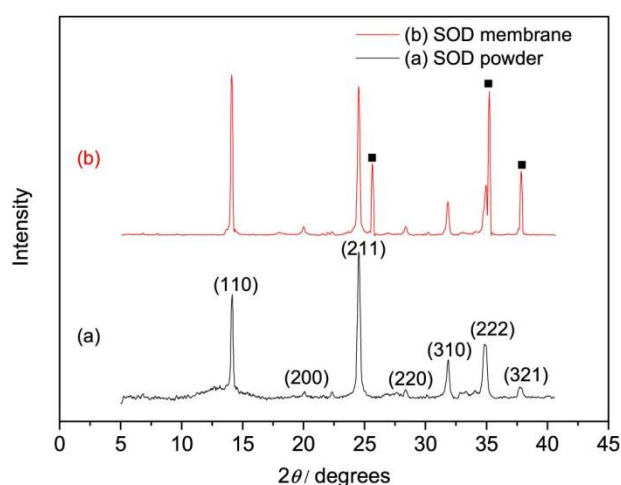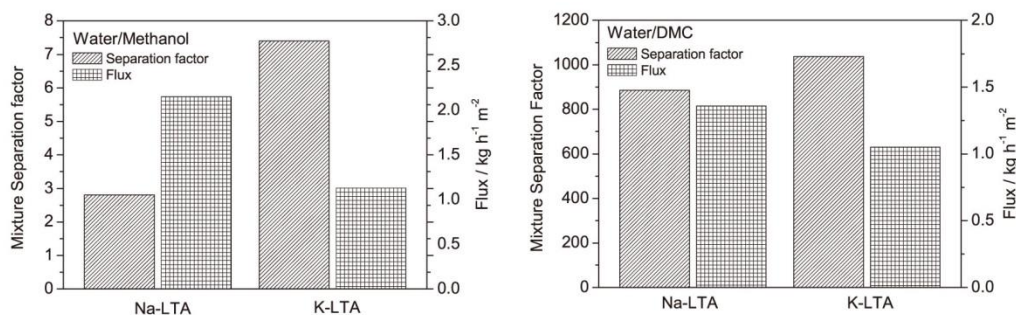# 2 Zeolite membranes for water pervaporation and separation

Fig. 6. Mixture separation factors and fluxes of the pervaporation for water against methanol (left) and water against DMC (right) through the supported Na-LTA membrane and ion-exchanged K-LTA membrane at room temperature.

Table 1
Mixture separation factors and fluxes for the pervaporation of water from methanol and DMC through the supported Na^+LTA and K^+-exchanged LTA membrane at room temperature.

Component	Na^+-LTA membrane				K^+-LTA membrane			
	H_2O	MeOH	H_2O	DMC	H_2O	MeOH	H_2O	DMC
x_{feed}/wt%	5.0	95.0	5.0	95.0	5.0	95.0	5.0	95.0
$x_{permeate}$/wt%	13.1	86.9	97.9	2.1	28.2	71.8	98.2	1.8
Separation factor	2.8		886		7.4		1037	
J/kg h^{-1} m^{-2}	2.15		1.36		1.13		1.05	

Table 2
Single gas permeances of H_2O, H_2 and CO_2 as well as mixture separation factors determined for equimolar mixtures acc. to Eq. (5) of H_2O/H_2 and H_2O/CO_2 through the SOD membrane at different temperatures.

Temperature (°C)	Permeance (mol m^{-2} s^{-1} Pa^{-1})			Mixture separation factor	
	H_2O	H_2	CO_2	H_2O/H_2	H_2O/CO_2
125	6.37×10^{-8}	1.79×10^{-8}	2.03×10^{-9}	8.1	31.4
150	6.50×10^{-8}	2.13×10^{-8}	2.84×10^{-9}	6.7	28.4
175	6.54×10^{-8}	2.88×10^{-8}	5.56×10^{-9}	5.2	25.2
200	6.59×10^{-8}	3.28×10^{-8}	6.84×10^{-9}	4.6	22.6

support after the repeated synthesis (Fig. 5), and no foreign phase is present by referring to the XRD. Compared to the XRD patterns SOD powder, the SOD membrane shows an obviously higher (110) peak, which indicates that an oriented SOD membrane was formed on the alumina support with their (110) face perpendicular to the support surface.

3.3. Pervaporation results of LTA membranes before and after K^+ ion-exchange

Fig. 6 and Table 1 show separation factors and fluxes of the pervaporation experiments for $H_2O/MeOH$ and H_2O/DMC mixtures through supported Na-LTA and K-LTA membranes at room temperature. After K^+ ion-exchange, the separation factor for the $H_2O/MeOH$ mixture increased from 2.8 to 7.4, while the separation factor for a H_2O/DMC mixture increased from ~800 to ~1000. Simultaneously, the water fluxes through the membranes after K^+

ion-exchange decreased. Since the pore size of the zeolite Na^+-LTA is 4.1 Å, DMC is spontaneously excluded from the LTA cages due to a molecular sieving effect. As a result, a H_2O/DMC mixture separation factor as high as 800 could be obtained on the Na^+-LTA membrane. However, for the $H_2O/MeOH$ mixture on Na^+-LTA membrane, a mixture separation factor of $\alpha = 2.8$ was measured, since the kinetic diameter of MeOH (3.8 Å) is smaller than the pore size of Na-LTA (4.1 Å).

3.4. Single and mixed gas permeation of SOD membranes

The single gas permeances of H_2O, H_2 and CO_2 as well as the separation factors of H_2O/H_2 and H_2O/CO_2 mixtures through the SOD membrane were evaluated in the temperature range from 125 to 200 °C. Related results, which were partly reported in our previous work [27], are summarized in Fig. 7 and Table 2.

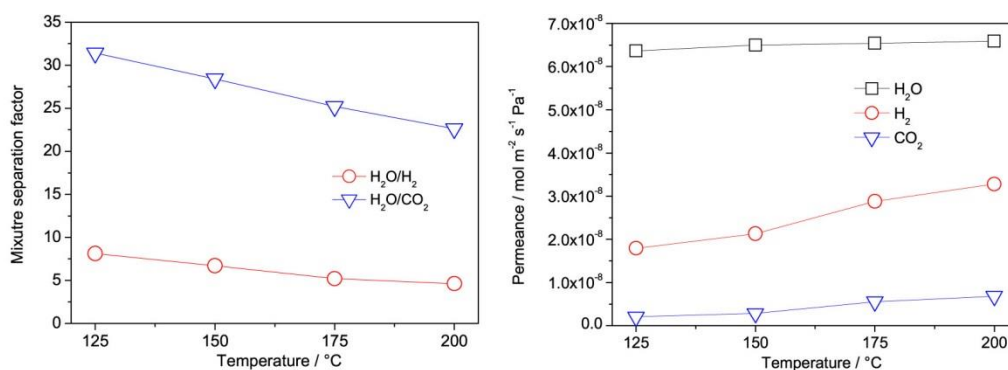**Fig. 7.** Mixture separation factors of equimolar mixtures of H_2O/H_2 and H_2O/CO_2 as well as single gas permeances of H_2O, H_2 and CO_2 through a supported zeolite SOD membrane prepared by two-step repeated hydrothermal synthesis as a function of temperature.

Table 3

Single gas permeances of H_2O, MeOH, DME and DMC as well as mixture separation factors of H_2O/MeOH, H_2O/DME and H_2O/DMC through the SOD membrane at different temperatures.

Temperature (°C)	Permeance (mol m^{-2} s^{-1} Pa^{-1})				Mixture separation factor		
	H_2O	MeOH	DME	DMC[a]	H_2O/MeOH	H_2O/DME	H_2O/DMC
125	6.37×10^{-8}	3.50×10^{-10}	2.90×10^{-10}	$<5 \times 10^{-11}$	180	220	>1000
150	6.50×10^{-8}	2.80×10^{-10}	2.87×10^{-10}		228	226	
175	6.54×10^{-8}	2.72×10^{-10}	2.71×10^{-10}		235	241	
200	6.59×10^{-8}	2.75×10^{-10}	2.60×10^{-10}		233	253	

[a] Since the area of the peaks of DMC, which was detected by gas chromatography was too small to integrate, the permeance of DMC cannot be evaluated exactly, when it was smaller than 5×10^{-11}.

The hydrophilic zeolite SOD membrane can be not only applied to separate steam from small gas molecules like H_2 and CO_2, but it also works well in the steam separation from larger molecules like MeOH, DME and DMC. Table 3 summarizes the separation performance of our zeolite SOD membrane for H_2O from MeOH, DME and DMC at temperatures from 125 °C to 200 °C. The removal of H_2O from MeOH, DME and DMC is also successful in the whole temperature range due to the hydrophilicity of the SOD membrane additionally supported by the molecular sieving effect. For instance, the separation factors of H_2O against MeOH, DME and DMC at 200 °C were around 230, 250 and >1000, respectively. Different to the steam separation from small molecules, when the temperatures increased from 125 to 200 °C, the mixture separation factors for the separation of H_2O from large molecules were improved, while the H_2O permeance also increased slightly, thus indicating an activated diffusion process. Owing to the extremely small pore size of SOD, large DMC molecules cannot permeate through a dense SOD membrane. The performance of SOD membrane to separate steam from either small gas molecules or large molecules like DME and DMC recommends SOD membrane an ideal candidate for the methanol, DME and DMC synthesis in membrane reactors with water removal.

4. Conclusions

Two hydrophilic zeolite membranes have been evaluated for the water separation from MeOH, DME and DMC:zeolite LTA membrane for pervaporation at room temperature, and zeolite SOD membrane for steam separation at high temperature up to 200 °C. A well-intergrown LTA membrane with a thickness of about 3.5 μm could be obtained on the APTES-modified α-alumina support. After the ion-exchange with K^+ for 12 h, the structure of the membrane remained unchanged but the free pore diameter of the 8-membered oxygen ring as bottleneck of the LTA membrane was reduced, which resulted in an increase of the selectivity but decrease of the permeance for the separation of water/methanol by pervaporation at room temperature. On the other hand, the LTA membrane was also suitable for the separation of water/DMC by pervaporation showing a high separation performance with a selectivity of around 800 and 1000, before and after ion-exchange, respectively.

With a repeated hydrothermal synthesis, a dense SOD membrane with a thickness of about 8 μm could be formed on the alumina support. The hydrophilic SOD membrane was also water selective, and displayed a high performance for the separation of steam from small gas molecules like H_2 and CO_2, which participated in the synthesis of DME and DMC. Moreover, water could also be separated successfully from MeOH, DME and DMC at high temperatures from 125 to 200 °C by using the SOD membrane.

References

[1] Y. Li, W. Yang, J. Membr. Sci. 316 (2008) 3–17.
[2] Y. Li, H. Zhou, G. Zhu, J. Liu, W. Yang, J. Membr. Sci. 297 (2007) 10–15.
[3] A. Huang, J. Caro, Chem. Commun. 46 (2010) 7748–7750.
[4] A. Huang, J. Caro, Chem. Mater. 22 (2010) 4353–4355.
[5] K. Aoki, K. Kusakabe, S. Morooka, J. Membr. Sci. 141 (1998) 197–205.
[6] X.C. Xu, W.S. Yang, J. Liu, L.W. Lin, Adv. Mater. 12 (2000) 195–198.
[7] J.J. Jafar, M. Budd, Microporous Mater. 12 (1997) 305–311.
[8] M. Kondo, M. Komori, H. Kita, K.I. Okamota, J. Membr. Sci. 133 (1997) 133–141.
[9] D. Shah, K. Kissick, A. Ghorpade, R. Hannah, D. Bhattacharyya, J. Membr. Sci. 179 (2000) 185–205.
[10] A.S. Huang, W.S. Yang, Microporous Mesoporous Mater. 102 (2007) 58–69.
[11] K. Sato, K. Aoki, K. Sugimoto, K. Izumi, S. Inoue, J. Saito, S. Ikeda, T. Nakane, Microporous Mesoporous Mater. 115 (2008) 184–188.
[12] Y. Li, H. Chen, J. Liu, H. Li, W. Yang, Sep. Purif. Technol. 57 (2007) 140–146.
[13] F.J. Varela-Gandía, A. Berenguer-Murcia, D. Lozano-Castelló, D. Cazorla-Amorós, J. Membr. Sci. 351 (2010) 123–130.
[14] R. Navarrete-Casas, A. Navarrete-Guijosa, C. Valenzuela-Calahorro, J.D. López-González, A. García-Rodríguez, J. Colloid Interface Sci. 306 (2007) 345–353.
[15] D.W. Breck, Zeolite Molecular Sieves, Wiley, New York (, 1974, pp. 83–86.
[16] A. Huang, J. Caro, J. Mater. Chem. 21 (2011) 11424–11429.
[17] R. Krishna, J.M. van Baten, Sep. Purif. Technol. 61 (2008) 414–423.
[18] E. Jaramillo, M. Chandross, J. Phys. Chem. B 108 (2004) 20155–20159.
[19] H. Lührs, J. Derr, R.X. Fischer, Microporous Mesoporous Mater. 151 (2012) 457–465.
[20] A. Basch, M. Hartl, P. Behrens, Microporous Mesoporous Mater. 99 (2007) 244–250.
[21] B. Xiao, P.S. Wheatley, R.E. Morris, Stud. Surf. Sci. Catal. 170A (2007) 902–909.
[22] G.T. Kerr, Sci. Am. 261 (1989) 100–105.
[23] R.A. Rakoczy, Y. Traa, Microporous Mesoporous Mater. 60 (2003) 69–78.
[24] H. Yahiro, K. Kurohagi, G. Okada, Y. Itagaki, M. Shiotani, A. Lund, Phys. Chem. Chem. Phys. 4 (2002) 4255–4259.
[25] G. Guan, K. Kusakabe, S. Morooka, Sep. Sci. Technol. 36 (2001) 2233–2245.
[26] S. Khajavi, S. Sartipi, J. Gascon, J.C. Jansen, F. Kapteijn, Microporous Mesoporous Mater. 132 (2010) 510–517.
[27] D.W. Breck, Zeolite Molecular Sieves, John Wiley, New York (, 1974.
[28] S. Khajavi, F. Kapteijn, J.C. Jansen, J. Membr. Sci. 299 (2007) 63–72.
[29] S.-R. Lee, Y.-H. Son, A. Julbe, J.-H. Choy, Thin Solid Films 495 (2006) 92–96.
[30] A. Julbe, J. Motuzas, F. Cazeville, G. Volle, C. Guizard, Sep. Purif. Technol. 32 (2003) 139–149.
[31] A. Huang, F. Liang, F. Steinbach, J. Caro, J. Membr. Sci. 350 (2010) 5–9.
[32] A. Huang, N. Wang, J. Caro, Microporous Mesoporous Mater. 164 (2012) 294–301.
[33] A. Van der Drift, Philips Res. Rep. 22 (1967) 267–288.
[34] H. Bux, A. Feldhoff, J. Cravillon, M. Wiebcke, Y. Li, J. Caro, Chem. Mater. 23 (2011) 2262–2269.
[35] N. Wang, Y. Liu, A. Huang, J. Caro, Microporous Mesoporous Mater. 192 (2014) 8–13.

3 Metal-organic framework membranes for H_2 purification

3.1 Summary

Due to the demand for clean energy, hydrogen purification becomes one of the most important tasks. Compared with traditional purification methods, membrane separation for hydrogen purification is more attractive because of its low cost. MOF membranes with various structures and adjustable properties attracted lots of attention in the past ten years. The three publications in this chapter introduce three novel MOF membranes, which can be applied for gas separations. Pre- or post-modification methods for synthesis are also reported for different MOF membranes.

The publication in Section 3.2 reports an amine-modified Mg-MOF-74 membrane with improved H_2/CO_2 selectivity. Although Mg-MOF-74 with 1D structure has a relative large pore size of about 10 Å, it shows a high CO_2 uptake ability which could have potential for H_2/CO_2 separation. For synthesis of a Mg-MOF-74 membrane, we used MgO as seeds, which can support nucleation points for Mg-MOF-74 crystals and promote the growth of the membrane. Another post-modification strategy was used for the as-prepared Mg-MOF-74 membrane. By post-modification of the open Mg sites with ethylenediamine, the selectivity of Mg-MOF-74 membrane enhanced obviously.

A highly permselective ZIF-100 membrane is introduced in Section 3.3. We have prepared the ZIF-100 membrane on a PDA-modified support. By this pre-modification method, covalent bonds between PDA and ZIF-100 could be formed, and the growth of ZIF-100 membrane on alumina support surface was improved. Due to its excellent CO_2 adsorption behavior and unique framework structure for CO_2 storage, ZIF-100 membrane showed high H_2/CO_2 selectivity.

The publication in Section 3.4 describes a ZIF-90 membrane for gas separation. APTES was used to post-modify the as-prepared ZIF-90 membrane. By the imine condensation between amino groups of APTES and aldehyde groups of the ZIF-90, the window aperture of the pore in ZIF-90 was narrowed, and intercrystalline defects could also be sealed. After the amine-modification, ZIF-100 membrane shows high separation factors of H_2/CO_2, H_2/CH_4, H_2/C_2H_6 and H_2/C_3H_8. The modification did not block the pores, since the H_2 permeances of the membrane reduced only slightly.

3.2 Amine-modified Mg-MOF-74/CPO-27-Mg membrane with enhanced H$_2$/CO$_2$ separation

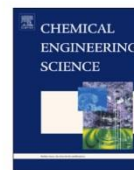Nanyi Wang, Alexander Mundstock, Yi Liu, Aisheng Huang and Jürgen Caro

Chemical Engineering Science 2015, 124, 27-36.

CHEMICAL
ENGINEERING
SCIENCE

Amine-modified Mg-MOF-74/CPO-27-Mg membrane with enhanced H_2/CO_2 separation

CrossMark

Nanyi Wang [a], Alexander Mundstock [a], Yi Liu [a], Aisheng Huang [b,*], Jürgen Caro [a,*]

[a] Institute of Physical Chemistry and Electrochemistry, Leibniz University Hannover, Callinstr. 22, D-30167 Hannover, Germany
[b] Institute of New Energy Technology, Ningbo Institute of Material Technology and Engineering, CAS, 1219 Zhongguan Road, 315201 Ningbo, PR China

HIGHLIGHTS

- Amination of the open metal sites in Mg-MOF-74 leads to retardation of CO_2 and doubles the selectivity for H_2/CO_2 separation.
- The size of Mg-MOF-74 crystals in membrane can be reduced after optimization of synthesis solution.
- Only by using MgO as seeds, a dense and continuous Mg-MOF-74 layer could be obtained.
- The selectivity of the Mg-MOF-74 membrane for H_2/CO_2 is far above the Robeson bound.

GRAPHICAL ABSTRACT
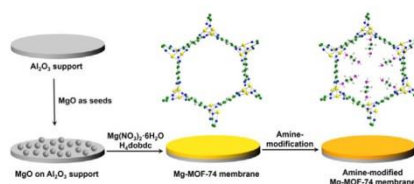
ABSTRACT

Mg-MOF-74 has attracted intense attention due to its high CO_2 uptake ability. In this work, a new strategy by using magnesium oxide as seeds was developed to synthesize a dense, defect-free Mg-MOF-74 membrane with hydrogen-selectivity. The mixed gas separation factor of H_2/CO_2 mixture could be improved by the post-modification of the Mg-MOF-74 membrane with ethylenediamine, since the modification with amine groups enhanced the strong adsorption of CO_2 molecules, which reduces the permeance of CO_2. The separation factors for both as-synthesized and amino-functionalized Mg-MOF-74 membranes reduce gradually with increasing temperature. After amination of the open Mg sites, the separation performance of the Mg-MOF-74 membrane was remarkably enhanced, and the H_2/CO_2 selectivity increased from 10.5 to 28 at room temperature.

© 2014 Elsevier Ltd. All rights reserved.

1. Introduction

As a high-quality and clean energy carrier, hydrogen has attracted renewed and increasing attention around the world in recent years. Currently, the majority of hydrogen is produced by steam-methane reforming (SMR) followed by a water-gas shift (WGS) strategy. Before hydrogen can be used in fuel cell, it has to be purified from the resulting SMR gas mixture which mainly contains CO_2. Also in the pre-combustion technology of CO_2 sequestration, H_2-selective membranes are desired. In the case of pre-combustion CO_2 capture, H_2-selective membranes can be applied at moderate temperatures (150–250 °C) in a one-step separation process. This approach offers the advantages that (i) the mixture of CO_2 and H_2 has already a high pressure, and that (ii) the application of selective H_2-permeable membranes can deliver CO_2 at high pressure, thus reducing compression costs. Therefore, the separation of H_2 from CO_2 is of high interest. Compared with conventional separation methods such as pressure swing adsorption (PSA), membrane separation is the most promising alternative because of its low energy consumption, ease of operation, and cost effectiveness (Rostrup-Nielsen and

* Corresponding authors. Tel.: +49 511762 3175; fax: +49 511 762 1912.
E-mail addresses: huangaisheng@nimte.ac.cn (A. Huang),
juergen.caro@pci.uni-hannover.de (J. Caro).

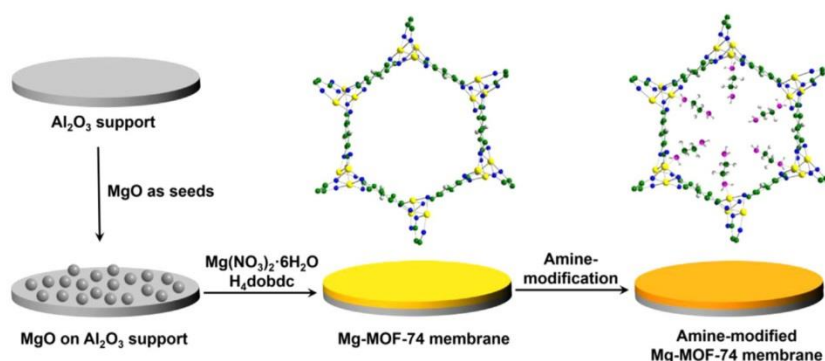# 3 Metal-organic framework membranes for H₂ purification

Fig. 1. Scheme of the synthesis of Mg-MOF-74 membrane on MgO-seeded Al$_2$O$_3$ supports and amine-modification of the as-prepared Mg-MOF-74 membrane.

Rostrup-Nielsen, 2002; Brown et al., 2014; Rodenas et al., 2014). Inorganic membranes like zeolites, Pt-alloys and carbon are of special interest since – different to organic polymer membranes – they can be operated under harsh separation conditions. In the recent 20 years, various hydrogen permselective inorganic membranes have been developed for the separation of H$_2$ from CO$_2$ (Shiflett and Foley, 1999; Uemiya et al., 1991; Ockwig and Nenoff, 2007; de Vos and Verweij, 1998; Hong et al., 2008; Huang et al., 2010). However, the preparation of highly H$_2$-permselective membranes is still a challenge.

Metal–organic frameworks (MOFs), which consist of metal ions or metal oxide clusters interconnected by anionic organic linkers, have attracted intense attention for potential applications in catalysis, separation, gas adsorption and gas storage due to their well-defined pore structure and specific adsorption affinities. (Yaghi et al., 2003; Seo et al., 2000; Ranjan and Tsapatsis, 2009; Lu and Hupp, 2010; Hermes et al., 2005; Zhao et al., 2009; Yoo et al., 2009; Li et al., 2010; Huang et al., 2012; Liu et al., 2013) Magnesium dioxybenzenedicarboxylate (Mg-MOF-74 or Mg/dobdc, also known as CPO-27-Mg, hereafter termed Mg-MOF-74) (Rosi et al., 2005), one of the iso-structural compounds of M$_2$(dhtp)(H$_2$O)$_2 \cdot$ 8H$_2$O (M-MOF-74, M=Ni, Co, Zn, Mg, Mn, dhtp=dihydroxyterephthalic) (Dietzel et al., 2005, 2008, 2006; Britt et al., 2009) is under intense investigation due to its significantly high CO$_2$ adsorption capacities. (Ranjan and Tsapatsis, 2009; Dietzel et al., 2009) Mg-MOF-74 is built up by the linkage of the Mg^{2+} ions with 2,5-dioxido-1,4-benzenedicarboxylate (DOBDC), where the metal ions build a distorted octahedron and the carboxylate groups act as ligand of the metal cations, to form a well-defined hexagonal, one-dimensional (1D) pore structure with a pore diameter of about 11 Å (Caskey et al., 2008; Bétard et al., 2010).

Attributing to the unique feature of its framework structure, where metal cations are bonded with five oxygen atoms to form a square-pyramid coordination, and the unsaturated metal sites in the center of the square plane are free to interact with CO$_2$ molecules, Mg-MOF-74 has a high CO$_2$ adsorption capacity (380 mg CO$_2$/g at room temperature under dry conditions) (Yazaydin et al., 2009). Due to its high gas adsorption ability, many studies have been focused on the gas separation efficiency of Mg-MOF-74 (Mason et al., 2011; Yang et al., 2012; Dietzel et al., 2010; Herm et al., 2012; Yu and Balbuena, 2013; Böhme et al., 2013; Mundstock et al., 2013).

Although there are numerous of studies of Mg-MOF-74 powders on the gas adsorption incl. simulation (Kong et al., 2012; Dzubak et al., 2012; Remy et al., 2013), to date no Mg-MOF-74 membrane with successful gas separation performance has been reported. In a first attempt, a supported Mg-MOF-74 membrane with a mean tilt angle of 31° of the 1D pore system from the

direction perpendicular to the membrane surface could be developed (Mundstock et al., 2013). Lee et al. (2012) have prepared a Ni-MOF-74 membrane by using the layer-by-layer synthesis technique with a H$_2$/CO$_2$ selectivity of 9.1 at 25 °C. Bae and Long (2013) used Mg-MOF-74 nanocrystals in mixed-matrix membranes to improve the CO$_2$/N$_2$ selectivity of the polymer membrane. In the present work, we have developed a new strategy by using magnesium oxide as seeds to synthesize a dense, defect-free Mg-MOF-74 membrane for gas separation. Moreover, the post-synthesis modification with ethylenediamine, which was developed by Choi et al. (2012), was employed to improve its gas separation efficiency (Fig. 1). When preparing supported MOF membranes with a 1D pore system, the orientation of the pores in a suitable direction remains a challenge as addressed for the first time for the Mn formate membrane (Arnold et al., 2007).

2. Experimental

2.1. Materials

Chemicals were used as received. 2,5-dihydroxyterephthalic acid (H$_4$dobdc, 98%, Aldrich), magnesium nitrate hexahydrate (99%, Sigma-Aldrich), magnesium oxide (99.9%, ChemPur), poly-ethyleneimine (branched, avg MW$\sim$25000 by LS, Aldrich), ethylenediamine ($\geq$99%, Sigma-Aldrich), toluene ($\geq$99.8%, Acros), N,N-dimethylformamide (DMF, water $<$50 ppm, Acros), ethanol ($\geq$99.8%, Sigma-Aldrich). Porous α-Al$_2$O$_3$ disks (Fraunhofer Institute IKTS, former HITK/Inocermic, Hermsdorf, Germany: 18 mm in diameter, 1.0 mm in thickness, 70 nm particles in the top layer) were used as supports.

2.2. Preparation of Mg-MOF-74 membranes

2.2.1. Seeding on the support surface

The seeding suspension was prepared by adding 1.5 g MgO and 1.2 g polyethyleneimine (PEI) in 100 mL water. PEI was used to ensure that the MgO particles ($<$50 nm) adhered to the support surface. The suspension was then stirred overnight, and the α-Al$_2$O$_3$ supports were dipped in the seeding suspension by using an automatic dip-coating device with a dip- and withdraw-speed of 300 and 100 mm/min, respectively. The seeded supports were then air-dried at 100 °C overnight.

2.2.2. Synthesis of Mg-MOF-74 membrane

The Mg-MOF-74 membrane was prepared by a solvothermal reaction. Mg(NO$_3$)$_2 \cdot$ 6H$_2$O (0.2375 g, 0.925 mmol) and H$_4$dobdc (0.1011 g, 0.509 mmol) were added to a 15 mL solution which was

prepared by mixing DMF, water and ethanol with a volumetric ratio of 15:1:1. The MgO-coated supports were then placed vertically in a Teflon-lined stainless steel autoclave which was filled with the synthesis solution and then heated at 120 °C in an air-conditioned oven for 24 h. After solvothermal reaction, the Mg-MOF-74 membranes were washed with DMF three times, and then dried in air overnight.

2.2.3. Post-modification of the membrane

The as-prepared Mg-MOF-74 membranes were treated with ethylenediamine (0.5 g in 10 mL toluene) at 110 °C for 2 h under reflux in argon atmosphere. The membranes were then directly removed from the solution and dried in argon at room temperature.

2.3. Characterization

Scanning electron microscopy (SEM) micrographs were taken on a JEOL JSM-6700F with a cold field emission gun operating at 2 kV and 10 μA. The X-ray diffraction (XRD) patterns were recorded at room temperature under ambient conditions with Bruker D8 ADVANCE X-ray diffractometer with Cu$K\alpha$ radiation at 40 kV and 40 mA. FT-IR spectrums were recorded with a Tensor 27 instrument (Bruker) through KBr pellets using Ar/Xe laser line with $\lambda = 633$ nm.

2.4. Evaluation of single gas permeation and mixed gas separation

The as-prepared and amine-modified Mg-MOF-74 membranes synthesized on MgO-seeded α-Al$_2$O$_3$ supports at 120 °C for 24 h were evaluated by single gas permeation and mixture gas separation with Wicke–Kallenbach (Huang et al., 2010). For the measurements of gas separation performances, the supported Mg-MOF-74 membrane was sealed in a permeation module with silicone O-rings. The mounting of the membranes into the housing was done in a glove box under argon to avoid the influence of humid air. According to the Wicke–Kallenbach technique, on both sides of the membrane was atmospheric pressure, N$_2$ was used on the permeate side as sweep gas, except for the measurement of N$_2$ permeance where CH$_4$ was used as sweep gas. The flow rate on the feed side was kept constant for each gas with 50 mL min^{-1}, and the flow rate on the permeate side was kept at 50 mL min^{-1} as well. The fluxes of both the feed and sweep gas were controlled by mass flow controllers, and a calibrated gas chromatograph (HP6890) was used to detect the gas concentrations on the permeate side. The gas chromatograph (GC) was calibrated every week anew with standard gas mixtures. The accuracy of the GC analysis of our H$_2$/CO$_2$ mixture with TCD detection is about ± 5 vol%. The permeance P is obtained by division of the flux by the transmembrane pressure difference, as shown in Eq.(1), where n is the amount of gas in mol, A is the membrane area, t is the permeation time, and Δp is the pressure difference. The separation factor $\alpha_{i,j}$ of a binary mixture permeation is defined as the quotient of the molar ratios of the components (i,j) in the permeate, divided by the quotient of the molar ratio of the components (i,j) in the retentate, as show in Eq. (2). Since less than 1% of the feed gas pass the membrane, the retentate composition is de facto identical with the feed composition.

$$P = \frac{n}{A \times t \times \Delta p} \tag{1}$$

$$\alpha_{i/j} = \frac{y_{i,perm}/y_{j,perm}}{y_{i,ret}/y_{j,ret}} \tag{2}$$

Originally, the Wicke–Kallenbach method has been developed for the determination of CO$_2$ surface diffusion with N$_2$ as sweep gas (Wicke and Kallenbach, 1941). It could happen therefore in our

case that the adsorption of nitrogen on the permeate side of the membrane would falsify the separation factor, also the counter-diffusion of the sweep gas to the feed side can happen. Therefore, to prove the feasibility of the Wicke–Kallenbach technique, gas permeation measurements were also carried out without sweep gas. In one scenario, the feed side was at 1 bar, and the permeate side was at reduced pressure (vacuum). In another case, scenario 2, the pressure on the feed side was 2 bar, and the pressure on the permeate side was 1 bar. It was found that the fluxes of the components of the feed gases were increased in scenario 1 and decreased in scenario 2. This experimental finding can be understood by modified concentrations gradients over the membrane as driving force for permeation. However, the mixture separation factors kept almost unchanged (less than $\pm 5\%$).

We have also excluded another source of experimental errors. Before every gas permeation measurement, the membranes were first activated in situ at 100 °C by using 50 mL min^{-1}H$_2$ in the Wicke–Kallenbach permeation apparatus. All permeation data were collected in steady state of permeation after at least 5 h equilibration time. Sometimes, after 5 h equilibration time we waited for another 12 h. Since there was no change in the permeation data, we assume that the H$_2$/CO$_2$ mixed gas system was in steady state after 5 h.

The apparent activation energy E_{act} of permeation can be calculated according to the Arrhenius equation (Eq. (3)), where P_i is the permeance of component i, P_i^0 is the pre-exponential factor, R is the ideal gas constant (8.314 J mol^{-1} K^{-1}), and T is the temperature in Kelvin. Then E_{act} has been determined through the slope of the plot, which is obtained from the straight line of lnP_i against T^{-1} (Li et al., 2010) (see Section 3.4. Results of single gas permeation and mixture gas separation).

$$P_i = P_i^0 \exp\left(-\frac{E_{act}}{RT}\right) \tag{3}$$

3. Results and discussion

3.1. Effects of the synthesis solution on the membrane preparation

We first tried to grow a Mg-MOF-74 membrane following Caskey's recipe with a solution composition of 3.3 equiv. Mg(NO$_3$)$_2$·6H$_2$O: 1 equiv. H$_4$dobdc (Caskey et al., 2008). However, we failed to prepare a continuous Mg-MOF-74 membrane after solvothermal synthesis for 24 h at 120 °C. As shown in Fig. 2(a), the crystals are too large to intergrow to a continuous layer, and big inter-crystalline gaps are easily observed in the Mg-MOF-74 layer. In order to control the size of the Mg-MOF-74 crystal and to avoid inter-crystalline voids, we modified the chemical composition of the synthesis solution by adjusting the ratio of Mg^{2+} and the dobdc^{4-} linker. By use of the new recipe with a solution composition of 1.8 equiv. Mg(NO$_3$)$_2$·6H$_2$O:1 equiv. H$_4$dobdc, the size of Mg-MOF-74 crystals can be remarkably reduced, and thus the crystals become well intergrown and form a dense Mg-MOF-74 membrane on the alumina support (Fig. 2(b)). XRD pattern of the Mg-MOF-74 membrane further confirms that the as-synthesized layer is a pure Mg-MOF-74 phase after the adjustment of the synthesis solution.

Due to the poor heterogeneous nucleation of Mg-MOF-74 crystals on the alumina support surface, it is difficult to form a continuous Mg-MOF-74 layer simply by in-situ hydrothermal synthesis. Fig. 3(a) shows the Mg-MOF-74 membrane prepared directly on the un-modified alumina support. It can be seen that the crystals don't grow into a dense membrane layer, and inter-crystalline gaps can be observed between the Mg-MOF-74 crystals. Therefore, we tried to improve their intergrowth by pre-coating
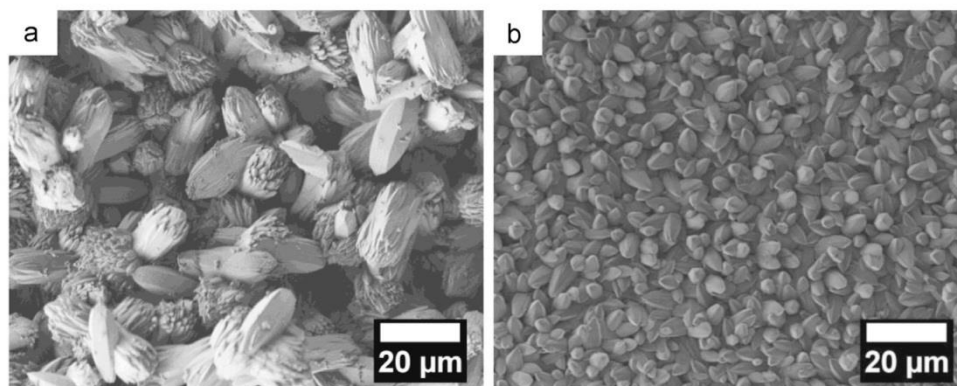
Fig. 2. Top view SEM images of Mg-MOF-74 membranes prepared on α-Al$_2$O$_3$ supports (a) before and (b) after the optimization of the synthesis solution (a cross-section of membrane (b) is shown in Fig. 6(b)).
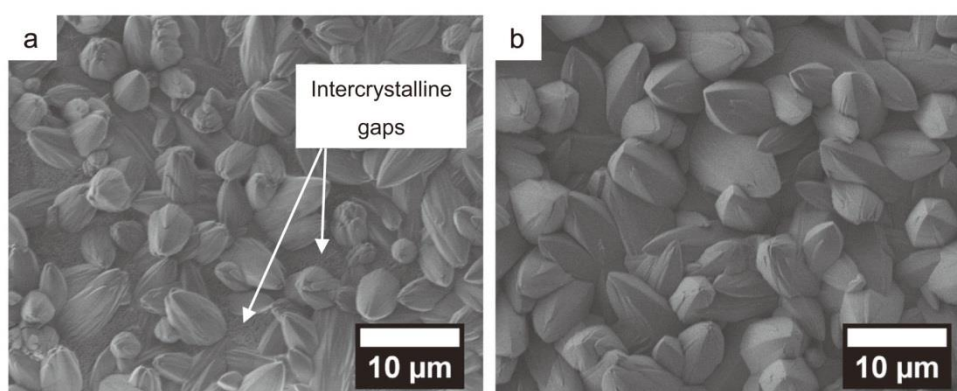

Fig. 3. Top view SEM images of Mg-MOF-74 membranes prepared (a) directly on the α-Al$_2$O$_3$ support and (b) on MgO-seeded α-Al$_2$O$_3$ support at 120 °C for 24 h.

the alumina substrate surface with MgO seeds, which are expected to promote both nucleation and growth of the Mg-MOF-74 layer. As shown in Fig. 3(b), the membranes prepared on MgO-seeded α-Al$_2$O$_3$ supports are indeed dense and no inter-crystalline voids can be observed. In the present work, MgO powders (< 50 nm) were coated on the surface of the support with the help of PEI, and served as nucleation centers which released Mg^{2+} ions into the synthesis solution, thus promoting the following growth of the Mg-MOF-74 crystals. After the synthesis of the membranes, the MgO seeds have transformed fully into the Mg-MOF-74. On the one hand, we cannot see any MgO seeds from the cross-section view of the membrane. On the other hand, the XRD patterns (Fig. 4) also indicate that the peaks of MgO disappeared after the membrane was grown on the support. Before choosing the MgO as seeds, we have also tried using Mg-MOF-74 nano crystals as seeds. However, these membrane preparations on the Mg-MOF-74-seeded supports, either by seeding in DMF or in ethanol, were not successful. The crystals grew too fast to large 10 μm sized crystals, and intercrystalline cracks were unavoidable.

3.2. Effects of the synthesis time

With the secondary growth method, the effect of the synthesis time on the membrane microstructure was followed. Fig. 5 shows SEM images of the Mg-MOF-74 membranes prepared on MgO-seeded α-Al$_2$O$_3$ supports for different synthesis times at 120 °C. As shown in Fig. 5(a), after 12 h, the alumina support surface has been covered by separate Mg-MOF-74 crystals. As the synthesis
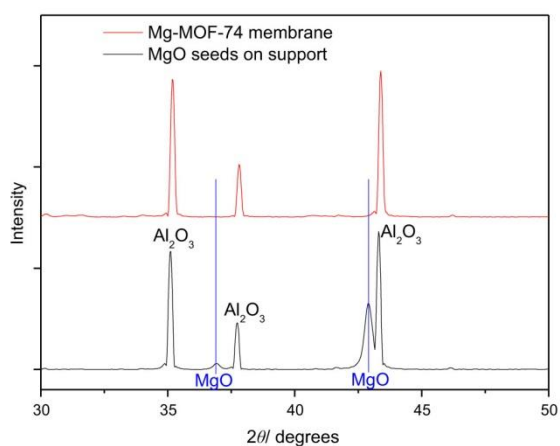
Fig. 4. XRD patterns of MgO seeds on the Al$_2$O$_3$ support and synthesized Mg-MOF-74 membranes.

time increases to 20 h, more Mg-MOF-74 crystals are attached to the substrate and gradually form a thin and continuous layer, although there are still observable inter-crystalline gaps between the Mg-MOF-74 crystals (Fig. 5(b)). A dense Mg-MOF-74 membrane can be formed if the synthesis time increases up to 24 h. It can be seen that the support surface was completely covered by

3 Metal-organic framework membranes for H₂ purification
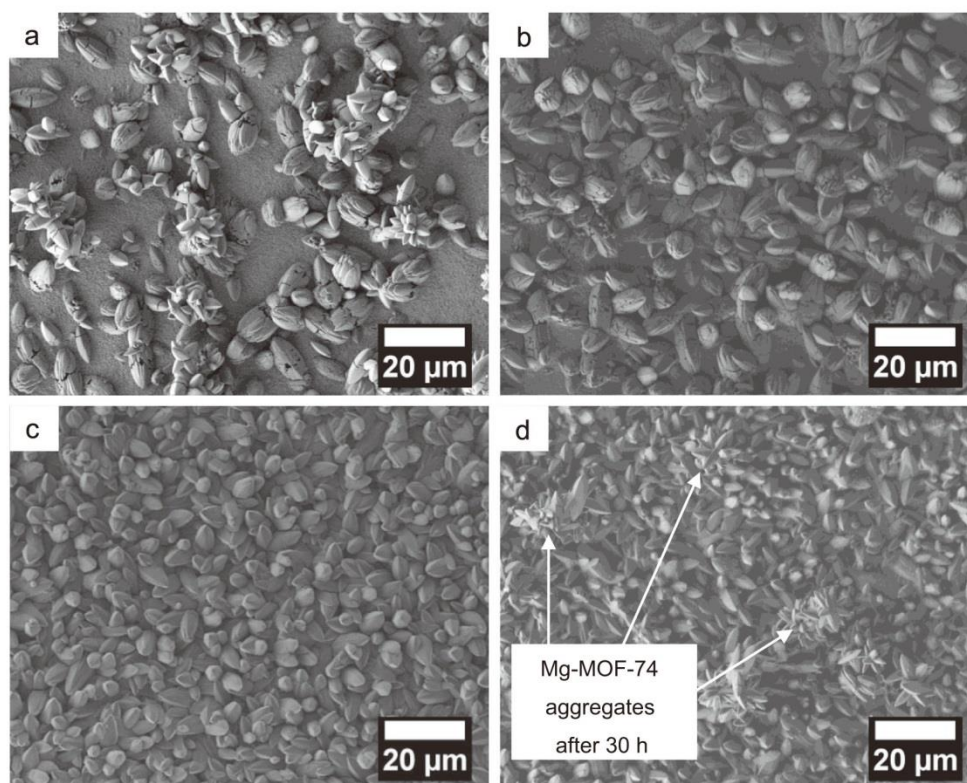
Fig. 5. Top view SEM images of Mg-MOF-74 membranes prepared on MgO-seeded α-Al₂O₃ supports at 120 °C for different synthesis times: (a) 16 h, (b) 20 h, (c) 24 h and (d) 30 h (for the XRD see Fig. 6).

uniform Mg-MOF-74 crystals with a grain size of about 10 μm, and no cracks or other macroscopic defects are visible (Fig. 5(c)). By further extending the synthesis time to 30 h, more Mg-MOF-74 crystals agglomerate on the as-prepared membrane, resulting in a rough membrane surface (Fig. 5(d)). The evolution of the Mg-MOF-74 membrane formation is also characterized by XRD, as shown in Fig. 6, compared with the XRD patterns of Mg-MOF-74 powder (Fig. 6(a)). After an elapse of 16 h, the first peaks of the Mg-MOF-74 crystals have been detected on the support surface (Fig. 6(b)). The heights of the Mg-MOF-74 diffraction peaks relative to the α-Al₂O₃ support increase with synthesis time, which indicates that the thickness of the membrane increases with time. After 24 h, the heights of the Mg-MOF-74 peaks relative to the α-Al₂O₃ support remain unchanged, which indicates that the Mg-MOF-74 crystals completely have covered the surface of the substrate (Fig. 6e). We conclude therefore, that 24 h at 120 °C is the optimum synthesis condition for the preparation of Mg-MOF-74 membranes.

Unfortunately, in this special case, it is impossible to draw from the XRD any conclusions about the crystal and – therefore – channel orientation in the membrane by simply comparing the XRD patterns of the isotropic powder and the membrane (Fig. 6(a) and (e)). This is due to the fact that all dominant peaks in the powder XRD pattern can be allocated to Miller indices $(-1\,2\,0)$, $(0\,3\,0)$ and $(-1\,5\,0)$ with l values of 0. Therefore, the formation of a "crystallographic preferred orientation" (CPO) index (Jeong et al., 2002) gives no information on the channel orientation in l direction. It has to be mentioned, that our XRD of the supported Mg-MOF-74 is similar to the XRD of Ni-MOF-74 and Zn-MOF-74 grown on alumina support (Bétard et al., 2010).
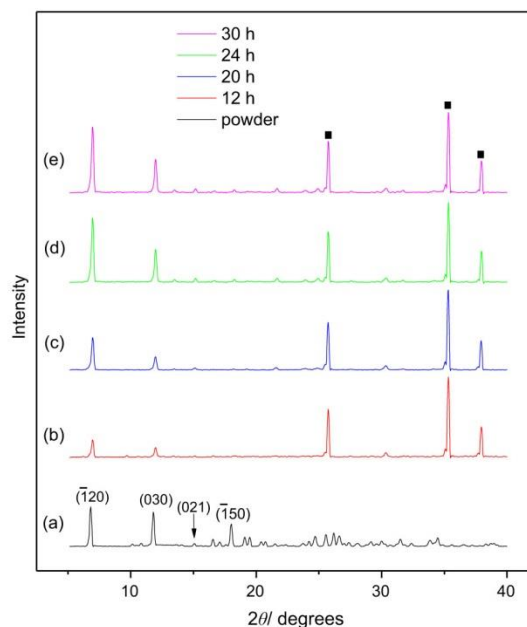

Fig. 6. XRD patterns of Mg-MOF-74 membranes prepared on MgO-seeded α-Al₂O₃ supports at 120 °C for different synthesis times: (b) 16 h, (c) 20 h, (d) 24 h and (e) 30 h, compared with (a) the XRD patterns of Mg-MOF-74 powder. (■): Al₂O₃ support, (not marked): Mg-MOF-74 (for the SEM see Fig. 5).
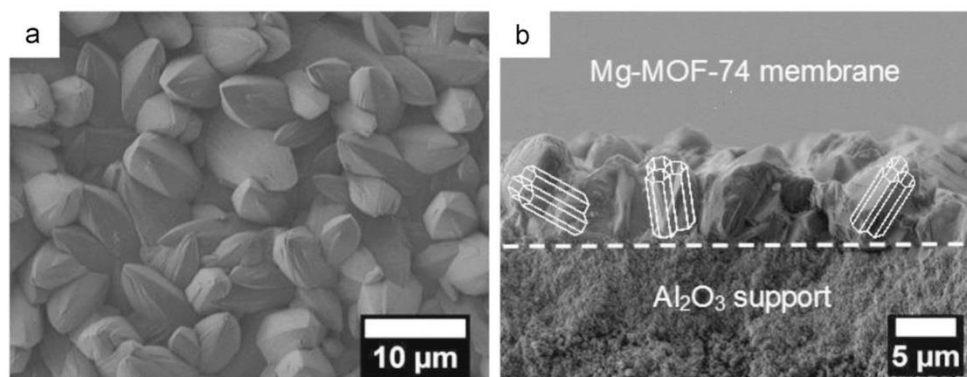
Fig. 7. (a) Top view and (b) cross-section SEM images of the Mg-MOF-74 membrane prepared on MgO-seeded α-Al$_2$O$_3$ supports at 120 °C for 24 h. The white channels in (b) stand for the orientation of the 1 D pores in Mg-MOF-74 crystals.
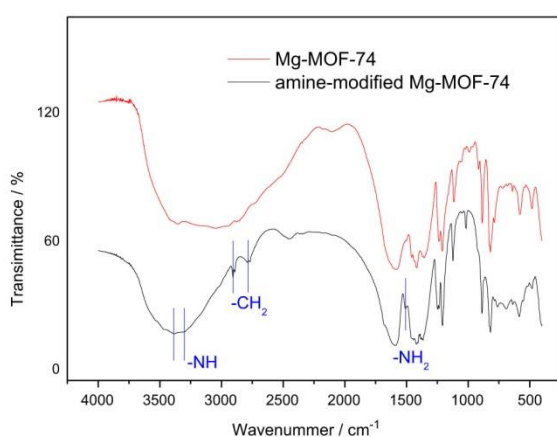

Fig. 8. FT-IR spectra of as-prepared and amine-modified Mg-MOF-74 crystals at room temperature.

Fig. 7 shows the Mg-MOF-74 membrane prepared on a MgO-seeded support for 24 h at 120 °C. From the cross-section view (Fig. 7(b)), the membrane is well intergrown with a thickness of about 10 μm. The shown membrane top view and the cross-section (Fig. 7) indicate that the crystals in the membrane show no statistical arrangement on the support but rather a tilted orientation with their trigonal axis perpendicular to the support. Thanks to this, a major part of all the 1D channels, which run along the *c*-axis of the trigonal structure, should be available for gas separation. Because of this tilted orientation of the *c*-axis, a huge amount of crystal planes and edges without an l ≠ 0 value such as (−1 2 0) and (0 3 0) are present and dominate the XRD as another reason for the above mentioned problematic orientation determination via XRD.

3.3. Effects of the post-modification

The Mg-MOF-74 membranes prepared on MgO-seeded α-Al$_2$O$_3$ supports were then post-modified with ethylenediamine. Fig. 8 shows the FT-IR spectra of non-modified and ethylenediamine-modified Mg-MOF-74 membranes. Both two samples contain a broad band at around 3450 cm^{-1}, which can be assigned to O-H stretching vibrations of adsorbed water, and most of the bands in the region from about 1600 to 800 cm^{-1} are due to the stretching of the aromatic ring. Although lots of bands in the fingerprint region cannot be recognized clearly due to the overlapping of

functional groups, some remarkable bands can still be distinguished. Compared with the FT-IR spectrum of non-modified Mg-MOF-74, the FT-IR spectrum of ethylenediamine-modified Mg-MOF-74 contains characteristic bands at 3370, 3285, 2932, 2814 and 1545 cm^{-1}, which match well with the FT-IR spectrum of ethylenediamine (Bétard et al., 2010; Su et al., 2010; Chang et al., 2003; Sabo et al., 2006). The bands shown at 3370, 3285 and 1545 cm^{-1} are related to NH$_2$ vibration in the primary amine group. The absorptions of the CH$_2$ groups of the aliphatic chains of ethylenediamine are observed at 2935 and 2814 cm^{-1} and are attributed to the asymmetric and symmetric stretching vibrations and deformation vibrations. The presence of –NH$_2$ and –CH$_2$ of the aliphatic chain after the amine modification confirms that ethylenediamine has been successfully grafted onto the Mg-MOF-74 crystals according to the recipe given in Choi et al. (2012). Judged by the SEM image and XRD pattern (not shown here), both the morphology and structure of the Mg-MOF-74 membrane remain unchanged after the amine-modification.

3.4. Results of single gas permeation and mixture gas separation

The single gas permeances on the as-prepared and amine-modified Mg-MOF-74 membranes at 25 °C and 1 bar as a function of the kinetic diameter of the gas molecules are shown in Fig. 9, and the inset gives the mixture separation factors for H$_2$ over other gases from their equimolar mixtures. The single gas permeances and ideal separation factors are summarized in Table 1, and the permeation data for mixed gases are listed in Table 2.

It follows from Fig. 9 to Table 1 that the single gas permeances of the as-prepared Mg-MOF-74 membrane follow the order: H$_2$ > CH$_4$ > N$_2$ > CO$_2$, with a H$_2$ permeance of 1.2 × 10^{-7} mol m^{-2} s^{-1} Pa^{-1}. The mixture separation factor of H$_2$/CO$_2$ with 10.5 is much higher than those of H$_2$/CH$_4$ (5.4) and H$_2$/N$_2$ (3.8) (inset in Fig. 9). This surprising experimental finding can be described by the diffusivity-solubility model of permeation (Krishna and van Baten, 2011). According to the rough estimate "permeation selectivity=adsorption selectivity x diffusion selectivity", a strong CO$_2$ adsorption over H$_2$ could lead to a CO$_2$-selective membrane. As reported previously (Yazaydin et al., 2009), Mg-MOF-74 shows very high CO$_2$ capture ability due to the unsaturated Mg^{2+} site, thus CO$_2$ can be stored in the pore structure Mg-MOF-74 especially. However, this strong CO$_2$ adsorption reduces the CO$_2$ mobility over proportional so that the Mg-MOF-74 membrane shows by the end a H$_2$ over CO$_2$ selectivity.

It is known that CO$_2$ interacts electronically also with amines (Langeroudi et al., 2009; Serna-Guerrero et al., 2008; Planas et al., 2013). It was our concept, therefore, to further enhance the H$_2$/CO$_2$ selectivity by increasing the adsorptive interaction of CO$_2$ by

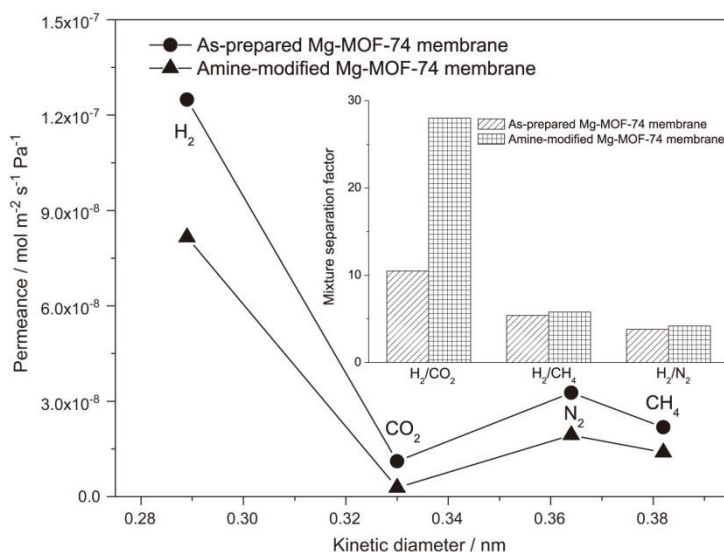# 3 Metal-organic framework membranes for H$_2$ purification

Fig. 9. Single gas permeances on the as-prepared and amine-modified Mg-MOF-74 membranes at 25 °C and 1 bar as a function of the kinetic diameter. The inset shows the mixture separation factors for H$_2$ over other gases from equimolar mixtures (for the temperature dependence of the H$_2$/CO$_2$ mixed gas selectivities see Fig. 10).

Table 1
Single gas permeation performances of the as-prepared and amine-modified Mg-MOF-74 membrane at 25 °C and 1 bar.

Gas$_{ij}$	KC*	As-prepared Mg-MOF-74 membrane			Amine-modified Mg-MOF-74 membrane		
		Permeances (i) (mol m^{-2} s^{-1} Pa^{-1})	Permeances (j) (mol m^{-2} s^{-1} Pa^{-1})	Ideal separation factor	Permeances (i) (mol m^{-2} s^{-1} Pa^{-1})	Permeances (j) (mol m^{-2} s^{-1} Pa^{-1})	Ideal separation factor
H$_2$/CO$_2$	4.7		1.1×10^{-8}	11		2.8×10^{-9}	29
H$_2$/CH$_4$	2.8	1.24×10^{-7}	2.2×10^{-8}	5.6	8.2×10^{-8}	1.4×10^{-8}	5.8
H$_2$/N$_2$	3.7		3.5×10^{-8}	3.5		1.9×10^{-8}	4.3

* KC: Knudsen constant.

Table 2
Mixed gas separation performances of the as-prepared and amine-modified Mg-MOF-74 membrane at 25 °C and 1 bar with 1:1 binary mixtures.

Gas$_{ij}$	KC*	As-prepared Mg-MOF-74 membrane			Amine-modified Mg-MOF-74 membrane		
		Permeances (i) (mol m^{-2} s^{-1} Pa^{-1})	Permeances (j) (mol m^{-2} s^{-1} Pa^{-1})	Mixture separation factor	Permeances (i) (mol m^{-2} s^{-1} Pa^{-1})	Permeances (j) (mol m^{-2} s^{-1} Pa^{-1})	Mixture separation factor
H$_2$/CO$_2$	4.7	1.0×10^{-7}	9.8×10^{-9}	10.5	7.6×10^{-8}	2.7×10^{-9}	28
H$_2$/CH$_4$	2.8	1.1×10^{-7}	2.1×10^{-8}	5.4	7.5×10^{-8}	1.3×10^{-8}	5.8
H$_2$/N$_2$	3.7	1.2×10^{-7}	3.3×10^{-9}	3.8	7.6×10^{-8}	1.8×10^{-8}	4.2

* KC: Knudsen constant.

amine-modification of prepared Mg-MOF-74 membrane. As expected, after the amine-modification, due to the narrowed pore size of MOF-74 the single gas permeances of H$_2$, CH$_4$ and N$_2$, decreased slightly by only a factor of 1.5, 1.6, and 1.8, respectively. However, the CO$_2$ permeance has been reduced by a factor of 4 from 1.1×10^{-8} mol m^{-2} s^{-1} Pa^{-1} to 2.8×10^{-9} mol m^{-2} s^{-1} Pa^{-1}. As a result, the mixed separation factors of H$_2$ against CH$_4$ and N$_2$ remained almost unchanged after the amine-functionalization, but the mixture separation factor of H$_2$/CO$_2$ dramatically increased from 10.5 to 28.

Due to the large pore size of about 11 Å, the size-based molecular sieve effect of Mg-MOF-74 was negligible. After the amine-modification, the pore size of the membrane was narrowed, but the pores are still large enough for the passage of small molecules like H$_2$, CH$_4$, N$_2$ and CO$_2$. Therefore, the mixture separation factors of H$_2$/CH$_4$ and H$_2$/N$_2$ do not change much when the membrane is modified by the diamine. On the contrary, the surface modification with amine groups has enhanced the strong adsorption of CO$_2$ molecules, which in turn reduces the permeance of CO$_2$, leading to an increase of the separation performance of H$_2$ over CO$_2$. As reported previously (Choi et al., 2012), one side of the amine group of ethylenediamine is bound to the open coordination sites of the Mg in the framework structure by direct ligation, while the amine group on the other side remains free in space (Hwang et al., 2008). Fig. 10 shows the mixture separation factors for equimolar H$_2$/CO$_2$ mixtures and the single
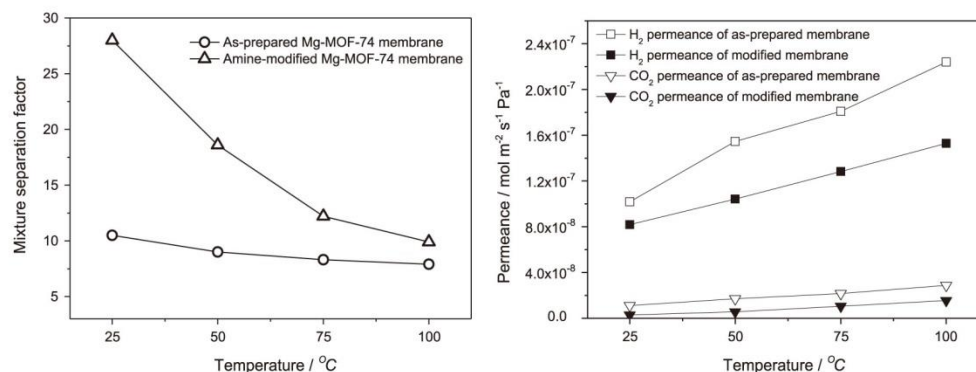
61

Fig. 10. Mixture separation factors for H_2/CO_2 from equimolar mixture (left) and single gas permeances of H_2 and CO_2 (right) on the as-prepared and amine-modified Mg-MOF-74 membranes at 1 bar as a function of temperature.

Table 3
Activation energies of H_2 and CO_2 permeation for Mg-MOF-74 membrane before and after amine-modification.

	Activation energy E_{act} (kJ mol^{-1})
H_2 before amine-modification	7.65
H_2 after amine-modification	7.71
CO_2 before amine-modification	11.4
CO_2 after amine-modification	20.9

gas permeances of H_2 and CO_2 on the as-prepared and amine-modified Mg-MOF-74 membranes at 1 bar as a function of temperature from 25 to 100 °C. For both the as-synthesized and amino-functionalized Mg-MOF-74 membranes the separation factors reduce gradually with increasing temperature. However, the reduction of the separation factors for the modified Mg-MOF-74 membrane was more remarkable since rising temperature has reduced the preferential adsorption of CO_2 on the amine groups. This trend is a good argument, that the interplay of adsorption and diffusion dominates the gas separation performance, rather than the size-based molecular sieving mechanism. As temperature increases, less CO_2 becomes adsorbed and more gas molecules can go through in the resulting free volume, leading to an increase in the hydrogen permeance and a reduction of the H_2/CO_2 selectivity. The grafted ethylenediamine was also proven to be stable at 100 °C, since the heating process of 1 °C min^{-1} from 25 to 100 °C is also reversible. The apparent activation energies E_{act} for H_2 and CO_2 permeation before and after modification, which are shown in Table 3, were obtained by fitting the data between 25 and 100 °C. Whereas the activation energy of H_2 permeation remains unchanged by the amination process, the activation energy of CO_2 has been almost doubled. This experimental finding can be explained by both steric effects (pore narrowing) and energetic effects (amine-CO_2 interaction). Our activation energies of H_2 and CO_2 permeation are similar to literature data of other microporous membranes for H_2/CO_2 separation, like CVD modified DDR zeolite membrane developed by Kanezashi et al. (2008) (the activation energy for H_2 and CO_2 are 9.62 and 12.8, respectively), but different to CVI modified silica membrane by Koutsonikolasa et al. (2009) (the activation energy for H_2 and CO_2 are 15.8 and 7.4, respectively).

As shown in a Robeson plot (Robeson 1991; Robeson 2008) in Fig. 11, the H_2/CO_2 selectivities and H_2 permeances of both the as-synthesized and the amine-modified Mg-MOF-74 membranes exceed by far the "upper-bound" for polymeric membranes, and the H_2/CO_2 selectivity after amine-modification increases with

Fig. 11. H_2/CO_2 selectivity versus H_2 permeability for as-prepared and amine-modified Mg-MOF-74 membranes at 25 °C and 1 bar, compared with the previously reported MOF membranes. The upper bound lines for polymeric membranes are based on Robeson (1991) and Robeson (2008).

only a slight decrease of the permeability. Furthermore, also compared with other MOF membranes, our amine-modified MOF-74 membrane is a promising material for the H_2/CO_2 separation (Fig. 11 and Table 4). As shown in Fig. 11, compared with the existing polymer membranes, the amine-modified MOF-74 membrane exhibits a both much higher H_2/CO_2 selectivity and H_2 permeability which recommends amine-modified MOF-74 powder also a promising candidate for the preparation of mixed matrix membranes (MMM) (Mahajan and Koros, 2000). The MMM concept avoids the difficulty to prepare and scale up pure supported MOF membranes and can be produced more easily as spiral wound or hollow fiber module, compared to the pure MOF membranes.

As a proof of the good reproducibility of the MgO-seeding synthesis method and amine-modification, Table 5 shows the results of gas permeation performance for four tested amine-modified Mg-MOF-74 membranes prepared following identical synthesis method. The selectivities of H_2/CO_2 and H_2 and CO_2 permeance at room temperature do not scatter more than $\pm 10\%$, which indicates the good reproducibility of the Mg-MOF-74 membranes.

Table 4

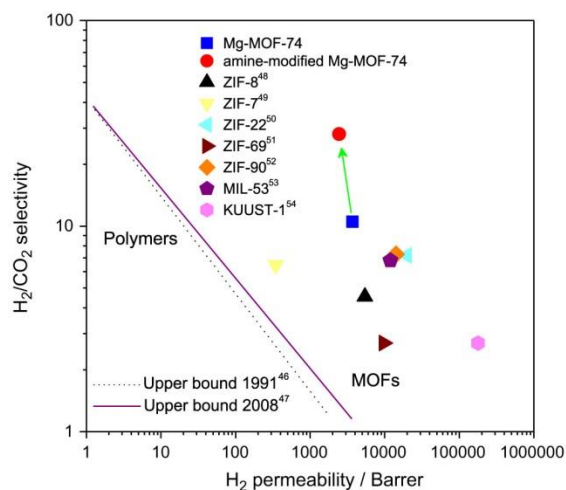H$_2$/CO$_2$ selectivity versus H$_2$ permeability for as-prepared and amine-modified Mg-MOF-74 membranes at 25 °C and 1 bar, compared with the previously reported MOF membranes.

MOF membranes	Thickness (μm)	H$_2$ permeance (mol m^{-2} s^1 Pa^1)	H$_2$ permeability* (Barrer)	H$_2$/CO$_2$ selectivity	References
Mg-MOF-74	10	1.2×10^{-07}	3.7×10^3	10.5	This study
Amine-modified Mg-MOF-74	10	8.2×10^{-08}	2.5×10^3	28	This study
ZIF-8	30	6.0×10^{-08}	5.4×10^3	4.5	Bux et al. (2009)
ZIF-7	1.5	7.7×10^{-08}	3.5×10^2	6.5	Li et al. (2010)
ZIF-22	40	1.7×10^{-07}	2.0×10^4	7.2	Huang et al. (2010)
ZIF-69	50	6.5×10^{-08}	9.7×10^3	2.7	Liu et al. (2010)
ZIF-90	20	2.4×10^{-07}	1.4×10^4	7.3	Huang et al. (2010)
MIL-53	8	5.0×10^{-08}	1.2×10^4	6.8	Hu et al. (2011)
KUUST-1	60	1.0×10^{-06}	1.8×10^5	2.7	Guo et al. (2009)

* Permeability is calculated as the membrane permeance multiplied by the membrane thickness. 1 Barrer = 3.348×10^{-16} mol m/(m^2 s Pa).

Table 5

Gas permeances of H$_2$ and CO$_2$ and mixture separation factors of H$_2$/CO$_2$ from equimolar mixtures at room temperature and 1 bar of 4 tested Mg-MOF-74 membranes.

	H$_2$ permeance (mol m^{-1} s^{-1} Pa^{-1})	CO$_2$ permeance (mol m^{-2} s^{-1} Pa^{-1})	Mixture separation factor H$_2$/CO$_2$
1	8.2×10^{-8}	2.8×10^{-9}	28
2	9.0×10^{-8}	3.1×10^{-9}	30
3	7.4×10^{-8}	2.8×10^{-9}	25
4	7.5×10^{-8}	2.9×10^{-9}	26

4. Conclusion

Phase-pure and compact Mg-MOF-74 membranes have been prepared successfully on MgO-seeded porous Al$_2$O$_3$ supports at 120 °C for 24 h after optimization of the synthesis solution. The mixture separation factor of H$_2$/CO$_2$ was much higher than those of H$_2$/CH$_4$ and H$_2$/N$_2$, especially at lower temperature. After amine-functionalization of the Mg-MOF-74 membrane by using ethylenediamine, the separation performance of H$_2$/CO$_2$ was remarkably enhanced and the mixture separation performance increased from 10.5 to 28 at room temperature. This increase is ascribed to two effects: (i) One amino group of the diamine is docked to the open Mg site, thus the diamine narrows the effective pore size which retards for steric reasons the carbon dioxide (kinetic diameter 3.3 Å) permeation stronger than the hydrogen one (2.9 Å), and (ii) the other amino group interacts with CO$_2$ thus reducing its mobility.

Acknowledgements

References

Arnold, M., Kortunov, P., Jones, D., Nedellec, Y., Kärger, J., Caro, J., 2007. Oriented crystallization on supports and anisotropic mass transport of the metal organic framework manganese formate. Eur. J. Inorg. Chem. 1, 60–64.

Bae, T., Long, J.R., 2013. CO2/N2 separations with mixed-matrix membranes containing Mg2(dobdc) nanocrystals. Energy Environ. Sci. 6, 3565–3569.

Bétard, A., Zander, D., Fischer, R.A., 2010. Dense and homogeneous coatings of CPO-27-M type metal–organic frameworks on alumina substrates. CrystEngComm 12, 3768–3772.

Böhme, U., Barth, B., Paula, C., Kuhnt, A., Schwieger, W., Mundstock, A., Caro, J., 2013. Martin Hartmann, Ethene/ethane and propene/propane separation via the olefin and paraffin selective metal–organic framework adsorbents CPO-27 and ZIF-8. Langmuir 29, 8592–8600.

Britt, D., Furukawa, H., Wang, B., Glover, T.G., Yaghi, O.M., 2009. Highly efficient separation of carbon dioxide by a metal–organic framework replete with open metal sites. Proc. Natl. Acad. Sci. 106, 20637–20640.

Brown, A.J., Brunelli, N.A., Eum, K., Rashidi, F., Johnson, J.R., Koros, W.J., Jones, C.W., Nair, S., 2014. Interfacial microfluidic processing of metal–organic framework hollow fiber membranes. Science 345, 72–75.

Bux, H., Liang, F., Li, Y., Cravillon, J., Wiebcke, M., Caro, J., 2009. Zeolitic imidazolate framework membrane with molecular sieving properties by microwave-assisted solvothermal synthesis. J. Am. Chem. Soc. 131, 16000–16001.

Caskey, S.R., Wong-Foy, A.G., Matzger, A.J., 2008. Dramatic tuning of carbon dioxide uptake via metal substitution in a coordination polymer with cylindrical pores. J. Am. Chem. Soc. 130, 10870–10871.

Chang, A.C.C., Chuang, S.S.C., Gray, M., Soong, Y., 2003. In-situ infrared study of CO2 adsorption on SBA-15 grafted with gamma-(aminopropyl)triethoxysilane. Energy Fuels 17, 468–473.

Choi, S., Watanabe, T., Bae, T., Sholl, D.S., Jones, C.W., 2012. Modification of the Mg/DOBDC MOF with amines to enhance CO2 adsorption from ultradilute gases. J. Phys. Chem. Lett. 3, 1136–1141.

de Vos, R.M., Verweij, H., 1998. High-selectivity, high-flux silica membranes for gas separation. Science 279, 1710–1711.

Dietzel, P.D.C., Besikiotis, V., Blom, R., 2009. Application of metal–organic frameworks with coordinatively unsaturated metal sites in storage and separation of methane and carbon dioxide. J. Mater. Chem. 19, 7362–7370.

Dietzel, P.D.C., Georgiev, P.A., Eckert, J., Blom, R., Strässle, T., Unruh, T., 2010. Interaction of hydrogen with accessible metal sites in the metal–organic frameworks M2(dhtp) (CPO-27-M; M=Ni, Co, Mg). Chem. Commun. 46, 4962–4964.

Dietzel, P.D.C., Johnsen, R.E., Blom, R., Fjellvag, H., 2008. Structural changes and coordinatively unsaturated metal atoms on dehydration of honeycomb analogous microporous metal–organic frameworks. Chem. A Eur. J. 14, 2389–2397.

Dietzel, P.D.C., Morita, Y., Blom, R., Fjellvag, H., 2005. An in situ high-temperature single-crystal investigation of a dehydrated metal–organic framework compound and field-induced magnetization of one-dimensional metaloxygen chains. Angew. Chem. Int. Ed. 44, 6354–6358.

Dietzel, P.D.C., Panella, B., Hirscher, M., Blom, R., Fjellvag, H., 2006. Hydrogen adsorption in a nickel based coordination polymer with open metal sites in the cylindrical cavities of the desolvated framework. Chem. Commun. 9, 959–961.

Dzubak, A.L., Lin, L., Kim, J., Swisher, J.A., Poloni, R., Maximoff, S.N., Smit, B., Gagliardi, L., 2012. Ab initio carbon capture in open-site metal–organic frameworks. Nat. Chem. 4, 810–816.

Guo, H., Zhu, G., Hewitt, I.J., Qiu, S., 2009. "Twin copper source" growth of metal–organic framework membrane: Cu3(BTC)2 with high permeability and selectivity for recycling H2. J. Am. Chem. Soc. 131, 1646–1647.

Herm, Z.R., Krishna, R., Long, J.R., 2012. CO2/CH4, CH4/H2 and CO2/CH4/H2 separations at high pressures using Mg2(dobdc). Microporous Mesoporous Mater. 151, 481–487.

Hermes, S., Schroder, F., Chelmowski, R., Woll, C., Fischer, R.A., 2005. Selective nucleation and growth of metal–organic open framework thin films on patterned COOH/CF3-terminated self-assembled monolayers on Au(111). J. Am. Chem. Soc. 127, 13744–13745.

Hong, M., Li, S., Falconer, J.L., Noble, R.D., 2008. Hydrogen purification using a SAPO-34 membrane. J. Membr. Sci. 307, 277–283.

Hu, Y., Dong, X., Nan, J., Jin, W., Ren, X., Xu, N., Lee, Y.M., 2011. Metal–organic framework membranes fabricated via reactive seeding. Chem. Commun. 47, 737–739.

Huang, A., Bux, H., Steinbach, F., Caro, J., 2010. Molecular-sieve membrane with hydrogen permselectivity: ZIF-22 in LTA topology prepared with 3-aminopropyltriethoxysilane as covalent linker. Angew. Chem. Int. Ed. 49, 4958–4961.

Huang, A., Dou, W., Caro, J., 2010. Steam-stable zeolitic imidazolate framework ZIF-90 membrane with hydrogen selectivity through covalent functionalization. J. Am. Chem. Soc. 132, 15562–15564.

Huang, A., Liang, F., Steinbach, F., Caro, J., 2010. Preparation and separation properties of LTA membranes by using 3-aminopropyltriethoxysilane as covalent linker. J. Membr. Sci. 350, 5–9.

Huang, A., Wang, N., Kong, C., Caro, J., 2012. Organosilica-functionalized zeolitic imidazolate framework ZIF-90 membrane with high gas-separation performance. Angew. Chem. Int. Ed. 51, 10551–10555.

Hwang, Y.K., Hong, D.Y., Chang, J.S., Jhung, S.H., Seo, Y.K, Kim, J., Vimont, A., Daturi, M., Serre, C., Ferey, G., 2008. Amine grafting on coordinatively unsaturated metal centers of MOFs: consequences for catalysis and metal encapsulation. Angew. Chem. Int. Ed. 47, 4144–4148.

Jeong, H.K., Krohn, J., Sujaoti, K., Tsapatsis, M., 2002. Oriented molecular sieve membranes by heteroepitaxial growth. J. Am. Chem. Soc. 124, 12966–12968.

Kanezashi, M., O' Brien-Abraham, J., Lin, Y.S., Suzuki, K., 2008. Gas permeation through DDR-type zeolite membranes at high temperatures. AIChE J. 54, 1478–1486.

Kong, X., Scott, E., Ding, W., Mason, J.A., Long, J.R., Reimer, J.A., 2012. CO2 dynamics in a metal–organic framework with open metal sites. J. Am. Chem. Soc. 134, 14341–14344.

Koutsonikolasa, D., Kaldisb, S., Sakellaropoulos, G.P., 2009. A low-temperature CVI method for pore modification of sol–gel silica membranes. J. Membr. Sci. 342, 131–137.

Krishna, R., van Baten, J.M., 2011. In silico screening of metal–organic frameworks in separation applications. Phys. Chem. Chem. Phys. 13, 10593–10616.

Langeroudi, E.G., Kleitz, F., Iliuta, M.C., Larachi, F., 2009. Grafted amine/CO2 interactions in (Gas-)liquid–solid adsorption/absorption equilibria. J. Phys. Chem. C 113 (52), 21866–21876.

Lee, D., Li, Q., Kim, H., Lee, K., 2012. Preparation of Ni-MOF-74 membrane for CO2 separation by layer-by-layer seeding technique. Microporous Mesoporous Mater. 163, 169–177.

Li, Y., Bux, H., Feldhoff, A., Li, G., Yang, W., Caro, J., 2010. Controllable synthesis of metal–organic frameworks: from MOF nanorods to oriented MOF membranes. Adv. Mater. 22, 3322–3326.

Li, Y., Liang, F., Bux, H., Feldhoff, A., Yang, W., Caro, J., 2010. Molecular sieve membrane: supported metal–organic framework with high hydrogen selectivity. Angew. Chem. Int. Ed. 49, 548–551.

Li, Y., Liang, F., Bux, H., A., Yang, W., Caro, J., 2010. Zeolitic imidazolate framework ZIF-7 based molecular sieve membrane for hydrogen separation. J. Membr. Sci. 354, 48–54.

Liu, Q., Wang, N., Caro, J., Huang, A., 2013. Bio-inspired polydopamine: a versatile and powerful platform for covalent synthesis of molecular sieve membranes. J. Am. Chem. Soc. 135, 17679–17682.

Liu, Y., Hu, E., Khan, E.A., Lai, Z., 2010. Synthesis and characterization of ZIF-69 membranes and separation for CO2/CO mixture. J. Membr. Sci. 353, 36–40.

Lu, G., Hupp, J.T., 2010. Metal–organic frameworks as sensors: a ZIF-8 based Fabry–Perot device as a selective sensor for chemical vapors and gases. J. Am. Chem. Soc. 132, 7832–7833.

Mahajan, R., Koros, W.J., 2000. Factors controlling successful formation of mixed-matrix gas separation materials. Ind. Eng. Chem. Res. 39, 2692–2696.

Mason, J.A., Sumida, K., Herm, Z.R., Krishna, R., Long, J.R., 2011. Evaluating metal–organic frameworks for post-combustion carbon dioxide capture via temperature swing adsorption. Energy Environ. Sci. 4, 3030–3040.

Mundstock, A., Böhme, U., Barth, B., Hartmann, M., Caro, J., 2013. Propylene/propane separation in fixed-Bed adsorber and membrane permeation. Chem. Ing. Tech. 85, 1694–1699.

Ockwig, N.W., Nenoff, T.M., 2007. Membranes for hydrogen separation. Chem. Rev. 107, 4078–4110.

Planas, N., Dzubak, A.L., Poloni, R., Chiang, L., McManus, A., McDonald, T.M., Neaton, J.B., Lange, J.R., Smit, B., Gagliardi, L., 2013. The mechanism of carbon dioxide adsorption in an alkylamine-functionalized metal–organic framework. J. Am. Chem. Soc. 135, 7402–7405.

Ranjan, R., Tsapatsis, M., 2009. Microporous metal organic framework membrane on porous support using the seeded growth method. Chem. Mater. 21, 4920–4924.

Remy, T., Peter, S.A., Van der Perre, S., Valvekens, P., de Vos, D.E., Baron, G.V., Denayer, J.F.M., 2013. Selective dynamic CO2 separations on Mg-MOF-74 at low pressures: a detailed comparison with 13X. J. Phys. Chem. C 117, 9301–9310.

Robeson, L.M., 1991. Correlation of separation factor versus permeability for polymeric membranes. J. Membr. Sci. 62, 165–185.

Robeson, L.M., 2008. The upper bound revisited. J. Membr. Sci. 320, 390–400.

Rodenas, T., van Dalen, M., García-Pérez, E., Serra-Crespo, P., Zornoza, B., Kapteijn, F., Gascon, J., 2014. Visualizing MOF mixed matrix membranes at the nanoscale: towards structure-performance relationships in CO2/CH4 separation over NH2-MIL-53(Al)@PI. Adv. Funct. Mater. 24, 249–256.

Rosi, N.L., Kim, J., Eddaoudi, M., Chen, B.L., O'Keeffe, M., Yaghi, O.M., 2005. Rod packings and metal–organic frameworks constructed from rod-shaped secondary building units. J. Am. Chem. Soc. 127, 1504–1518.

Rostrup-Nielsen, J.R., Rostrup-Nielsen, T., 2002. Large-scale hydrogen production. CATTECH 6, 150–159.

Sabo, M., Boehlmannb, W., Kaskel, S., 2006. Titanium terephthalate (TT-1) hybrid materials with high specific surface area. J. Mater. Chem. 16, 2354–2357.

Seo, J.S., Whang, D., Lee, H., Jun, S.I., Oh, J., Jeon, Y.J., Kim, K., 2000. A homochiral metal–organic porous material for enantioselective separation and catalysis. Nature 404, 982–986.

Serna-Guerrero, R., Da'na, E., Sayari, A., 2008. New insights into the interactions of CO2 with amine-functionalized silica. Ind. Eng. Chem. Res. 47, 9406–9412.

Shiflett, M.B., Foley, H.C., 1999. Ultrasonic deposition of high-selectivity nanoporous carbon membranes. Science 285, 1902–1905.

Su, F., Lu, C., Kuo, S., Zeng, W., 2010. Adsorption of CO2 on amine-functionalized Y-type zeolites. Energy Fuels 24, 1441–1448.

Uemiya, S., Matsuda, T., Kikuchi, E., 1991. Hydrogen permeable palladium-silver alloy membrane supported on porous ceramics. J. Membr. Sci. 56, 315–325.

Wicke, E., Kallenbach, R., 1941. Die Oberflächendiffusion von Kohlendioxyd in aktiven Kohlen 97, 135-151.

Yaghi, O.M., O'Keeffe, M., Ockwig, N.W., Chae, H.K., Eddaoudi, M., Kim, J., 2003. Reticular synthesis and the design of new materials. Nature 423, 705–714.

Yang, D., Cho, H., Kim, J., Yang, S., Ahn, W., 2012. CO2 capture and conversion using Mg-MOF-74 prepared by a sonochemical method. Energy Environ. Sci. 5, 6465–6473.

Yazaydin, A.Ö., Snurr, R.Q., Park, T., Koh, K., Liu, J., LeVan, M.D., Benin, A.I., Jakubczak, P., Lanuza, M., Galloway, D.B., Low, J.J., Willis, R.R., 2009. Screening of metal–organic frameworks for carbon dioxide capture from flue gas using a combined experimental and modeling approach. J. Am. Chem. Soc. 131, 18198–18199.

Yoo, Y., Lai, Z., Jeong, H., 2009. Fabrication of MOF-5 membranes using microwave-induced rapid seeding and solvothermal secondary growth. Microporous Mesoporous Mater. 123, 100–106.

Yu, J., Balbuena, P.B., 2013. Water effects on postcombustion CO2 capture in Mg-MOF-74. J. Phys. Chem. C 117 (7), 3383–3388.

Zhao, Z., Li, Z., Lin, Y., 2009. Adsorption and diffusion of carbon dioxide on metal–organic framework (MOF-5). Ind. Eng. Chem. Res. 48, 10015–10020.

3.3 Polydopamine-based synthesis of zeolite imidazolate framework ZIF-100 membrane with high H$_2$/CO$_2$ selectivity

Nanyi Wang, Yi Liu, Zhiwei Qiao, Lisa Diestel, Jian Zhou, Aisheng Huang and Jürgen Caro

CrossMark
click for updates

Polydopamine-based synthesis of a zeolite imidazolate framework ZIF-100 membrane with high H$_2$/CO$_2$ selectivity

Nanyi Wang,*[a] Yi Liu,[a] Zhiwei Qiao,[b] Lisa Diestel,[a] Jian Zhou,[b] Aisheng Huang*[c] and Jürgen Caro[a]

A highly permselective ZIF-100 molecular sieve membrane has been prepared on a polydopamine (PDA)-modified support. Attributed to the formation of strong covalent and non-covalent bonds between PDA and ZIF-100, the ZIF-100 nutrients are attracted and bound to the support surface, thus promoting the growth of well-intergrown and phase-pure ZIF-100 membranes. The developed ZIF-100 membranes show high H$_2$/CO$_2$ selectivity due to the outstanding CO$_2$ adsorption capacity of ZIF-100.

1. Introduction

The growing demand for energy and environmental issues has promoted the concept of "hydrogen economy".[1] Currently, up to 90% of hydrogen is produced by steam-methane reforming (SMR) followed by the water–gas shift (WGS). Before it can be used in fuel cells, H$_2$ has to be purified from the SMR gas mixture which mainly contains CO$_2$.[2] Moreover, H$_2$-selective membranes are also desired in the pre-combustion technology of CO$_2$ sequestration.[3] Compared with traditional separation methods like pressure swing adsorption (PSA) and cryogenic distillation, membrane-based separation techniques have attracted significant attention due to lower energy consumption and investment cost.[4] In the recent 20 years, inorganic membranes such as zeolite membranes,[5] Pd-based membranes,[6,7] amorphous microporous silica membranes[8] and carbon membranes[9] have been developed for the separation of H$_2$ from CO$_2$.

Recent efforts have been devoted to the fabrication of supported metal–organic framework (MOF) membranes due to their highly diversified structures and specific adsorption affinities.[10–17] In particular, great attention has been paid to zeolite imidazolate framework (ZIF) membranes since 2009 because of their relatively high stability and tunable pore size.[18,19] So far, a series of ZIF membranes with small pore sizes, including ZIF-7 (0.30 nm),[20] ZIF-22 (0.30 nm),[21] ZIF-8

(0.34 nm),[22–24] ZIF-90 (0.35 nm)[25–27] and ZIF-95 (0.37 nm),[28] were successively developed for gas separation. Despite much progress in the development of H$_2$-selective ZIF membranes, the development of thermally stable ZIF membranes with a high H$_2$/CO$_2$ selectivity is still desired.

Yaghi and co-workers have developed a novel ZIF-100 structure with the composition Zn$_{20}$(cbIM)$_{39}$(OH) through the reaction of Zn(O$_3$SCF$_3$)$_2$ with 5-chlorobenzimidazole (cbIM).[29] ZIF-100 was found to have a rather complex structure. The unit cell of ZIF-100 has a MOZ topology, which is constructed from 7524 atoms. This MOZ cage has a large inner sphere with a diameter of 35.6 Å and a constricted window aperture of only 3.35 Å. ZIF-100 shows a high affinity and capacity to CO$_2$, which results in an outstanding CO$_2$ uptake.[29] It is reported that ZIF-100 not only has high CO$_2$ capacity, but also a high thermal stability up to 500 °C.[29] It is worth mentioning that the high CO$_2$ adsorption capacity as found for MOFs with accessible metal ions like MIL-53[30] or MOF-74[31] is not common for ZIFs. However, the adsorption affinity of ZIF-100 for CO$_2$ outperforms that of ZIF-95 and BPL carbon,[32] which is widely used in industry for gas separation.

Although there have been a few studies of ZIF-100 powders on gas adsorption,[33] to date no ZIF-100 membrane with gas separation performance has been reported. In this study, we report the synthesis of a dense ZIF-100 membrane by covalent modification of the substrate surface using polydopamine (PDA), as shown in Fig. 1. During this pre-modification process, dopamine can easily polymerize into PDA, and stick on different kinds of organic and inorganic material surfaces.[34] Then the PDA-modified surface can be used as a versatile platform for further reactions.[35–37] Recently, PDA-based synthesis of ZIF-8 and zeolite LTA membranes has been developed to improve their gas separation performance and reproducibility.[38–40] It can be expected, therefore, that ZIF-100 membranes prepared on

[a]Institute of Physical Chemistry and Electrochemistry, Leibniz University of Hannover, Callinstrasse 22, 30167 Hannover, Germany. E-mail: nanyi.wang@pci.uni-hannover.de

[b]School of Chemistry and Chemical Engineering, Guangdong Provincial Key Lab for Green Chemical Product Technology, South China University of Technology, Guangzhou 510640, China

[c]Institute of New Energy Technology, Ningbo Institute of Material Technology and Engineering, CAS, 1219 Zhongguan Road, 315201 Ningbo, P. R. China. E-mail: huangaisheng@nimte.ac.cn
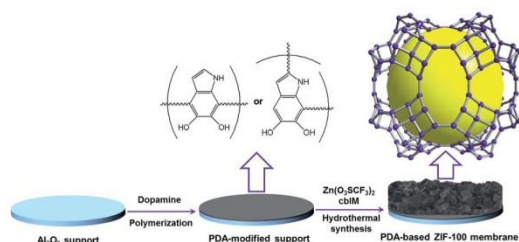
4722 | *J. Mater. Chem. A*, 2015, **3**, 4722–4728

This journal is © The Royal Society of Chemistry 2015

Fig. 1 Schematic diagram of the synthesis of ZIF-100 membranes on a polydopamine-modified Al$_2$O$_3$ support.

PDA-functionalized supports will show higher gas separation performances and reproducibility of membrane preparation.

2. Experimental

2.1. Materials

Chemicals were used as received: zinc trifluoromethane-sulfonate (98%, Aldrich), 5-chlorobenzimidazole (cbIM, 98%, Abcr), N,N-dimethylformamide (DMF, water < 50 ppm, Acros), dopamine hydrochloride (Sigma), and tris(hydroxymethyl)aminomethane (Tris–HCl, ≥99.8%, Sigma-Aldrich). Porous α-Al$_2$O$_3$ disks (Fraunhofer Institute IKTS, former HITK/Inocermic, Hermsdorf, Germany: 18 mm in diameter, 1.0 mm in thickness, 70 nm particles in the top layer) were used as supports.

2.2. Polydopamine (PDA) modification of the support surface

The PDA modification of the support surface was done according to a previous procedure.[38–40] Dopamine hydrochloride (2 mg mL^{-1}) was dissolved in 10 mM Tris–HCl (pH 8.5) in an open air vessel (diameter: 180 mm). And then the porous α-Al$_2$O$_3$ disks were placed facing up into the dopamine solution (50 mL). A magnetic stirrer was placed in the middle of the vessel surrounded in a satellite-shape by 6 support discs. The solution was then stirred for 20 h at room temperature, leading to the polymerization of dopamine into PDA on the alumina support surface. The oxygen needed for the dopamine polymerization dissolved from air.

2.3. Synthesis of the ZIF-100 membrane

The ZIF-100 membrane was prepared by a solvothermal reaction of trifluoromethanesulfonate and cbIM in DMF according to a previous report.[29] The PDA-modified or PDA-free α-Al$_2$O$_3$ supports were placed horizontally in a Teflon-lined stainless steel autoclave which was filled with 15 mL synthesis solution, and heated at 120 °C in an air oven for 48 h. After the solvothermal reaction, the ZIF-100 membranes were washed with DMF several times, and then dried in air at 110 °C overnight.

2.4. Characterization of the ZIF-100 membrane

The X-ray diffraction (XRD) patterns were recorded at room temperature under ambient conditions with an X-ray diffractometer (D8 Advance, Bruker-AXS, with Cu-Kα radiation at 40 kV and 40 mA). The morphology and thickness of the ZIF-100 membranes were characterized by scanning electron microscopy (SEM) at 2 keV and 10 μA by using a JEOL Jeol-JSM-6700F with a cold field emission gun. By using the same SEM microscope the chemical composition of the cross-section of ZIF-100 was characterized by energy-dispersive X-ray spectroscopy (EDXS) at 20 kV and 20 μA. The chemical composition of the cross-section of the ZIF-100 layer was characterized by energy-dispersive X-ray spectroscopy (EDXS) using the same SEM microscope at 20 kV and 20 μA.

2.5. Simulation models and methods

The Grand Canonical Monte Carlo (GCMC) simulation method in RASPA package[41] was used to calculate the H$_2$/CO$_2$ mixed gas adsorption in ZIF-100. In the GCMC ensemble, the chemical potential, the volume, and the temperature were kept fixed as in the adsorption experiments. The chemical potential was related to the system pressure by the Peng–Robinson equation of state. In this work, the structure of ZIF-100 was constructed from the experimental single-crystal X-ray diffraction data.[29] The standard 12-6 Lennard-Jones (LJ) potential was used to model the dispersive and repulsive interatomic interactions. The Lorentz–Berthelot mixing rules were employed to calculate gas/framework parameters. The LJ parameters of the ZIF-100 atoms were obtained from the Dreiding force field,[42] and if not available in Dreiding, from the Universal Force Field.[43] The partial charges of the ZIF-100 atoms were estimated using the CHELPG method[44] and the density functional theory (DFT) calculation using the B3LYP method[45,46] and the LANL2DZ basis set. A united-atom model was used for CH$_4$ with the LJ parameters from the TraPPE force field.[47] N$_2$ was mimicked by two-site models with a bond length of 1.10 Å.[48] Partial charges and LJ parameters for CO$_2$ were taken from the TraPPE force field. The electrostatic interactions for adsorbent–adsorbate and adsorbate–adsorbate were calculated by the Ewald summation technique.[49]

2.6. Permeation of single gas and separation of mixed gases

For the single and mixed gas permeation, every ZIF-100 membrane was sealed in a permeation cell with silicone O-rings. In our Wicke–Kallenbach permeation cell, we worked with feed and sweep gases at 1 bar. A calibrated gas chromatograph (HP6890) was used to detect the gas concentrations. The fluxes of both the feed and sweep gases were controlled by mass flow controllers. The flow rate on the feed side was kept constant for each gas at 50 mL min^{-1}, while the flow rate on the permeate side was kept at 50 mL min^{-1} as well. N$_2$ was usually used as the sweep gas, except for the measurement of N$_2$ permeance where CH$_4$ was used as the sweep gas instead.

The permeance P is obtained by the division of the flux by the transmembrane pressure difference, and the separation factor $\alpha_{i,j}$ of a binary mixture permeation is defined as the quotient of the molar ratios of the components (i, j) in the permeate, divided by the quotient of the molar ratio of the components (i, j) in the retentate. Since less than 1% of the feed gas can pass

This journal is © The Royal Society of Chemistry 2015

J. Mater. Chem. A, 2015, **3**, 4722–4728 | **4723**

67

through the membrane, the retentate composition is *de facto* identical to the feed composition.

To prove the feasibility of the Wicke–Kallenbach technique, the membranes were also tested under pressure difference. In this case, the pressure on the feed side was 4 bar (2 bar partial pressure of the binary mixture), while the pressure on the permeate side was 1 bar.

The gas chromatograph (GC) was calibrated every week anew with standard gas mixtures. The accuracy of the GC analysis of our H$_2$/CO$_2$ mixture using TCD detection is about ±5 vol%. Before gas permeation, the ZIF-100 membranes were activated at 100 °C with a heating rate of 0.2 °C min^{-1} by using an equimolar H$_2$/CO$_2$ mixture in the Wicke–Kallenbach permeation apparatus. All permeation data were collected in the steady state of permeation after 12 h equilibration time.

3. Results and discussion

3.1. Simulation study of gas adsorption isotherms of ZIF-100

The mixed gas adsorption isotherms in ZIF-100 were examined by molecular simulation. The adsorption of an equimolar H$_2$/CO$_2$ mixture in the pore structure of the ZIF-100 cage at 25 °C and 1 bar is shown as a snapshot in Fig. 2. It can be clearly seen that a huge number of CO$_2$ molecules are adsorbed in the pores of ZIF-100, while only a few H$_2$ molecules are found. The simulation results of the gas adsorption isotherms of H$_2$, CO$_2$, CH$_4$ and N$_2$ at 25 °C are compared to the available experimental data[29] in the pressure range from 10 to 750 Torr in Fig. 3. As shown in Fig. 3, the simulated isotherms of different gases coincide well with the measured ones in the whole pressure range. The adsorption of CO$_2$ exceeds by far the adsorption of the other gases. The simulated adsorption isotherms of an equimolar H$_2$/CO$_2$ mixture at 25 °C are shown in Fig. 4 as a
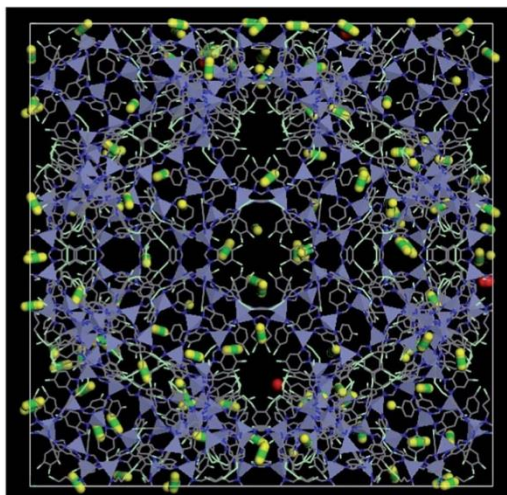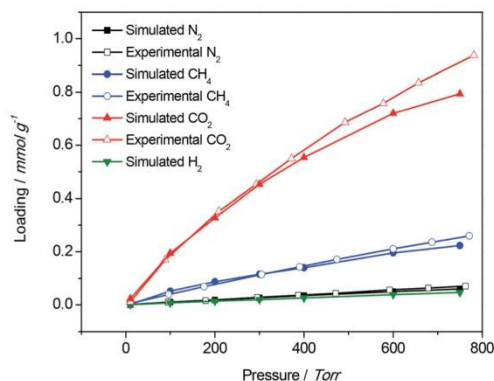

Fig. 3 Simulated single component adsorption isotherms of H$_2$, CO$_2$, CH$_4$ and N$_2$ at 25 °C in the pressure range from 10 to 750 Torr compared with the measured data.[29]

function of the total pressure. As shown in Fig. 4, CO$_2$ is predominantly adsorbed over H$_2$ in ZIF-100 in the whole pressure range due to the much stronger interaction between CO$_2$ and ZIF-100. As a result, the simulation study of the gas adsorption isotherm in ZIF-100 is in good accordance with the experimental data, and the experimentally found strong adsorption affinity of ZIF-100 to CO$_2$ was confirmed by the simulation.

3.2. Synthesis of the ZIF-100 membrane

We first tried to grow a ZIF-100 layer simply by *in situ* hydrothermal synthesis on an unmodified α-alumina support, as shown in Fig. 5(a). However, it turned out to be extremely difficult to form a continuous ZIF-100 layer directly on the support due to the poor heterogeneous nucleation of ZIF-100 crystals on the α-alumina support surface. Our recent study indicated that pre-modification of the support surface with PDA

Fig. 2 Snapshot of adsorption of an equimolar H$_2$/CO$_2$ mixture in ZIF-100 pores at 25 °C and 1 bar with CO$_2$ in yellow-green and H$_2$ in red.
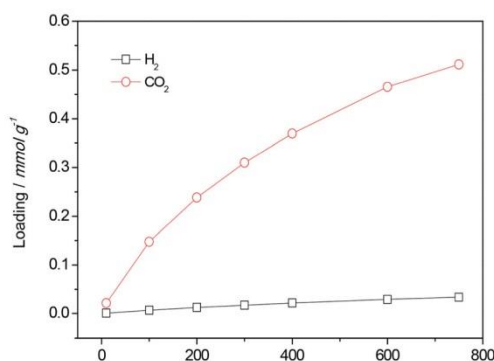

Fig. 4 Simulated mixed gas adsorption isotherms of equimolar H$_2$/CO$_2$ mixtures at 25 °C in the pressure range from 10 to 750 Torr. The pressure on the abscissa indicates the total pressure of the equimolar binary mixture.
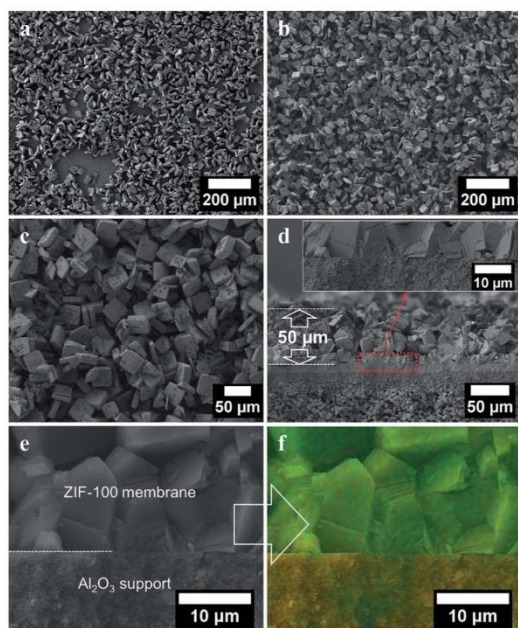
68

3 Metal-organic framework membranes for H$_2$ purification

Fig. 5 SEM top views of (a) ZIF-100 membranes prepared on a PDA-free Al$_2$O$_3$ support and (b and c) on a PDA-modified support, as well as (d and e) the cross-sectional view of the ZIF-100 membrane with PDA-modification. The inset of (d) shows a magnified part of the ZIF-100 membrane at the interface support–ZIF-100 layer. (f) shows the EDXS mapping of the magnified cross-section (green: Zn and Cl as tracers for ZIF-100; orange: Al as the tracer for the support). The $K_{\alpha1}$ transitions have been used.

Fig. 6 XRD patterns of ZIF-100 membranes prepared on PDA-free and PDA-modified supports, compared with the XRD patterns of ZIF-100 powder. (■) for the Al$_2$O$_3$ support. Signals of ZIF-100 crystals are not marked.

can be employed[38] as a simple and powerful strategy to improve the nucleation of MOFs and zeolites on the alumina support surface through the formation of strong covalent bonds with the MOF or zeolite crystals.[38–40] In the present work, therefore, we tried to prepare a dense ZIF-100 membrane on the pre-modified support with PDA. As shown in Fig. 5(b) and (c), a continuous ZIF-100 layer is formed on the PDA-modified supports. From the cross-sectional view shown in Fig. 5(d), it follows that big crystals are loosely packed on the top of the ZIF-100 membranes due to sedimentation, but as we can see from the magnified part (inset in Fig. 5(d)), a thin and well-inter-grown ZIF-100 zone is formed at the interface to the support, thus controlling the selectivity for gas separation. Fig. 5(f) shows the EDXS mapping of the cross-section of the ZIF-100 membrane near the support surface (Fig. 5(e)). A sharp transition can be seen between the ZIF-100 membrane (Zn and Cl signals) and the alumina support (Al signal) which means that there was no infiltration of the synthesis solution into the support. Also the above mentioned well-intergrown ZIF-100 zone near the support can be seen in Fig. 5(f).

The XRD patterns of ZIF-100 membranes are compared with those of ZIF-100 powder in Fig. 6. The results show that all diffraction peaks of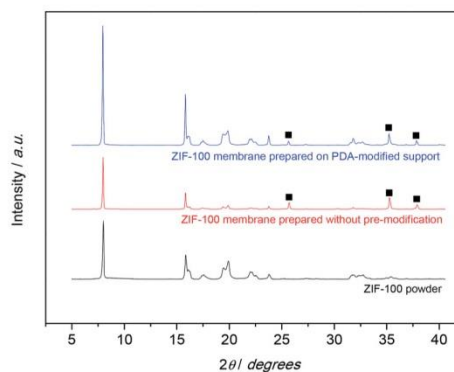 the ZIF-100 layer prepared on either PDA-modified or bare supports match well with those of the ZIF-100 powder besides the α-Al$_2$O$_3$ signals from the support, which indicates that the ZIF-100 membrane prepared on the PDA-modified substrate exhibits the pure ZIF-100 structure. Moreover, the XRD pattern of the PDA pre-modified ZIF-100 membrane shows higher ZIF-100 peak intensity compared to the membrane grown on the bare alumina support, since the ZIF-100 membrane grown on the PDA-based support is much denser and thicker.

3.3. Single gas permeation and mixture gas separation

It is worth noting that before the single gas permeation, the gas permeation performance of the mixed H$_2$/CO$_2$ gas pair on the PDA-modified alumina support was first measured and both the H$_2$ permeance and H$_2$/CO$_2$ separation factor remained unchanged when compared to the permeance through the bare Al$_2$O$_3$ support, which indicates that the PDA-layer itself is not gas-selective.

The single gas permeances of H$_2$, CO$_2$, N$_2$ and CH$_4$ through the ZIF-100 membrane prepared on the PDA-modified support at 25 °C and 1 bar as a function of the kinetic diameter of the gas molecules are shown in Fig. 7, and the results in detail are summarized in Table 1. The inset gives the mixed separation factor for H$_2$ over other gases from their equimolar mixtures. It can be seen that the single gas permeance of H$_2$ at room temperature is ~6.3 × 10^{-8} mol m^{-2} s^{-1} Pa^{-1}, and the single gas permeances through the ZIF-100 membrane follow the order H$_2$ > N$_2$ > CH$_4$ > CO$_2$, which leads to the highest H$_2$/CO$_2$ separation factor of 72. Although CO$_2$ has a smaller kinetic diameter than N$_2$ and CH$_4$, it was believed that the molecular sieving effect did not dominate the separation process, and the high H$_2$/CO$_2$ selectivity can be explained by the diffusivity–solubility model of gas permeation instead. As reported previously,[29] only CO$_2$ can be retained in the pore structure of ZIF-100 while other small gas molecules will easily permeate through the framework since ZIF-100 shows a strong adsorption of CO$_2$

This journal is © The Royal Society of Chemistry 2015

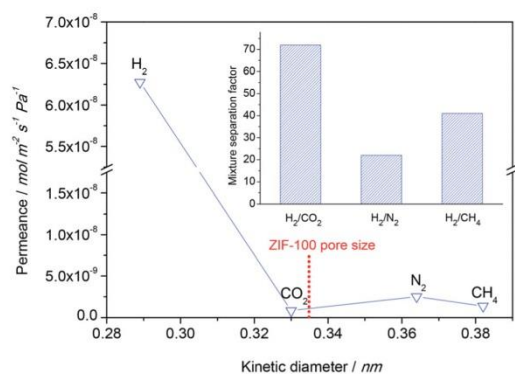*J. Mater. Chem. A*, 2015, **3**, 4722–4728 | **4725**

69

Fig. 7 Single gas permeances through the ZIF-100 membrane prepared by PDA-modification at 25 °C and 1 bar as a function of the kinetic diameter of permeated gases. The inset shows the mixture separation factors for H$_2$ over other gases from equimolar mixtures.
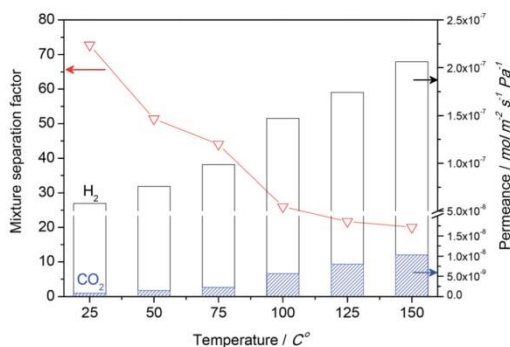

Fig. 8 Single gas permeances of H$_2$ and CO$_2$ and mixture separation factors for H$_2$/CO$_2$ from an equimolar mixture on the ZIF-100 membrane prepared by PDA-modification at 1 bar as a function of temperature.

originating from the strong quadrupolar interactions of carbon with nitrogen atoms in the linkers of ZIF-100. The strong adsorption ability of CO$_2$ has been confirmed by the simulation study, as shown in Section 3.1. The mobility of CO$_2$ was retarded by this strong adsorption, while H$_2$ can still pass through the pore network easily, leading to a high H$_2$/CO$_2$ selectivity. This experimental finding is similar to those reported on zeolite[50–52] and MOF membranes.[21,26,53–55]

Fig. 8 shows the single gas permeance of H$_2$ and CO$_2$ as well as the mixture separation factors for equimolar H$_2$/CO$_2$ mixtures at 1 bar as a function of temperature from 25 to 150 °C. It can be seen that the H$_2$/CO$_2$ separation factors reduce gradually with increasing temperature in a temperature window of 25 to 100 °C, and then only slightly decrease when the temperature is higher than 100 °C. This trend can be explained by the interplay of adsorption and diffusion of H$_2$ and CO$_2$ in the pore structure of ZIF-100. At low temperatures, a large amount of CO$_2$ molecules is adsorbed in the ZIF-100 pores and only the highly mobile H$_2$ can diffuse through the membrane. As the temperature increases, less CO$_2$ becomes adsorbed and both H$_2$ and CO$_2$ can diffuse more easily in the resulting free volume, which leads to an enhancement of both H$_2$ and CO$_2$ permeance. Since the CO$_2$ permeance increases faster than the

H$_2$ one, the H$_2$/CO$_2$ selectivity decreases with increasing temperature. After the temperature reached 100 °C, the effect of the CO$_2$ adsorption is substantially reduced and the gas separation behaviour of ZIF-100 becomes dominated by the kinetic molecular sieving effect since the width of the pore apertures of ZIF-100 is in a similar size to CO$_2$. However, because of the gate opening due to linker distortion, no sharp cut-off can be expected.[56–63] Further, the ZIF-100 membrane shows completely reversible separation behaviour between 25 and 150 °C. The permeances measured during the cooling-down are consistent well with those during the heating-up.

In addition, the ZIF-100 membrane can maintain its high H$_2$/CO$_2$ selectivity when the feed pressure increases. As shown in Fig. 9, when the H$_2$ and CO$_2$ partial pressure increased from 0.5 to 2 bar (corresponding to a change in the total feed pressure from 1 to 4 bar), the H$_2$/CO$_2$ separation factor reduces only slightly which is a direct proof that the membrane does not contain macroscopic defects.

Moreover, it was also found that the synthesis method with pre-modification of the α-alumina supports by PDA can contribute to a higher reproducibility of ZIF-100 membrane preparation, as shown in Table 2. The gas separation performances of 5 different membranes prepared by the same method were tested and the mixture separation factors of H$_2$/CO$_2$ do not scatter more than ±10%.

Table 1 Single and mixed gas (with 1 : 1 binary mixtures) permeances as well as the ideal and mixture separation factors on the ZIF-100 membrane prepared by pre-modification with PDA at 25 °C and 1 bar

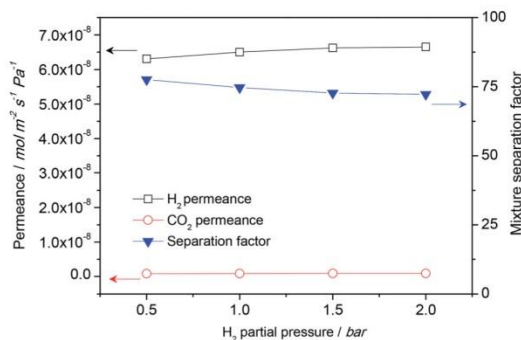|		Separation performance of the ZIF-100 membrane					
		Single gas			Mixed gases		
Gas$_{i/j}$	Knudsen constant	Permeances (i) (mol m^{-2} s^{-1} Pa^{-1})	Permeances (j) (mol m^{-2} s^{-1} Pa^{-1})	Ideal separation factor	Permeances (i) (mol m^{-2} s^{-1} Pa^{-1})	Permeances (j) (mol m^{-2} s^{-1} Pa^{-1})	Mixture separation factor (α)
H$_2$/CO$_2$	4.7	6.3×10^{-8}	8.1×10^{-10}	77	5.8×10^{-8}	8.0×10^{-10}	72
H$_2$/N$_2$	3.7		2.5×10^{-9}	25	6.2×10^{-8}	2.7×10^{-9}	22
H$_2$/CH$_4$	2.8		1.4×10^{-9}	46	5.8×10^{-8}	1.4×10^{-9}	41

70

Fig. 9 H$_2$ and CO$_2$ permeances and H$_2$/CO$_2$ mixed gas selectivity of the ZIF-100 membrane prepared by PDA-modification as a function of hydrogen partial pressure in the feed from equimolar mixtures at room temperature. Permeate pressure was kept constant at 1 bar.

Table 2 Single gas permeances of H$_2$ and CO$_2$ and mixture separation factors of H$_2$/CO$_2$ from equimolar mixtures at room temperature and 1 bar feed/1 bar permeate of 5 tested ZIF-100 membranes showing the reproducibility of membrane preparation and testing

	H$_2$ permeance (mol m^{-2} s^{-1} Pa^{-1})	CO$_2$ permeance (mol m^{-2} s^{-1} Pa^{-1})	Mixture separation factor H$_2$/CO$_2$
1	6.3×10^{-8}	8.1×10^{-10}	72
2	6.5×10^{-8}	8.0×10^{-10}	76
3	6.1×10^{-8}	7.9×10^{-10}	68
4	6.6×10^{-8}	8.1×10^{-10}	75
5	5.8×10^{-8}	7.8×10^{-10}	70

4. Conclusions

Dense and phase-pure ZIF-100 membranes have been prepared on the PDA-modified alumina support at 120 °C for 48 h. After the pre-modification with PDA, the ZIF-100 nutrients were attached to the support surface through the formation of covalent chemical bonds. The mixture separation factors of H$_2$/CO$_2$, H$_2$/N$_2$ and H$_2$/CH$_4$ through the PDA-based ZIF-100 membrane were 72, 22 and 41 at room temperature and 1 bar. The high H$_2$/CO$_2$ selectivity is ascribed to the high CO$_2$ uptake behaviour of ZIF-100 and a small window aperture of 3.35 Å.

Acknowledgements

Notes and references

1 S. Dunn, *Int. J. Hydrogen Energy*, 2002, **27**, 235.
2 J. R. Rostrup-Nielsen and T. Rostrup-Nielsen, *CATTECH*, 2002, **6**, 150.
3 A. A. Olagire, *Energy*, 2010, **35**, 2610.
4 A. J. Brown, N. A. Brunelli, K. Eum, F. Rashidi, J. R. Johnson, W. J. Koros, C. W. Jones and S. Nair, *Science*, 2014, **345**, 72.
5 M. Hong, S. Li, J. L. Falconer and R. D. Noble, *J. Membr. Sci.*, 2008, **307**, 277.
6 F. Gallucci, E. Fernandez, P. Corengia and M. S. Annaland, *Chem. Eng. Sci.*, 2013, **92**, 40.
7 S. Uemiya, T. Matsuda and E. Kikuchi, *J. Membr. Sci.*, 1991, **56**, 315.
8 R. M. de Vos and H. Verweij, *Science*, 1998, **279**, 1710.
9 M. B. Shiflett and H. C. Foley, *Science*, 1999, **285**, 1902.
10 H. Li, M. Eddaoudi, M. O. Keeffe and O. M. Yaghi, *Nature*, 1999, **402**, 276.
11 M. Dincâ, A. F. Yu and J. R. Long, *J. Am. Chem. Soc.*, 2006, **128**, 8904.
12 S. Hermes, F. Schroder, R. Chelmowski, C. Woll and R. A. Fischer, *J. Am. Chem. Soc.*, 2005, **127**, 13744.
13 R. Ranjan and M. Tsapatsis, *Chem. Mater.*, 2009, **21**, 4920.
14 A. Bétard, H. Bux, S. Henke, D. Zacher, J. Caro and R. A. Fischer, *Microporous Mesoporous Mater.*, 2012, **150**, 76.
15 Y. Yoo, Z. Lai and H. K. Jeong, *Microporous Mesoporous Mater.*, 2009, **123**, 100.
16 T. Rodenas, M. van Dalen, E. García-Pérez, P. Serra-Crespo, B. Zornoza, F. Kapteijn and J. Gascon, *Adv. Funct. Mater.*, 2014, **24**, 249.
17 F. Cacho-Bailo, B. Seoane, C. Téllez and J. Coronas, *J. Membr. Sci.*, 2014, **464**, 119.
18 R. Banerjee, A. Phan, B. Wang, C. Knobler, H. Furukawa, M. O'Keeffe and O. M. Yaghi, *Science*, 2008, **319**, 939.
19 A. Phan, C. J. Doonan, F. J. Uribe-romo, C. B. Knobler, M. O'Keeffe and O. M. Yaghi, *Acc. Chem. Res.*, 2010, **43**, 58.
20 Y. Li, F. Liang, H. Bux, A. Feldhoff, W. Yang and J. Caro, *Angew. Chem.*, 2010, **122**, 558; *Angew. Chem., Int. Ed.*, 2010, **49**, 548.
21 A. Huang, H. Bux, F. Steinbach and J. Caro, *Angew. Chem., Int. Ed.*, 2010, **49**, 4958.
22 H. Bux, F. Liang, Y. Li, J. Cravillon, M. Wiebcke and J. Caro, *J. Am. Chem. Soc.*, 2009, **131**, 16000.
23 H. Bux, A. Feldhoff, J. Cravillon, M. Wiebcke, Y. Li and J. Caro, *Chem. Mater.*, 2011, **23**, 2262.
24 Y. Pan and Z. Lai, *Chem. Commun.*, 2011, **47**, 10275.
25 A. Huang, W. Dou and J. Caro, *J. Am. Chem. Soc.*, 2010, **132**, 15562.
26 A. Huang and J. Caro, *Angew. Chem., Int. Ed.*, 2011, **50**, 4979.
27 A. Huang, N. Wang, C. Kong and J. Caro, *Angew. Chem., Int. Ed.*, 2012, **51**, 10551.
28 A. Huang, Y. Chen, N. Wang, Z. Hu, J. Jiang and J. Caro, *Chem. Commun.*, 2012, **48**, 10981.
29 B. Wang, A. P. Côté, H. Furukawa, M. O'Keeffe and O. M. Yaghi, *Nature*, 2008, **453**, 207.

Journal of Materials Chemistry A

30 S. Bourrelly, P. L. Llewellyn, C. Serre, F. Millange, T. Loiseau and G. Férey, *J. Am. Chem. Soc.*, 2009, **131**, 6326.

31 L. Valenzano, B. Civalleri, S. Chavan, G. T. Palomino, C. O. Areán and S. Bordiga, *J. Phys. Chem. C*, 2010, **114**, 11185.

32 S. Sircar, T. C. Golden and M. B. Rao, *Carbon*, 1996, **34**, 1.

33 M. Prakash, N. Sakhavand and R. Shahsavari, *J. Phys. Chem. C*, 2013, **117**, 24407.

34 H. Lee, S. M. Dellatore, W. M. Miller and P. B. Messersmith, *Science*, 2007, **318**, 426.

35 H. Lee, J. Rho and P. B. Messersmith, *Adv. Mater.*, 2009, **21**, 431.

36 J. Ryu, S. H. Ku, H. Lee and C. B. Park, *Adv. Funct. Mater.*, 2010, **20**, 2132.

37 D. Ling, W. Park, Y. I. Park, N. Lee, F. Li, C. Song, S. Yang, S. H. Choi, K. Na and T. Hyeon, *Angew. Chem., Int. Ed.*, 2011, **50**, 11360.

38 Q. Liu, N. Wang, J. Caro and A. Huang, *J. Am. Chem. Soc.*, 2013, **135**, 17679.

39 A. Huang, Q. Liu, N. Wang and J. Caro, *J. Mater. Chem. A*, 2014, **2**, 8246.

40 C. Yuan, Q. Liu, H. Chen and A. Huang, *RSC Adv.*, 2014, **4**, 41982.

41 *RASPA 1.0.*, ed. D. Dubbeldam, S. Calero, D. E. Ellis and R. Q. Snurr, Northwestern University, Evanston, IL, 2008.

42 S. L. Mayo, B. D. Olafson and W. A. Goddard, *J. Phys. Chem.*, 1990, **94**(26), 8897.

43 A. K. Rappe, C. J. Casewit, K. S. Colwell, W. A. Goddard III and W. M. Skiff, *J. Am. Chem. Soc.*, 1992, **114**(25), 10024.

44 C. M. Breneman and K. B. Wiberg, *J. Comput. Chem.*, 1990, **11**(3), 361.

45 C. Lee, W. Yang and R. G. Parr, *Phys. Rev. B: Condens. Matter Mater. Phys.*, 1988, **37**(2), 785.

46 A. D. Becke, *J. Chem. Phys.*, 1993, **98**, 5648.

47 M. G. Martin and J. I. Siepmann, *J. Phys. Chem. B*, 1998, **102**(14), 2569.

48 C. S. Murthy, K. Singer, M. L. Klein and I. R. McDonald, *Mol. Phys.*, 1980, **41**(6), 1387.

49 P. P. Ewald, *Ann. Phys.*, 1921, **64**(3), 253.

50 A. Huang, N. Wang and J. Caro, *J. Membr. Sci.*, 2012, **389**, 272.

51 A. Huang and J. Caro, *J. Mater. Chem.*, 2011, **21**, 11424.

52 N. Wang, Y. Liu, A. Huang and J. Caro, *Microporous Mesoporous Mater.*, 2014, **192**, 8.

53 Y. Li, F. Liang, H. Bux, A. Feldhoff, W. Yang and J. Caro, *Angew. Chem., Int. Ed.*, 2010, **49**, 548.

54 A. Huang, Y. Chen, N. Wang, Z. Hu, J. Jiang and J. Caro, *Chem. Commun.*, 2012, **48**, 10981.

55 N. Wang, A. Mundstock, Y. Liu, A. Huang and J. Caro, *Chem. Eng. Sci.*, DOI: 10.1016/j.ces.2014.10.037

56 C. Gücüyener, J. van den Bergh, J. Gascon and F. Kapteijn, *J. Am. Chem. Soc.*, 2010, **132**, 17704.

57 D. Fairen-Jimenez, S. A. Moggach, M. T. Wharmby, P. A. Wright, S. Parsons and T. Düren, *J. Am. Chem. Soc.*, 2001, **133**, 8900.

58 S. A. Moggach, T. D. Bennett and A. K. Cheetham, *Angew. Chem.*, 2009, **121**, 7221.

59 T. Chokbunpiam, R. Chanajaree, T. Remsungnen, O. Saengsawang, S. Fritzsche, C. Chmelik, J. Caro, W. Janke and S. Hannongbua, *Microporous Mesoporous Mater.*, 2014, **187**, 1.

60 S. Aguado, G. Bergeret, M. P. Titus, V. Moizan, C. Nieto-Draghi, N. Bats and D. Farrusseng, *New J. Chem.*, 2011, **35**, 546.

61 J. van den Bergh, C. Gücüyener, E. A. Pidko, E. J. M. Hensen, J. Gascon and F. Kapteijn, *Chem.–Eur. J.*, 2011, **17**, 8832.

62 D. L. Chen, N. Wang, F. F. Wang, J. Xie, Y. Zhong, W. Zhu, J. K. Johnson and R. Krishna, *J. Phys. Chem. C*, 2014, **118**, 17831.

63 C. O. Ania, E. García-Pérez, M. Haro, J. J. Gutiérrez-Sevillano, T. Valdés-Solís, J. B. Parra and S. Calero, *J. Phys. Chem. Lett.*, 2012, **3**, 1159.

3.4 Organosilica-functionalized zeolitic imidazolate framework ZIF-90 membrane with high gas-separation performance

Aisheng Huang, Nanyi Wang, Chunlong Kong and Jürgen Caro

Metal–Organic Frameworks

Organosilica-Functionalized Zeolitic Imidazolate Framework ZIF-90 Membrane with High Gas-Separation Performance**

Aisheng Huang,* Nanyi Wang, Chunlong Kong, and Jürgen Caro*

Membrane-based separation techniques are energy- and cost-intensive in comparison with conventional separation processes like distillation and adsorption.[1] Recently, supported metal-organic framework (MOF) films have attracted intense attention for potential applications as semiconductors, sensors, and molecular sieve membranes because of their highly diversified structures and pore sizes as well as specific adsorption affinities.[2–20] In particular, attributed to their zeolite-like properties such as permanent porosity, uniform pore size, exceptional thermal and chemical stabilities, zeolitic imidazolate frameworks (ZIFs) have emerged as a novel type of crystalline porous material for the preparation of superior molecular sieve membranes.[21–23] So far, a series of supported ZIF membranes, including ZIF-7,[24] ZIF-8,[14,25–27] ZIF-22,[28] ZIF-69,[29] and ZIF-90,[30,31] have been reported for permeation of single gases or separation of mixed gases. Despite much progress in the preparation of MOF membranes, there is still a long road ahead before highly permselective MOF membranes can be developed for practical applications, as highlighted recently.[32] It is often found that the as-prepared MOF layers have a polycrystalline structure containing intercrystalline defects, which are detrimental to the membrane selectivity. Therefore, post-modification of the as-prepared MOF membranes is helpful to minimize the nonselective transport pathways through the intercrystalline gaps.[18,31]

As proposed by Yaghi and co-workers,[33] the free aldehyde groups in the ZIF-90 framework allow the covalent functionalization with amine groups through an imine condensation reaction (see Figure S1 in the Supporting Information).[34–37] Therefore, the hydrogen selectivity of the as-prepared ZIF-90 membrane can be improved through the covalent post-functionalization with ethanolamine.[31] However, the membrane selectivity was enhanced at the expense of the permeance since the small ethanolamine molecules

could easily permeate into the ZIF-90 structure, resulting in a lower hydrogen permeance because of a homogeneous constriction of the pore network. In addition, the post-functionalization process using ethanolamine as reactant is rather long (usually over 10 h), leading to some decomposition of the ZIF-90 material. Therefore, the development of a facile and effective post-functionalization route is desirable to prepare ZIF-90 membranes with high selectivity, while maintaining their high permeance. In our previous report,[30] we found that the amine group of the 3-aminopropyltriethoxysilane (APTES) reacts easily with the free aldehyde groups in the ZIF-90 framework, as shown in Figure 1a. Thus, the organosilica APTES can be expected to modify the ZIF-90
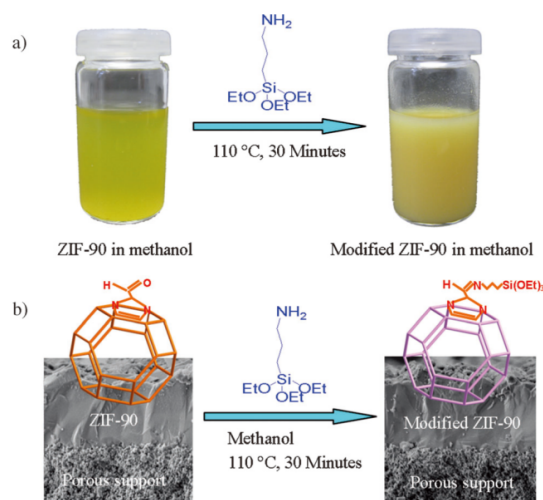

Figure 1. a) Covalent post-functionalization of suspended ZIF-90 crystals in methanol and b) molecular sieve membrane through amine condensation by using organosilica APTES.

membrane (Figure 1b). On one hand, the covalent post-functionalization is promising for the reduction of the intercrystalline defects of the polycrystalline ZIF-90 layer, thus enhancing the selectivity of gas separation. On the other hand, the relatively large APTES molecules are restrained from entering the interior of the ZIF-90 layer, thus making possible a high hydrogen permeance of the ZIF-90 membrane. Therefore, the APTES-modified ZIF-90 membranes will display a high gas-separation performance.

For covalent post-functionalization, the as-prepared ZIF-90 crystals and membranes were immersed in a solution of

[*] Prof. Dr. A. Huang, Dr. C. Kong
Institute of New Energy Technology
Ningbo Institute of Material Technology and Engineering, CAS
519 Zhuangshi Road, 315201 Ningbo (P. R. China)
E-mail: huangaisheng@nimte.ac.cn

M. Sc. N. Wang, Prof. Dr. J. Caro
Institute of Physical Chemistry and Electrochemistry
Leibniz University Hannover
Callinstraße 3A, 30167 Hannover (Germany)
E-mail: juergen.caro@pci.uni-hannover.de

Supporting information for this article is available on the WWW under http://dx.doi.org/10.1002/anie.201204621.

WILEY ONLINE LIBRARY

10551

Angewandte
Communications

APTES in methanol, and then refluxed for 30 minutes at 110 °C. As intuitively shown in Figure 1 a, when APTES was added to the green-yellow ZIF-90 clear solution, a beige colloidal solution which scatters the light because of particle aggregation is quickly observed, indicating that the linkages between the free aldehyde groups of the ZIF-90 and the amino group of APTES have been formed. Further, the reaction of ZIF-90 with APTES was confirmed by Fourier Transform infrared spectroscopy (FTIR). As shown in Figure S2 in the Supporting Information, the C=O band of the aldehyde at about 1668 cm^{-1} is replaced by the C=N bond of the imine at 1640 cm^{-1}. The presence of the H−CNR band at 2970 cm^{-1} and the Si−O band at 1080 cm^{-1} after APTES modification also suggests that APTES has been grafted on the surface of the ZIF-90 crystals.

After APTES functionalization, no remarkable differences in the membrane morphology are found between the as-prepared and the APTES-functionalized ZIF-90 membranes. A well intergrown ZIF-90 layer with a thickness of about 20 μm was formed on the porous alumina support, and no visible cracks, pinholes or other defects are observed for both ZIF-90 membranes (Figure S3 in the Supporting Information). The X-ray diffraction (XRD) pattern (Figure S4) shows that the high crystallinity of the ZIF-90 membrane is unchanged after APTES functionalization. All XRD peaks of the APTES-functionalized ZIF-90 membrane match well with those of the as-prepared ZIF-90 membrane.

Before permeation of single gases and separation of mixed gases, the as-prepared and APTES-functionalized ZIF-90 membranes were on-stream activated at 225 °C with a heating rate of 0.2 °C per minute by using an equimolar H$_2$/CH$_4$ mixture in the Wicke–Kallenbach permeation apparatus (Figure S5). Figure 2 shows the increase of the H$_2$ and CH$_4$ permeances as well as of the H$_2$/CH$_4$ selectivity from their binary mixture with increasing temperature during the on-stream activation. Whereas the H$_2$ permeance remarkably increases with increasing temperature from 25 to 225 °C, the CH$_4$ permeance only slightly increases, resulting in a remarkable enhancement of H$_2$/CH$_4$ selectivity from 8 to 71. Similar to the previous report,[31] the APTES-functionalized ZIF-90 membrane is more easily activated than the as-prepared ZIF-
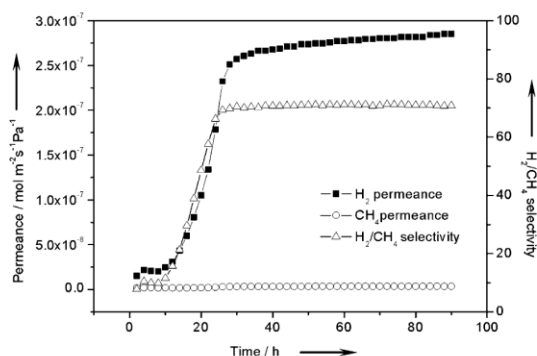
90 membrane since the guest molecule DMF that is difficult to remove has been exchanged by the more volatile methanol during the covalent post-functionalization (Figure S6). After on-stream activation at 225 °C for 60 h, the APTES-functionalized ZIF-90 membrane shows a constant H$_2$ permeance of about 2.9×10^{-7} mol m^{-2} s^{-1} Pa^{-1} and a H$_2$/CH$_4$ selectivity of 71.

After on-stream activation, the volumetric flow rates of the single gases H$_2$, CO$_2$, CH$_4$, C$_2$H$_6$, and C$_3$H$_8$ as well as of their equimolar binary mixtures of H$_2$ with CO$_2$, CH$_4$, C$_2$H$_6$, and C$_3$H$_8$ have been measured through the as-prepared and APTES-functionalized ZIF-90 membranes by using the Wicke–Kallenbach technique. The single-gas permeances and ideal separation factors are summarized in Table S1. Figure 3 shows the permeances of the single gases through the
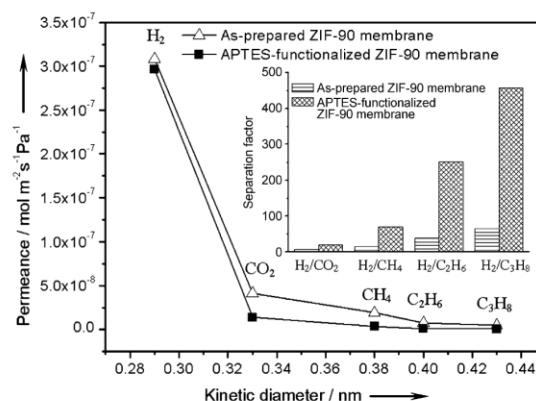

Figure 3. Permeances of single gases for the as-prepared and APTES-functionalized ZIF-90 membranes as a function of the kinetic diameter at 225 °C and 1 bar using the Wicke–Kallenbach technique. The inset shows the separation factors for equimolar mixtures of H$_2$ and other gases as determined by gas chromatography.

as-prepared and APTES-functionalized ZIF-90 membranes at 225 °C and 1 bar as a function of the kinetic diameters of the permeating molecules. As shown in Figure 3 and Table S1, for the APTES-functionalized ZIF-90 membrane, the H$_2$ permeance of 3.0×10^{-7} mol m^{-2} s^{-1} Pa^{-1} is much higher than those of the other gases, and a cut-off is observed between H$_2$ and the other more bulky gases. Compared with the as-prepared ZIF-90 membrane, the H$_2$ permeance of the APTES-functionalized ZIF-90 membrane keeps almost unchanged although all other gas permeances decrease. In our previous report,[31] a remarkable reduction of the H$_2$ permeance has been reported since the small ethanolamine molecules can easily enter the pore volume of the ZIF-90 layer, thus resulting in a severe constriction of the pore apertures in the whole bulk phase. In the present work, the bulky APTES molecules are restricted to enter the interior of the ZIF-90 layer in a short time, thus avoiding remarkable reduction of the H$_2$ permeance. At 225 °C and 1 bar, the ideal separation factors of H$_2$ from CO$_2$, CH$_4$, C$_2$H$_6$, and C$_3$H$_8$ are 22, 74, 261, and 473, which by far exceed the corresponding Knudsen coefficients (4.7, 2.8, 3.9, and 4.7) and those of the

Figure 2. H$_2$ and CH$_4$ permeances as well as H$_2$/CH$_4$ selectivity of an equimolar H$_2$/CH$_4$ mixture of the APTES-functionalized ZIF-90 membrane during the on-stream activation at 225 °C.

75

as-prepared ZIF-90 membrane (7.5, 16, 41, and 67). These results are in good agreement with our supposition that the hydrogen selectivity of the modified ZIF-90 membrane can be enhanced through APTES functionalization by eliminating the intercrystalline defects.

Compared with the permeance of H_2 as a single component, the H_2 permeance in the mixtures shows only a slight reduction with a H_2 permeance of about $2.9 \times 10^{-7} \, mol \, m^{-2} \, s^{-1} \, Pa^{-1}$, suggesting that no competitive adsorption between the species plays a significant role at a high temperature, and the larger molecules (CO_2, CH_4, C_2H_6, and C_3H_8) only slightly hinder the permeation of the highly mobile H_2. For the 1:1 binary mixtures, the separation factors of H_2/CO_2, H_2/CH_4, H_2/C_2H_6, and H_2/C_3H_8 mixtures are 20, 71, 250, and 458, respectively, which are higher than those on the as-prepared ZIF-90 membrane (7.2, 15, 39, and 65), as shown in the inset of Figure 3 and Table S2. As usual, with longer modification time, the permeances decrease parallel to the selectivity increase. As shown in Table S3, extending the modification time to 1 h, the H_2 permeance decreases to $6.8 \times 10^{-8} \, mol \, m^{-2} \, s^{-1} \, Pa^{-1}$ while the H_2/CH_4 selectivity increases to 146 since the covalent docking of APTES restricts the adsorption rate. Compared with literature data for permeation of mixed gases on MOF and zeolite membranes (Table S4),[16–20,24–31,38–44] the APTES-functionalized ZIF-90 membrane developed in this study shows higher gas separation performances. The obtained high H_2 selectivity of the ZIF-90 membrane is attributed to the narrowing of the pore mouth and minimizing of intercrystalline defects by APTES post-functionalization, and thus enhancing the reproducibility of the membrane preparation (Table S5).

To investigate the thermal stability of the APTES-functionalized ZIF-90 membrane, the operating temperature for the separation of the H_2/CH_4 mixture was increased from 25 to 225 °C. It can be seen that the H_2 permeance increases from 8.3×10^{-8} to $2.9 \times 10^{-7} \, mol \, m^{-2} \, s^{-1} \, Pa^{-1}$, while the CH_4 permeance only slightly increases from 3.0×10^{-9} to $4.0 \times 10^{-9} \, mol \, m^{-2} \, s^{-1} \, Pa^{-1}$, thus the separation factor of the H_2/CH_4 mixture rises from 27 to 71 (Figure S7). This phenomenon can also be explained by an adsorption–diffusion model. At low temperature, ZIF-90 adsorbs CH_4 more strongly than H_2, thus blocking the diffusion paths of the rarely adsorbed but highly mobile H_2. When the temperature increases, less CH_4 becomes adsorbed, and more H_2 can diffuse through the resulting free volume,[45] leading to an enhancement of the H_2 permeance. Furthermore, the APTES-functionalized ZIF-90 membrane shows a completely reversible separation behavior between 25 and 225 °C. In addition, the ZIF-90 membrane can keep its high H_2/CH_4 selectivity when the CH_4 partial pressure increases from 0.5 to 2.0 bar corresponding to total feed pressures of 1.0 to 4.0 bar while the permeate pressure was 1 bar constant. The slight reduction of the H_2/CH_4 selectivity with increasing feed pressure is due to an increased CH_4 loading of the membrane which reduces the H_2 diffusivity (Figure S8).

As reported previously,[30,31] the as-prepared and imine-functionalized ZIF-90 membranes show a high hydrothermal stability. Also the APTES-functionalized ZIF-90 membranes consistently exhibit a high stability in the presence of steam,

and both H_2 permeance and H_2/CH_4 selectivity are unchanged for at least 48 h (Figure 4), which shows that the ZIF-90 pore volume is not blocked by the adsorbed water. The slight reduction of the H_2 permeance can be attributed to the parallel permeation of H_2O and H_2 through the ZIF-90 membrane since the kinetic diameter of H_2O is only 0.26 nm,
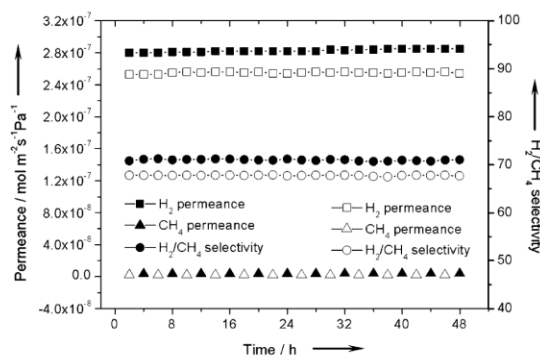

Figure 4. Hydrothermal stability measurement of the APTES-functionalized ZIF-90 membrane for the separation of an equimolar H_2/CH_4 mixture and addition of 3 mol% steam at 225 °C. Filled symbols (■▲●): without steam, and open symbols (□△○): with steam.

which is smaller than the pore size of ZIF-90.[45] In the presence of steam, the aminopropyl groups are hydrolytically stable and will not split from the surface of the ZIF-90 layer. Although the ethoxy bonds of APTES are hydrolyzed, the transient silanol groups will condense with other silanol groups to form stable linkages. This covalent attachment of APTES to the linker could prevent or at least reduce the so called "gate opening" effect by a linker flip-flop movement as observed for ZIF-8.[46] This minimized framework flexibility could also be a reason for the increase of the separation factor for mixed gases as shown in Table S2.

In conclusion, in the present work we have developed a facile post-functionalization road for the preparation of highly permselective ZIF-90 molecular sieve membranes through an imine condensation reaction by using the organo-silica APTES. By covalent linkages between the free aldehyde groups of the ZIF-90 and the amino group of APTES, both narrowing of the pore mouth and sealing of intercrystalline defects of the polycrystalline ZIF-90 layer are achieved, and thus the selectivity for gas separation was enhanced. For binary mixtures at 225 °C and 1 bar, the separation factors of H_2/CO_2, H_2/CH_4, H_2/C_2H_6, and H_2/C_3H_8 mixtures were found to be 20, 71, 250, and 458, and a relatively high H_2 permeance of about $2.9 \times 10^{-7} \, mol \, m^{-2} \, s^{-1} \, Pa^{-1}$ can be obtained to avoid pore blocking. Further, the APTES-functionalized ZIF-90 molecular sieve membranes display a high thermal and hydrothermal stability. These properties recommend APTES-functionalized ZIF-90 membranes as a promising candidate for industrial hydrogen separation.

Angewandte
Communications

Experimental Section

All chemicals were used as received: zinc nitrate tetrahydrate (>99%, Merck), imidazolate-2-carboxyaldehyde (ICA, >99%, Alfa Aesar), 3-aminopropyltriethoxysilane (APTES, 98%, Abcr), toluene (Acros), and *N,N*-dimethylformamide (DMF, water <50 ppm, Acros). Porous α-Al$_2$O$_3$ disks (Fraunhofer Institute IKTS, former HITK/Inocermic, Hermsdorf, Germany: 18 mm in diameter, 1.0 mm in thickness, 70 nm particles in the top layer) were used as support materials.

Synthesis of ZIF-90 crystals and membranes: The ZIF-90 crystals and membranes were prepared as reported previously.[30,34] The APTES-treated α-Al$_2$O$_3$ support materials[47,48] were placed horizontally in a Teflon-lined stainless steel autoclave which was filled with synthesis solution, and heated at 100°C in an air-circulating oven for 18 h. After solvothermal reaction, the ZIF-90 crystals and membranes were washed with DMF several times, and then dried in air at 60°C over night.

Covalent functionalization of ZIF-90 crystals and membranes: The as-prepared ZIF-90 crystals and membranes were immersed in methanol and APTES solution, and refluxed at 110°C for 0–1.0 h. After the reaction, the modified ZIF-90 crystals and membranes were washed with methanol several times and then dried in air at room temperature over night before characterization and permeation measurements.

Characterization of ZIF-90 crystals and membranes: The as-prepared and APTES-functionalized ZIF-90 crystals were measured by FTIR spectroscopy and XRD. The as-prepared and APTES-functionalized ZIF-90 mebranes were measured by SEM and XRD. FTIR spectra were recorded with a Tensor 27 instrument (Bruker) through KBr pellets using an Ar/Xe laser line at 633 nm. SEM micrographs were taken on a JEOL JSM-6700F with a cold field emission gun operating at 2 kV and 10 μA. The XRD patterns were recorded at room temperature under ambient conditions with a Bruker D8 ADVANCE X-ray diffractometer with CuKα radiation at 40 kV and 40 mA.

Permeation of single gases and separation of mixed gases: For the permeation of single gases and separation of mixed gases, the as-prepared and APTES-functionalized ZIF-90 membranes were sealed in a permeation module with silicone O-rings. The sweep gas N$_2$ was fed on the permeate side to keep the concentration of permeating gas as low as possible thus providing a driving force for permeation. The total pressure on each side of the membrane was atmospheric. The fluxes of feed and sweep gases were determined with mass-flow controllers, and a calibrated gas chromotograph (HP6890) was used to measure the gas concentrations (Figure S6). The separation factor $\alpha_{i,j}$ of a binary mixture after permeation is defined as the quotient of the molar ratios of the components (i,j) in the permeate, divided by the quotient of the molar ratio of the components (i,j) in the retentate.

[1] N. W. Ockwig, T. M. Nenoff, *Chem. Rev.* **2007**, *107*, 4078–4110.

[2] H. Li, M. Eddaoudi, M. O'Keeffe, O. M. Yaghi, *Nature* **1999**, *402*, 276–279.

[3] J. S. Seo, D. Whang, H. Lee, S. I. Jun, J. Oh, Y. J. Jeon, K. Kim, *Nature* **2000**, *404*, 982–986.

[4] O. M. Yaghi, M. O'Keeffe, N. W. Ockwig, H. K. Chae, M. Eddaoudi, J. Kim, *Nature* **2003**, *423*, 705–714.

[5] M. Dincâ, A. F. Yu, J. R. Long, *J. Am. Chem. Soc.* **2006**, *128*, 8904–8913.

[6] L. J. Murray, M. Dincâ, J. R. Long, *Chem. Soc. Rev.* **2009**, *38*, 1294–1314.

[7] C. G. Silva, A. Corma, H. García, *J. Mater. Chem.* **2010**, *20*, 3141–3156.

[8] E. Biemmi, C. Scherb, T. Bein, *J. Am. Chem. Soc.* **2007**, *129*, 8054–8055.

[9] S. Hermes, F. Schroder, R. Chelmowski, C. Woll, R. A. Fischer, *J. Am. Chem. Soc.* **2005**, *127*, 13744–13745.

[10] L. E. Kreno, K. Leong, O. K. Farha, M. Allendorf, R. P. Van Duyne, J. T. Hupp, *Chem. Rev.* **2012**, *112*, 1105–1125.

[11] A. Bétard, R. A. Fischer, *Chem. Rev.* **2012**, *112*, 1055–1083.

[12] R. Ranjan, M. Tsapatsis, *Chem. Mater.* **2009**, *21*, 4920–4924.

[13] A. Bétard, H. Bux, S. Henke, D. Zacher, J. Caro, R. A. Fischer, *Microporous Mesoporous Mater.* **2012**, *150*, 76–82.

[14] S. R. Venna, M. A. Carreon, *J. Am. Chem. Soc.* **2010**, *132*, 76–78.

[15] Y. Yoo, Z. Lai, H. K. Jeong, *Microporous Mesoporous Mater.* **2009**, *123*, 100–106.

[16] H. Guo, G. Zhu, I. J. Hewitt, S. Qiu, *J. Am. Chem. Soc.* **2009**, *131*, 1646–1647.

[17] J. Nan, X. Dong, W. Wang, W. Jin, N. Xu, *Langmuir* **2011**, *27*, 4309–4312.

[18] Y. Yoo, V. Varela-Guerrero, H.-K. Jeong, *Langmuir* **2011**, *27*, 2652–2657.

[19] Y. Hu, X. Dong, J. Nan, W. Jin, X. Ren, N. Xu, Y. M. Lee, *Chem. Commun.* **2011**, *47*, 737–739.

[20] S. Aguado, C. H. Nicolas, V. Moizan-Baslé, C. Nieto, H. Amrouche, N. Bats, N. Audebrandd, D. Farrusseng, *New J. Chem.* **2011**, *35*, 41–44.

[21] K. S. Park, Z. Ni, A. P. Côté, J. Y. Choi, R. Huang, F. J. Uribe-Romo, H. K. Chae, M. O'Keeffe, O. M. Yaghi, *Proc. Natl. Acad. Sci. USA* **2006**, *103*, 10186–10191.

[22] R. Banerjee, A. Phan, B. Wang, C. Knobler, H. Furukawa, M. O'Keeffe, O. M. Yaghi, *Science* **2008**, *319*, 939–943.

[23] A. Phan, C. J. Doonan, F. J. Uribe-romo, C. B. Knobler, M. O'Keeffe, O. M. Yaghi, *Acc. Chem. Res.* **2010**, *43*, 58–67.

[24] Y. Li, F. Liang, H. Bux, A. Feldhoff, W. Yang, J. Caro, *Angew. Chem.* **2010**, *122*, 558–561; *Angew. Chem. Int. Ed.* **2010**, *49*, 548–551.

[25] H. Bux, F. Liang, Y. Li, J. Cravillon, M. Wiebcke, J. Caro, *J. Am. Chem. Soc.* **2009**, *131*, 16000–16001.

[26] H. Bux, A. Feldhoff, J. Cravillon, M. Wiebcke, Y. Li, J. Caro, *Chem. Mater.* **2011**, *23*, 2262–2269.

[27] Y. Pan, Z. Lai, *Chem. Commun.* **2011**, *47*, 10275–10277.

[28] A. Huang, H. Bux, F. Steinbach, J. Caro, *Angew. Chem.* **2010**, *122*, 5078–5081; *Angew. Chem. Int. Ed.* **2010**, *49*, 4958–4961.

[29] Y. Liu, E. Hu, E. A. Khan, Z. Lai, *J. Membr. Sci.* **2010**, *353*, 36–40.

[30] A. Huang, W. Dou, J. Caro, *J. Am. Chem. Soc.* **2010**, *132*, 15562–15564.

[31] A. Huang, J. Caro, *Angew. Chem.* **2011**, *123*, 5083–5086; *Angew. Chem. Int. Ed.* **2011**, *50*, 4979–4982.

[32] J. Gascon, F. Kapteijn, *Angew. Chem.* **2010**, *122*, 1572–1574; *Angew. Chem. Int. Ed.* **2010**, *49*, 1530–1532.

[33] W. Morris, C. J. Doonan, H. Furukawa, R. Banerjee, O. M. Yaghi, *J. Am. Chem. Soc.* **2008**, *130*, 12626–12627.

[34] Z. Wang, S. M. Cohen, *Angew. Chem.* **2008**, *120*, 4777–4780; *Angew. Chem. Int. Ed.* **2008**, *47*, 4699–4702.

[35] S. M. Cohen, *Chem. Rev.* **2012**, *112*, 970–1000.

[36] T. Haneda, M. Kawano, T. Kawamichi, M. Fujita, *J. Am. Chem. Soc.* **2008**, *130*, 1578–1579.

[37] A. D. Burrows, C. G. Frost, M. F. Mahon, C. Richardson, *Angew. Chem.* **2008**, *120*, 8610–8614; *Angew. Chem. Int. Ed.* **2008**, *47*, 8482–8486.

[38] M. Kanezashi, J. O'Brien-Abraham, Y. S. Lin, *AIChE J.* **2008**, *54*, 1478–1486.

[39] G. Guan, T. Tanaka, K. Kusakabe, K. Sotowa, S. Morooka, *J. Membr. Sci.* **2003**, *214*, 191–198.

Angewandte
International Edition Chemie

[40] M. Yu, H. H. Funke, R. D. Noble, J. L. Falconer, *J. Am. Chem. Soc.* **2011**, *133*, 1748–1750.

[41] A. Huang, F. Liang, F. Steinbach, T. M. Gesing, J. Caro, *J. Am. Chem. Soc.* **2010**, *132*, 2140–2141.

[42] A. Huang, J. Caro, *J. Mater. Chem.* **2011**, *21*, 11424–11429.

[43] A. Huang, J. Caro, *Chem. Commun.* **2010**, *46*, 7748–7750.

[44] U. Illgen, R. Schäfer, M. Noack, P. Kölsch, A. Kühnle, J. Caro, *Catal. Commun.* **2001**, *2*, 339–345.

[45] Y. Li, F. Liang, H. Bux, W. Yang, J. Caro, *J. Membr. Sci.* **2010**, *354*, 48–54.

[46] D. Fairen-Jimenez, S. A. Moggach, M. T. Wharmby, P. A. Wright, S. Parsons, T. Düren, *J. Am. Chem. Soc.* **2011**, *133*, 8900–8902.

[47] A. Huang, F. Liang, F. Steinbach, J. Caro, *J. Membr. Sci.* **2010**, *350*, 5–9.

[48] A. Kulak, Y. Lee, Y. S. Park, K. B. Yoon, *Angew. Chem.* **2000**, *112*, 980–983; *Angew. Chem. Int. Ed.* **2000**, *39*, 950–953.

78

Support information

Supporting Information

© Wiley-VCH 2012

69451 Weinheim, Germany

Organosilica-Functionalized Zeolitic Imidazolate Framework ZIF-90 Membrane with High Gas-Separation Performance**

Aisheng Huang,* Nanyi Wang, Chunlong Kong, and Jürgen Caro*

anie_201204621_sm_miscellaneous_information.pdf

Figure S1
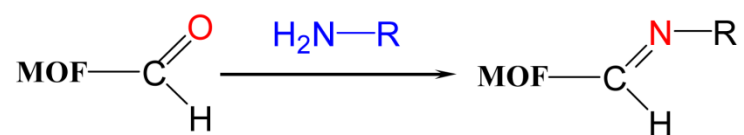
Figure S1. Scheme of covalent postfunctionalization of MOFs via imines condensation reaction.

Figure S2
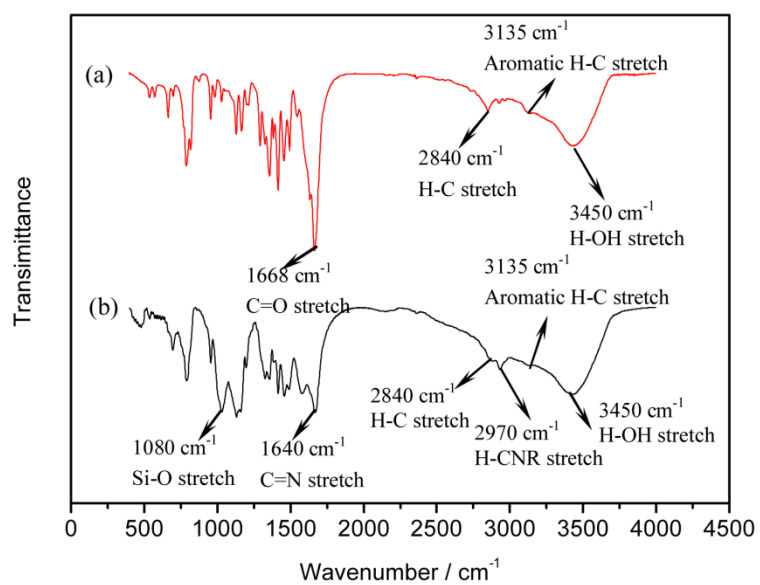
Figure S2. FTIR spectrums of the as-prepared ZIF-90 crystals (a),

and organosilica-functionalized ZIF-90 crystals (b).

Figure S3
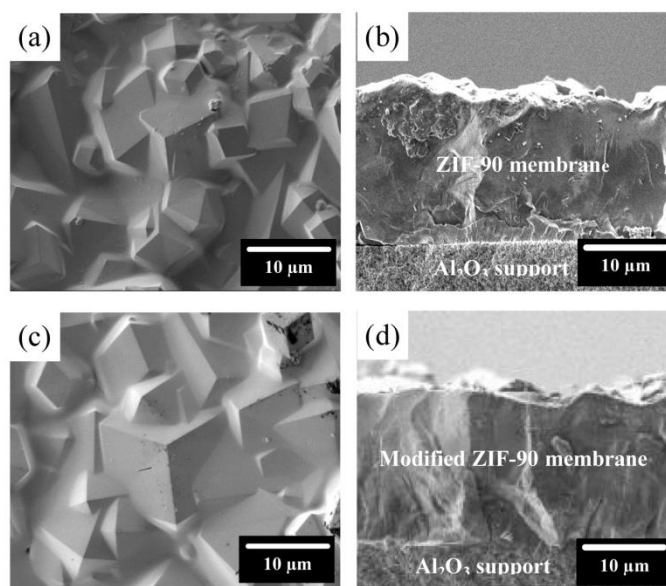
Figure S3. (a) Top view and (b) cross-section SEM images of the as-prepared ZIF-90 membrane on the porous Al$_2$O$_3$ support; (c) Top view and (d) cross-section SEM of the APTES-modified ZIF-90 membrane via covalent postfunctionalization on the porous Al$_2$O$_3$ support.

Figure S4
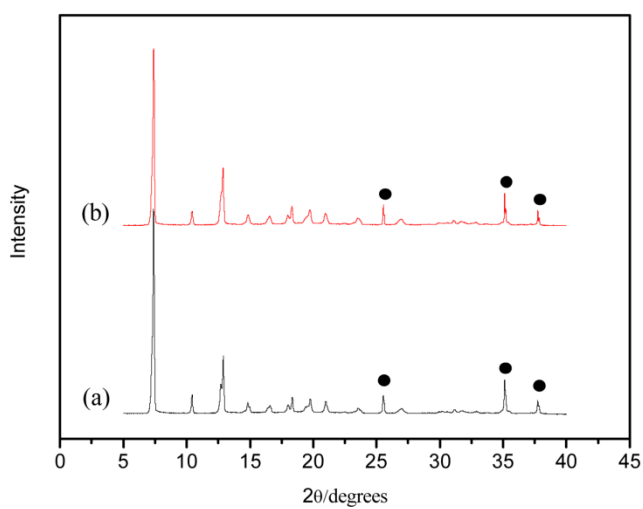
Figure S4. XRD patterns of the as-made ZIF-90 membrane (a) and organosilica-functionalized ZIF-90 membrane on Al$_2$O$_3$ support. (?): Al$_2$O$_3$ support, (not marked): ZIF-90 crystals.

Figure S5
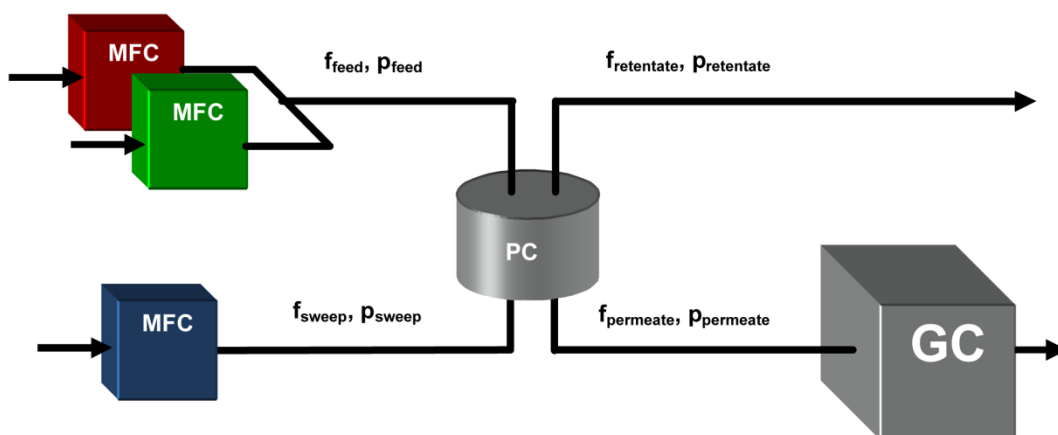
Figure S5. Measurement equipment for both single and mixed gas permeation.

Legend:

MFC: mass flow controller

PC: permeation cell with mounted membrane

GC: gas chromatograph

f: volumetric flow rate

p: pressure

Figure S6
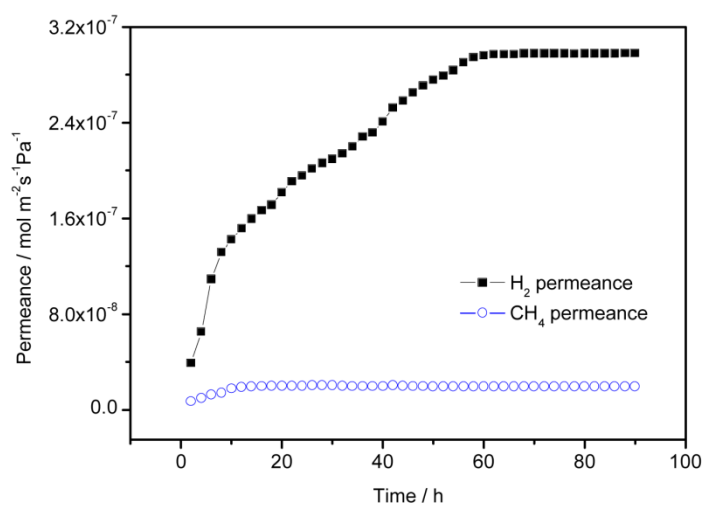
Figure S6. H$_2$ and CH$_4$ permeances obtained from an equimolar H$_2$/CH$_4$ mixture through the as-prepared ZIF-90 membrane during the on-stream activation process at 225 ºC.
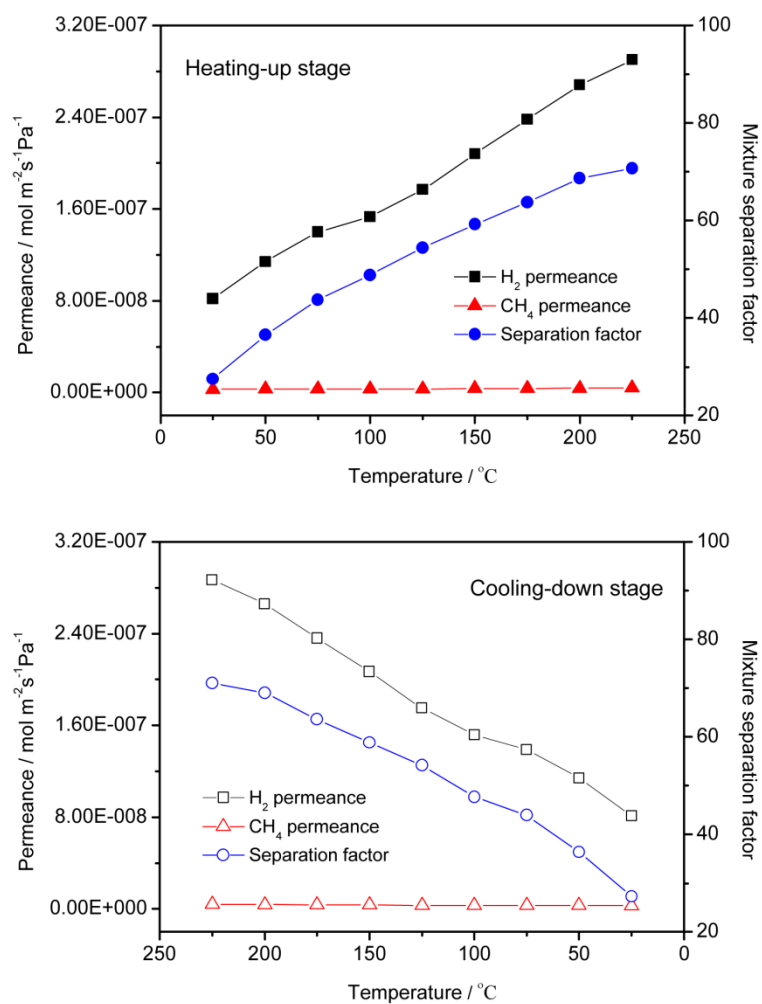
Figure S7

Figure S7. Gas permeances and H$_2$/CH$_4$ selectivity of the APTES-functionalized ZIF-90 membrane as function of the temperature at 1 bar.

Figure S8
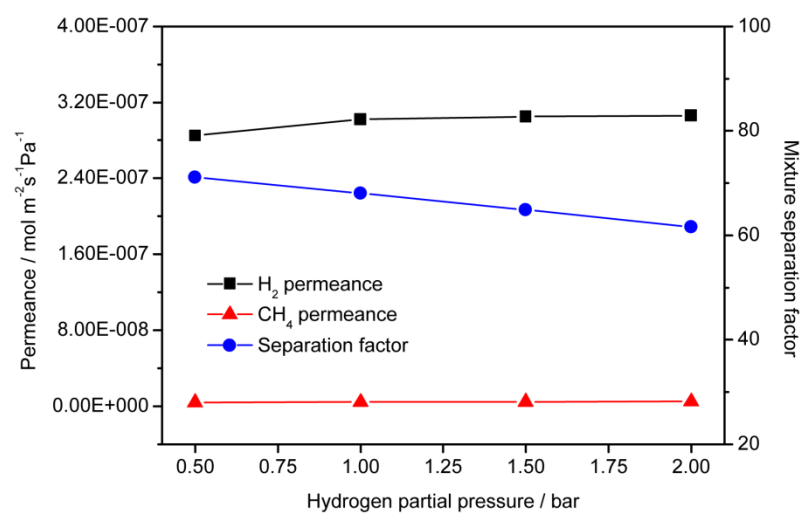
Figure S8. Gas permeances and H_2/CH_4 selectivity of the APTES-functionalized ZIF-90 membrane as function of the hydrogen partial pressure at 225 ºC.

Table S1

Table S1 Single gases permeation performances of the as-prepared and APTES-functionalized ZIF-90 membrane at 225 °C and 1 bar.

Gas$_{i/j}$	KC*	Single gas permeation performances of the ZIF-90 membrane					
		As-prepared ZIF-90 membrane			APTES-functionalized ZIF-90 membrane s		
		Permeances(i) (mol/m^2·S^1·Pa^1)	Permeances(j) (mol/m^2·S^1·Pa^1)	Ideal Separation factor	Permeances(i) (mol/m^2·S^1·Pa^1)	Permeances(j) (mol/m^2·S^1·Pa^1)	Ideal Separation factor
H_2/CO_2	4.7	3.08×10^{-7}	4.10×10^{-8}	7.51	2.96×10^{-7}	1.37×10^{-8}	21.6
H_2/CH_4	2.8	3.08×10^{-7}	1.90×10^{-8}	16.2	2.96×10^{-7}	3.72×10^{-9}	79.6
H_2/C_2H_6	3.9	3.08×10^{-7}	7.49×10^{-9}	41.1	2.96×10^{-7}	1.14×10^{-9}	261
H_2/C_3H_8	4.7	3.08×10^{-7}	4.61×10^{-9}	66.8	2.96×10^{-7}	6.26×10^{-10}	473

* KC: Knudsen constant.

Table S2

Table S2 Mixture gases separation performances of the as-prepared and APTES-functionalized

ZIF-90 membrane at 225 ºC and 1 bar with 1:1 binary mixtures.

		Mixture gases separation performances of the ZIF-90 membrane					
Gas$_{i/j}$	KC*	As-prepared ZIF-90 membrane			APTES-functionalized ZIF-90 membrane		
		Permeances(i) (mol/m^2·S^1·Pa^1)	Permeances(j) (mol/m^2·S^1·Pa^1)	Separation factor	Permeances(i) (mol/m^2·S^1·Pa^1)	Permeances(j) (mol/m^2·S^1·Pa^1)	Separation factor
H$_2$/CO$_2$	4.7	2.91 x 10^{-7}	4.04 x 10^{-8}	7.20	2.82 x 10^{-7}	1.37 x 10^{-8}	20.1
H$_2$/CH$_4$	2.8	2.90 x 10^{-7}	1.94 x 10^{-8}	15.4	2.85 x 10^{-7}	4.02 x 10^{-9}	70.5
H$_2$/C$_2$H$_6$	3.9	2.87 x 10^{-7}	7.40x 10^{-9}	38.8	2.80 x 10^{-7}	1.14 x 10^{-9}	250
H$_2$/C$_3$H$_8$	4.7	2.85 x 10^{-7}	4.36 x 10^{-9}	65.4	2.78 x 10^{-7}	6.26 x 10^{-10}	458

* KC: Knudsen constant.

Table S3

Table S3 H$_2$/CH$_4$ separation performances of the ZIF-90 membranes as functional of modification time with APTES at 225 ºC and 1 bar with 1:1 binary mixtures.

Membrane	Post-modification	Permeance[a]		H$_2$/CH$_4$ selectivity
		H$_2$	CH$_4$	
M1	No	2.98×10^{-7}	1.94×10^{-8}	15.4
M2	110°C 0.5 h	2.85×10^{-7}	4.02×10^{-9}	70.5
M3	110°C 1.0 h	6.77×10^{-8}	4.64×10^{-10}	146

[a] (mol/m^2·S^1·Pa^1).

Table S4

Table S4 Comparison of the mixture gas separation performances of the APTES-functionalized ZIF-90 membrane in this study with other zeolite and MOF membranes from literatures.

Membrane	Pore size (nm)	Temperature (°C)	Mixture as separation performances				Reference
			Selectivity			H_2 permeances $(mol/m^2 \cdot S^1 \cdot Pa^1)$	
			H_2/CO_2	H_2/CH_4	H_2/C_3H_8		
DDR	0.36 x 0.44	300	3.5	/	/	7.9×10^{-6}	S1
Matrix AlPO$_4$	/	35	9.7	/	/	1.1×10^{-7}	S2
SAPO-34	0.38	200	23	/	/	7.0×10^{-8}	S3
LTA AlPO$_4$	0.40	25	7.6	4.3	146	2.5×10^{-7}	S4
NaA	0.41	20	6.7	4.9	15.8	2.3×10^{-7}	S5
ITQ-29	0. 41	300	7.8 [a]	6.2 [a]	127	3.6×10^{-7}	S6
MOF-5	1.40	/	KD [b]	KD [b]	/	4.7×10^{-6}	S7
HKUST-1	0.90	25	6.8	6	7.0	1.0×10^{-6}	S8
HKUST-1	0.90	25	4.6	3.0	/	6.7×10^{-7}	S9
IRMOF-3 [c]	/	25	4.1	2.0	2.4	1.1×10^{-6}	S10
MIL-53	0.73 x 0.77	/	5.4	4.0	/	5.0×10^{-7}	S11
SIM-1	0.34	25	2.4 [a]	2.6 [a]	/	8.2×10^{-7}	S12
ZIF-7	0.30	200	6.5	5.9	/	8.0×10^{-8}	S13
ZIF-8	0.34	25	4.5 [a]	11.3	/	5.1×10^{-8}	S14
ZIF-8	0.34	25	6.0	15	300	1.0×10^{-7}	S15
ZIF-8	0.34	23	/	/	545	4.4×10^{-7}	S16
ZIF-22	0.29	50	7.2	5.2	/	1.9×10^{-7}	S17
ZIF-69	4.4	25	2.7 [a]	3.7 [a]	/	6.50×10^{-8}	S18
ZIF-90	0.37	200	7.2 [a]	15.3	/	2.51×10^{-7}	S19
ZIF-90 [d]	/	200	15.3	18.9	/	2.02×10^{-7}	S20
ZIF-90 [e]	/	225	20.1	70.5	458	2.85×10^{-7}	This work

[a] ideal separation factor, [b] Knudsen diffusion, [c] AM6 modified IRMOF-3, [d] ethanolamine modified ZIF-90, [e] APTES modified ZIF-90.

Table S5

Table S5. Separation performances of APTES-functionalized ZIF-90 membranes modified by 30 minutes for the separation of H$_2$/CH$_4$ mixtures at 225 ºC and 1 bar.

Membrane	H$_2$ permeance (mol·m^{-2}·s^{-1}·Pa^{-1})	CO$_2$ permeance (mol·m^{-2}·s^{-1}·Pa^{-1})	H$_2$/CO$_2$ selectivity	Average selectivity	standard deviation of selectivity
M1	2.80 x 10^{-7}	3.93 x 10^{-9}	70.4		
M2	2.86 x 10^{-7}	4.08x 10^{-9}	70.1	70.37	0.12
M3	2.83 x 10^{-7}	4.01 x 10^{-9}	70.6		

References:

(S1) M. Kanezashi, J. O'Brien-Abraham, Y. S. Lin, *AIChE Journal* **2008**, *54*, 1478–1486.

(S2) G. Guan, T. Tanaka, K. Kusakabe, K. Sotowa, S. Morooka, *J. Membr. Sci.* **2003**, *214*, 191–198.

(S3) M. Yu, H.H. Funke, R. D. Noble, J. L. Falconer, *J. Am. Chem. Soc.* **2011**, *133*, 1748–1750.

(S4) A. Huang, F. Liang, F. Steinbach, T. M. Gesing, J. Caro, *J. Am. Chem. Soc.* **2010**, *132*, 2140–2141.

(S5) A. Huang, J. Caro, *J. Mater. Chem.* **2011**, *21*, 11424–11429.

(S6) A. Huang, J. Caro, *Chem. Commun.* **2010**, *46*, 7748–7750.

(S7) Y. Yoo, Z. Lai, H. K. Jeong, *Microporous Mesoporous Mater.* **2009**, *123*, 100–106.

(S8) H. Guo, G. Zhu, I. J. Hewitt, S. Qiu, *J. Am. Chem. Soc.* **2009**, *131*, 1646–1647.

(S9) J. Nan, X. Dong, W. Wang, W. Jin, N. Xu, *Langmuir* **2011**, *27*, 4309–4312.

(S10) Y. Yoo, V. Varela-Guerrero, H.-K. Jeong, *Langmuir* **2011**, *27*, 2652–265.

(S11) Y. Hu, X. Dong, J. Nan, W. Jin, X. Ren, N. Xu, Y. M. Lee, *Chem. Commun.* **2011**, *47*, 737–739.

(S12) S. Aguado, C. H. Nicolas, V. Moizan-Baslé, C. Nieto, H. Amrouche, N. Bats, N. Audebrandd, D. Farrusseng, *New J. Chem.* **2011**, *35*, 41–44.

(S13) Y. Li, F. Liang, H. Bux, A. Feldhoff, W. Yang, J. Caro, *Angew. Chem. Int. Ed.* **2010**, *49*, 548–551.

(S14) H. Bux, F. Liang, Y. Li, J. Cravillon, M. Wiebcke, J. Caro, *J. Am. Chem. Soc.* **2009**, *131*, 16000–16001.

(S15) H. Bux, A. Feldhoff, J. Cravillon, M. Wiebcke, Y. Li, J. Caro, *Chem. Mater.* **2011**, *23*, 2262–2269.

(S16). Y. Pan, Z. Lai, *Chem. Commun.* **2011**, *47*, 10275–10277

(S17) A. Huang, H. Bux, F. Steinbach, J. Caro, *Angew. Chem. Int. Ed.* **2010**, *49*, 4958-4961.

(S18) Y. Liu, E. Hu, E. A. Khan, Z. Lai, *J. Membr. Sci.* **2010**, *353*, 36–40.

(S19) A. Huang, W. Dou, J. Caro, *J. Am. Chem. Soc.* **2010**, *132*, 15562–15564.

(S20) A. Huang, J. Caro, *Angew. Chem. Int. Ed.* **2011**, *50*, 4979–4982.

4 Conclusions

This thesis is dedicated to the preparation and evaluation of two zeolite membranes (zeolite SOD and LTA membranes) and three MOF membranes (Mg-MOF-74, ZIF-90 and ZIF-100 membranes). As clean environmental process, separation by molecular sieve zeolite and MOF membranes has already shown potential applications in industry, such as for gas separation, as well as in membrane reactors.

The first part of this thesis was focused on the hydrophilic zeolite membrane for water separation, either for water vapor separation at high temperatures and for water pervaporation at room temperature, as described in Section 2. To synthesize a dense SOD membrane, we have developed a two-step repeated hydrothermal synthesis method. After the repeated synthesis method, well-intergrown SOD membrane with a thickness of around 8 μm could be obtained on the alumina support. The SOD membranes were evaluated from 125 to 200 ℃ in steam permeation of equimolar mixtures of H_2O/H_2, H_2O/CH_4, H_2O/CO_2, $H_2O/MeOH$, H_2O/DME and H_2O/DMC. The stability of SOD membrane at high temperatures and the selectivity results reported in Sections 2.2 and 2.3 are promising for the application of SOD membranes in membrane reactors such as for esterification. Since less water could be adsorbed in the SOD framework as temperature increases, it was found that the mixed gas separation factors of H_2O/H_2, H_2O/CH_4, and H_2O/CO_2 decreased slightly with increasing temperature. It is worth to mention that by using SOD membranes water can be very effectively separated from other molecules like methanol (MeOH), dimethylether (DME) and dimethylcarbonate (DMC), with mixture separation factors near 200, >200 and >1000, respectively. Due to the thickness of the SOD membrane, however, the water permeance (0.43 kg/m^2 h bar) is relative low.

Zeolite LTA membrane was developed for water separation from MeOH and DMC by pervaporation at room temperature. After the alumina support was pre-modified by 3-aminopropyltriethoxysilane (APTES), a supported well-intergrown LTA membrane could be obtained. LTA membranes are usually synthesized in the Na$^+$ form, with a pore size of about 4 Å. However, it is not small enough to separate water form methanol, since both of H_2O and MeOH are smaller than the pore size (with kinetic diameters of 2.6 Å and 3.8 Å, respectively). We tried to solve the problem by using ion-exchange of

the Na^+ with larger K^+ ions, thus the pore size was narrowed to 3 Å. After the ion-exchange for 12 h, the selectivity of $H_2O/MeOH$ in mixture was improved from 2.8 to 7.4 at room temperature by pervaporation. On the other hand, the LTA membrane also showed good selectivity for water/DMC separation. The separation factors of H_2O/DMC by pervaporation at room temperature were around 800 and 1000 (before and after ion-exchange, respectively).

In the second part we introduced three MOF membranes, namely Mg-MOF-74, ZIF-90 and ZIF-100 membranes, for hydrogen purification. We focused on the synthesis method of these MOF membranes, especially pre- and post-modification method to improve the membrane quality and gas separation performances. We used a secondary growth method to prepare Mg-MOF-74 membrane after optimization of the synthesis solution. By seeding MgO nanocrystals on the alumina support, a phase-pure and compact Mg-MOF-74 membrane can grow on the seeded support. Although Mg-MOF-74 has relatively larger pore size of about 10 Å, a mixture separation factor of H_2/CO_2 with 10.5 (obviously higher than those of H_2/CH_4 and H_2/N_2) could be obtained at room temperature. After a post-functionalization of the as-prepared Mg-MOF-74 membrane by ethylenediamine, the H_2/CO_2 selectivity was remarkably increased to 28 at room temperature. Attributed to the unsaturated Mg^{2+} site in the framework structure of Mg-MOF-74, CO_2 can be stored in the pore structure Mg-MOF-74, thus resulting in a high H_2/CO_2 selectivity. By modification using a diamine, one amino group was interacted with the open Mg site to narrow the pore size, and the other amino group interacts with CO_2 thus further reducing CO_2 mobility.

Dense and continuous ZIF-100 membrane was prepared on polydopamine (PDA)-modified alumina support. After the pre-modification by PDA, covalent and non-covalent bonds between PDA and ZIF-100 were formed and ZIF-100 nutrients could be attracted better on the support. Due to the outstanding CO_2 uptake behavior and the small pore aperture of ZIF-100, the PDA-based ZIF-100 membrane showed a high H_2/CO_2 selectivity of about 72 at room temperature and 1 bar. In Section 3.3, we have also investigated the gas adsorption isotherm of ZIF-100 by a simulation study. In good accordance with the experimental data, it was found in simulation study that CO_2 is predominantly adsorbed over H_2 in the whole pressure range attributing to the much stronger interaction between CO_2 and ZIF-100.

As described in Section 3.4, a post-modification method was used to modify the as-prepared ZIF-90 membrane by using APTES. Through an imine condensation between the free aldehyde groups of the ZIF-90 and the amino group of APTES, the mixture separation factors of H_2/CO_2, H_2/CH_4, H_2/C_2H_6 and H_2/C_3H_8 could be improved to 20.1, 70.5, 250 and 458, respectively, while the high H_2 permeances could be kept after the modification as well. The increase of the separation factors is ascribed to two effects: the pore mouth of ZIF-100 was narrowed, and defects of the polycrystalline ZIF-90 layer were also sealed during the APTES-modification.

In summary, this work presented five molecular sieving membranes for gas/liquid separation. Various synthesis skills were investigated based on the properties of each membrane. Pre-modification methods (with APTES or PDA), secondary growth method as well as two-step synthesis method were introduced to improve the membrane quality and reproducibility, so that the membranes could grow better on the alumina support. Post-modifications (with APTES or ethylenediamine) and ion-exchange of the as-prepared membranes were applied to improve the gas/liquid separation performance of the obtained membranes.

So far, zeolite and MOF molecular sieve membranes have not found any industrial applications in technical gas separation. An exception is the use of LTA and FAU membranes in the de-watering of different solvents by steam permeation or pervaporation. At present, the higher production costs of zeolite and MOF membranes are not justified by a higher separation performance (selectivity, flux) or by a longer live time. Special problems for MOFs are their instability against moisture and their non-constant pore size. As coordination polymer, MOFs show the phenomenon of framework flexibility which is linked to such termini like "breathing", "gate opening", "linker distortion" and results in no sharp pore size "cut off" in adsorption and permeation.

Mixed Matrix Membranes (MMM) combine the excellent processing properties of polymers (spring of hollow fibers, casting of foils) with the adsorption and diffusion selectivities of zeolites and MOFs when the polymer is modified by 10…30 vol. % of zeolite or MOF (nano)powder. The analysis of the open literatures of the last few years leads to the assumption that in MOF-based MMM must be a synergistic interplay of

MOF particles and the continuous polymer phase. The dramatic improvements of flux and selectivity of MMM cannot by understood on the base of the classical Maxwell theory. One possible explanation of the improved selectivity of MMM is that the polymer matrix stops linker distortion which increases selectivity.

Appendix

Publications

Publications included in this thesis

1. **N. Wang**, Y. Liu, A. Huang, J. Caro, Supported SOD membrane with steam selectivity by a two-step repeated hydrothermal synthesis, Microporous and Mesoporous Materials 2014, 192, 8-13.

2. **N. Wang**, Y. Liu, A. Huang, J. Caro, Hydrophilic SOD and LTA membranes for membrane-supported methanol, dimethylether and dimethylcarbonate synthesis. Microporous and Mesoporous Materials 2015, 207, 33-38.

3. **N. Wang**, A. Mundstock, Y. Liu, A. Huang, J. Caro, Amine-modified Mg-MOF-74/CPO-27-Mg membrane with enhanced H_2/CO_2 separation. Chemical Engineering Science 2015, 124, 27-36.

4. **N. Wang**, Y. Liu, Z. Qiao, L. Diestel, J. Zhou, A. Huang, J. Caro, Polydopamine-based synthesis of zeolite imidazolate framework ZIF-100 membrane with high H_2/CO_2 selectivity. Journal of Materials Chemistry A 2015, 3, 4722-4728.

5. A. Huang, **N. Wang**, C. Kong, and J. Caro, Organosilica-functionalized zeolitic imidazolate framework ZIF-90 membrane with high gas-separation performance, Angewandte Chemie International Edition 2012, 51, 10551-10555.

Publications not included in this thesis

6. L. Diestel, **N. Wang**, A. Schulz, F. Steinbach, J. Caro, Matrimid-based mixed matrix membranes: interpretation and correlation of experimental findings for zeolitic imidazolate frameworks as fillers in H_2/CO_2 separation, Industrial & Engineering Chemistry Research 2015, 54, 1103-1112.

7. Y. Liu, J. Pan, **N. Wang**, F. Steinbach, X. Liu, J. Caro, Remarkably enhanced gas separation by partial self-conversion of a laminated membrane to metal–organic frameworks, Angewandte Chemie International Edition 2015, 54, 3028 –3032

8. A. Huang, Q. Liu, **N. Wang**, Y. Zhu, J. Caro, Bicontinuous zeolitic imidazolate framework ZIF-8@GO membrane with enhanced hydrogen selectivity, Journal of the American Chemical Society 2014, 136, 14686-14689.

9. Y. Liu, **N. Wang**, J. Pan, F. Steinbach, J. Caro, In situ synthesis of MOF membranes on ZnAl-CO$_3$ LDH buffer layer-modified substrates, Journal of the American Chemical Society 2014, 136, 14353-14356.

10. A. Huang, Q. Liu, **N. Wang**, J. Caro, Organosilica functionalized zeolitic imidazolate framework ZIF-90 membrane for CO$_2$/CH$_4$ separation, Microporous and Mesoporous Materials 2014, 192, 18-22.

11. A. Huang, Y. Chen, Q. Liu, **N. Wang**, J. Jiang, J. Caro, Synthesis of highly hydrophobic and permselective metal-organic framework Zn(BDC)(TED)0.5 membranes for H$_2$/CO$_2$ separation, Journal of Membrane Science 2014, 454, 126-132.

12. A. Huang, Q. Liu, **N Wang**, J. Caro, Highly hydrogen permselective ZIF-8 membranes supported on polydopamine functionalized macroporous stainless-steel- nets, Journal of Materials Chemistry A 2014, 2, 8246-8251.

13. Y. Liu, **N. Wang**, L. Diestel, F. Steinbach, J. Caro, MOF membrane synthesis in the confined space of a vertically aligned LDH network, Chemical Communications 2014, 50, 4225-4227.

14. Y. Liu, **N. Wang**, J. Caro, In situ formation of LDH membranes of different microstructures with molecular sieve gas selectivity, Journal of Materials Chemistry A 2014, 2, 5716-5723.

15. Y. Liu, **N. Wang**, Z. Cao, J. Caro, Molecular sieving through interlayer galleries, Journal of Materials Chemistry A 2014, 2, 1235-1238.

16. Q. Liu, **N. Wang**, J. Caro, A. Huang, Bio-Inspired polydopamine: A versatile and powerful platform for covalent synthesis of molecular sieve membranes, Journal of the American Chemical Society 2013, 135, 17679-17682.

17. A. Huang, Q. Liu, **N. Wang**, X. Tong, B. Huang, M. Wang, J. Caro, Covalent synthesis of dense zeolite LTA membranes on various 3-chloropropyltrimethoxy-silane functionalized supports, Journal of Membrane Science 2013, 437, 57-64.

18. A. Huang, **N. Wang**, J. Caro, Synthesis of multi-layer zeolite LTA membranes with enhanced gas separation performance by using 3-aminopropyltriethoxysilane as interlayer, Microporous and Mesoporous Materials 2012, 164, 294-301.

19. A. Huang, Y. Chen, **N. Wang**, Z. Hu, J. Jiang, J. Caro, A highly permeable and selective zeolitic imidazolate framework ZIF-95 membrane for H_2/CO_2 separation, Chemical Communications 2012, 48, 10981-10983.

20. A. Huang, **N. Wan**g, J. Caro, Seeding-free synthesis of dense zeolite FAU membranes on 3-aminopropyltriethoxysilane-functionalized alumina supports, Journal of Membrane Science 2012, 389, 272-279.

21. A. Huang, **N. Wang**, J. Caro, Stepwise synthesis of sandwich-structured composite zeolite membranes with enhanced separation selectivity, Chemical Communications 2012, 48, 3542-3544.

Contrubutions to conferences

1. A. Huang, **N. Wang***, J. Caro, Stepwise synthesis of sandwich-structured composite zeolite membranes with enhanced separation selectivity, 24. Deutsche Zeolith-Tagung, 7th-09th March 2012, Magdeburg, poster presentation.

2. **N. Wang***, A. Huang, J. Caro, Improved MOF and zeolite membranes by support modification, EUROMEMBRANE 23th-27th September 2012, London, poster presentation.

3. A. Huang, **N. Wang***, C. Kong, and J. Caro, Organosilica functionalized zeolitic imidazolate framework ZIF-90 membrane with high gas separation performances, 25. Deutsche Zeolith-Tagung, 6th-8th March 2013, Hamburg, poster presentation.

4. **N. Wang***, A. Mundstock, Y. Liu, A. Huang, J. Caro, Amine-modified Mg-MOF-74/CPO-27-Mg membrane with enhanced H2/CO2 separation, IZMM6 (6th International Zeolite Membrane Meeting) 15th-19th June 2013, Jeju Island, Korea, poster presentation.

5. **N. Wang***, Y. Liu, A. Huang, J. Caro, Supported SOD membrane with steam selectivity by a two-step repeated hydrothermal synthesis, 26. Deutsche Zeolith-Tagung, 26th-28th February 2014, Paderborn, poster presentation.

6. Q. Liu, **N. Wang***, J. Caro, A. Huang, Bio-Inspired polydopamine: A versatile and powerful platform for covalent synthesis of molecular sieve membranes, 6th FEZA Conference, 8th-11th September 2014, Leipzig, poster presentation.

Curriculum Vitae

Personal data:

Name:	Nanyi Wang
Date of birth:	26.11.1986
Place of birth:	Jiangsu, China
Nationality:	Chinese
Marital status:	Married

Higher education:

Since 01/2012	Ph. D. research at **Gottfried Wilhelm Leibniz University Hannover**, Germany.
	Scientific co-worker in the group of Prof. Dr. Jürgen Caro, Institute of Physical Chemistry and Electrochemistry.
10/2009 – 11/2011	Study at **Gottfried Wilhelm Leibniz University Hannover**, Germany.
	Degree: Master of Science in "Material- and Nanochemistry".
	Master thesis with Prof. Dr. Jürgen Caro: Seeding-free synthesis of zeolite FAU molecular sieve membranes by using 3-aminopropyltriethoxysilane as covalent linker
01/2007 – 02/2009	Study as exchange-student at **Fachhochschule Reutlingen**, Germany.
	Degree: Bachelor in "Chemistry with Marketing"
09/2004 – 02/2009	Study at **Donghua University**, Shanghai, China.
	Degree: Bachelor in "Light chemical engineering".

Erklärung zur Dissertation

gemäß §6(1) der Promotionsordung der Naturwissenschaftlichen Fakultät der Gottfried Wilhelm Leibniz Universität Hannover für die Promotion zum Dr. rer. nat.

Hiermit erkläre ich, dass ich die vorgelegende Dissertation selbstständig verfasst und unter Verwendung der angegebenen Quelle und Hilfsmittel angefertigt habe. Die Dissertation wurde nicht schon als Masterarbeit oder andere Prüfungsarbeit verwendet.

Nanyi Wang

Hannover, Januar 2015